Electronic Supplementary Material (ESI) for Materials Advances.

Supporting Information:

Pentatomic Carbon Ring Conjugated Nitrogen-Doped Nanographene

Jinku Bai,[a] Xiao Xu,[b] Xin-Yue Wang,[a] Xin Sun,[a] Jiaqi Liang,[a] Tongling Liang[c] and Han-Yuan Gong*[a]

[a] College of Chemistry, Beijing Normal University, No. 19, XinJieKouWai St, HaiDian District, Beijing 100875, China
[b] Goods and Material Department of CASIC Tertiary Research Institute, Building 30, No.1 Xili, Beiqu, Fengtai District, Beijing 100074, China
[c] Institute of Chemistry, Chinese Academy of Science, Beijing 100190, P. R. China; University of Chinese Academy of Sciences, Beijing 100049, China

*Correspondence: hanyuangong@bnu.edu.cn (H.-Y.G.)

Table of Contents

Section S1: *General Considerations*

All solvents and reagents were purchased from Innochem, Hwrk, Chem, Energy Chemical or Cambridge Isotope Laboratories commercial suppliers and used without further purification. ^{1}H and ^{13}C NMR spectra were detected on 400 JNM-ECZ 400S or 600 JNM-ECZ 400S instrument. The ^{1}H and ^{13}C NMR chemical shifts are referenced to residual solvent signals ($CDCl_3$: δ_H = 7.26 ppm, δ_C = 77.16 ppm).[1] High resolution mass spectra (HMRS) were performed on AB SCIEX Triple TOF 56q00+ instrument. Uv-vis spectra were collected on a Shimadzu UV-2450 spectrometer. Fluorescence emission spectra were obtained with an Edinburgh Instruments FS5 spectrometer. Fluorescence lifetimes (τ) were detected on an Edinburgh Instruments FS980. Fluorescence quantum yields were obtained using a HAMAMATSU Quantaurus-QY instrument.

All single crystals used to obtain the X-ray diffraction structures reported in the text grew as yellow or red needle. The .cif documents are available as the separate supporting information files, which provide details regarding the specific crystals used for the analysis, along with the structures in question. Diffraction grade crystals were obtained via slowly evaporation from a mixture of CH_2Cl_2/C_2H_5OH or $ClCH_2CH_2Cl/CH_3OH$ as described below.

The crystals used for single crystal analyses were cut from clusters of the corresponding crystals and had the approximate dimensions given in the .cif documents. The data were collected on XtalLAB Synergy diffractor. Data reduction was performed using CrysAlispro (Rigaku OD) software packages. The structures were refined by full-matrix least-squares on F2 with anisotropic displacement parameters for the non-H atoms using SHELXL-2018/3.[2-4] Definitions used for calculating R(F), Rw(F2) and the goodness of fit, S, are given below and in the .cif documents.[5] Tables of positional and thermal parameters, bond lengths and angles, torsion angles, figures and lists of observed and calculated structure factors are located in the corresponding .cif documents available from the Cambridge Crystallographic Centre and may be obtained by quoting the CCDC ref. numbers 2305337, 2305338 and 2305344. The cif. documents also contain details of the crystal data, data collection, and structure refinement for each structure.

Section S2: *Synthesis and characterization of 1,14-dichloro-6,9-dimethoxyquinolino [2',3',4':3,4] indeno [2,1,7-ghi]phenanthridine* (**1**)

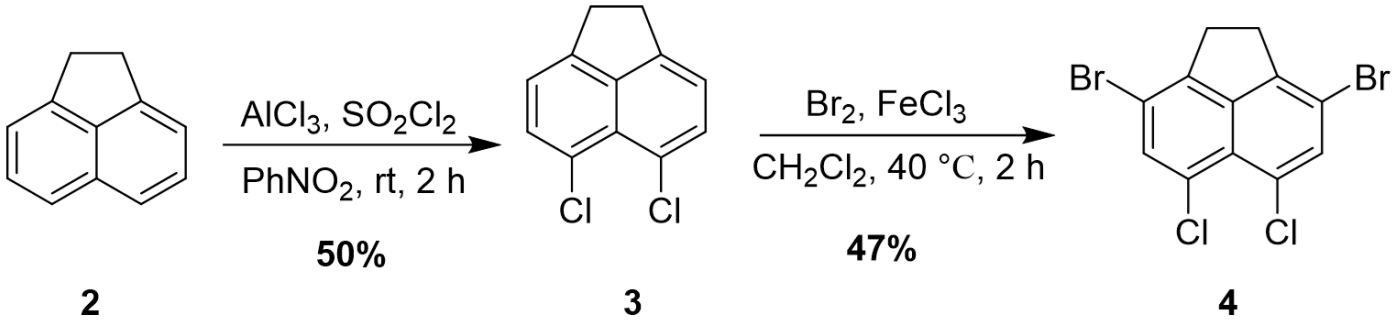

2 **3** **4**

Synthesis of 3,8-dibromo-5,6-dichloro-1,2-dihydroacenaphthylene 4[6]

According to the literature[6], sulfuryl chloride (110.0 g, 66.0 mL, 815 mmol) was dropwise added to a solution containing acenaphthene (**2**) (60.0 g, 390 mmol) and aluminum chloride (10.4 g, 78.0 mmol) in nitrobenzene (250 mL) over 2 h. The solution was stirred for further 2 h and then poured into 600 mL mixture of methanol and water (5:1, *v/v*). The precipitate was collected, washed with methanol, and dried to generate a tan solid (43.3 g, 50% yield). ^{1}H NMR (400 MHz, $CDCl_3$) δ (ppm): 7.49 (d, J = 7.6 Hz, 2H), 7.15 (d, J = 7.6 Hz, 2H), 3.33 (s, 4H).

Bromine (35.9 g, 22.4 mmol) was added in five portions (every 30 min) to a refluxing solution containing 5,6-dichloroacenaphthene **3** (25.0 g, 112 mmol) and ferric chloride (1.82 g, 11.2 mmol) in CH_2Cl_2 (500 mL). Then the mixture kept stirring at reflux for 2 h, then cooled to ambient temperature, washed with water (2 × 250 mL), and evaporated. The brownish solid was triturated with methanol (250 mL) to give a light brown solid **4** (20.0 g, 47%). ^{1}H NMR (400 MHz, $CDCl_3$) δ (ppm): 7.63 (s, 2H), 3.28 (s, 4H). The results are consistent with the literature[6].

Synthesis of 2,2'-(5,6-dichloro-1,2-dihydroacenaphthylene-3,8-diyl)bis(4,4,5,5-tetramethyl-1,3,2-dioxaborolane) 5[7]

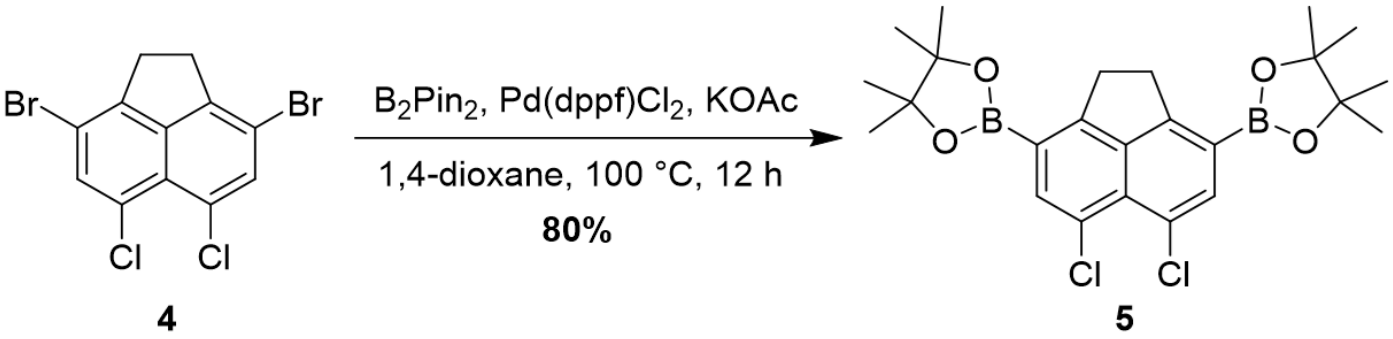

4 **5**

Under argon protection, a 500 mL three-necked flask was charged with 3,8-dibromo-5,6-dichloro-1,2-dihydroacenaphthylene **4** (7.62 g, 20.0 mmol), B_2Pin_2 (15.2 g, 60.0 mmol), $Pd(dppf)Cl_2$ (730 mg, 1.00 mmol) and KOAc (19.6 g, 200 mmol). Then 200 mL 1,4-dioxane was added and the resulting mixture was heated at 100 ℃ for 12 h. The mixture was cooled to room temperature. The solvent was removed with rotary evaporator and the residue was diluted with 25 mL CH_2Cl_2 and filtered through celite. The filtrate was concentrated. Then the crude product was purified via column chromatography (silica gel, 200-300 mesh; elute as petroleum ether (PE: B.P., 60-90 ℃)/ethyl acetate (EA), 2:1, *v/v*) to give compound **5** as a white solid (7.6 g, 80%). Mp: 272-274 ℃. ^{1}H NMR (400 MHz, $CDCl_3$) δ (ppm): 7.91 (s, 2H), 3.47 (s, 4H), 1.37 (s, 24H). ^{13}C NMR (100 MHz, $CDCl_3$) δ (ppm): 156.8, 141.4, 137.6, 128.8, 125.2, 84.0, 31.9, 25.1; MALDI-TOF HRMS (*m/z*): $[M]^+$ calcd. for $C_{24}H_{30}B_2Cl_2O_4$, 474.1707; found: 474.1707.

Synthesis of 5,6-dichloro-3,8-bis(3-methoxy-2-nitrophenyl)-1,2-dihydroacenaphthylene 7

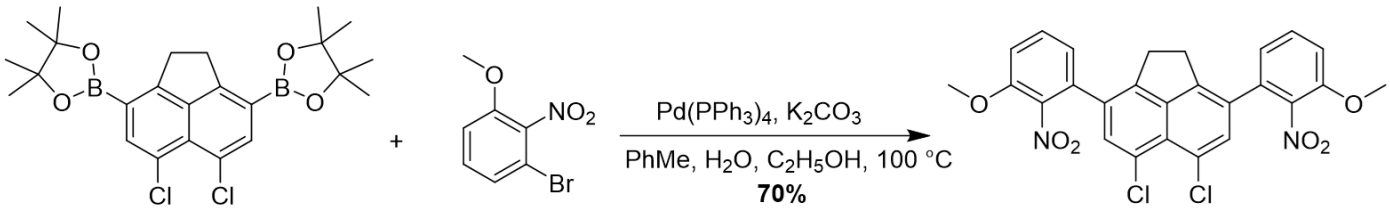

5 **6** **7**

Under argon atmosphere, a 250 mL three-necked flask was charged with **5** (2.85 g, 6.00 mmol), **6** (3.48 g, 15.0 mmol), $Pd(PPh_3)_4$ (416 mg, 0.360 mmol) and K_2CO_3 (6.63 g, 48.0 mmol). Then 50 mL toluene, 1 mL water and 1 mL ethanol were added. The resulting mixture was heated at 100 ℃ for 12 h. Then the reaction was cooled to room temperature. After removing the solvent with rotary evaporator, the crude product was purified with flash chromatography (silica gel, 200-300 mesh; elute as PE/EA (5:1, *v/v*)) to afford compound **7** as a white solid (2.21 g, 70 %). Mp: 242-246 ℃. ^{1}H NMR (400 MHz, $CDCl_3$) δ (ppm): 7.50 (t, *J* = 8.4 Hz, 2H), 7.46 (s, 2H), 7.10 (d, *J* = 7.6 Hz, 2H), 6.95 (d, *J* = 6.8 Hz, 2H), 3.96 (s, 6H), 3.15 (s, 4H). ^{13}C NMR (100 MHz, $CDCl_3$) δ (ppm): 151.1, 145.1, 141.6, 141.2, 132.9, 132.1, 131.2, 129.3, 126.8, 125.8, 122.1, 112.3, 56.6,

29.3; MALDI-TOF HRMS (*m/z*): $[M]^{+\bullet}$ calcd. for $C_{26}H_{18}Cl_2N_2O_6$, 524.0542; found: 524.0541.

Synthesis of 5,6-dichloro-3,8-bis(3-methoxy-2-nitrophenyl)acenaphthylene-1,2-dione 8[6]

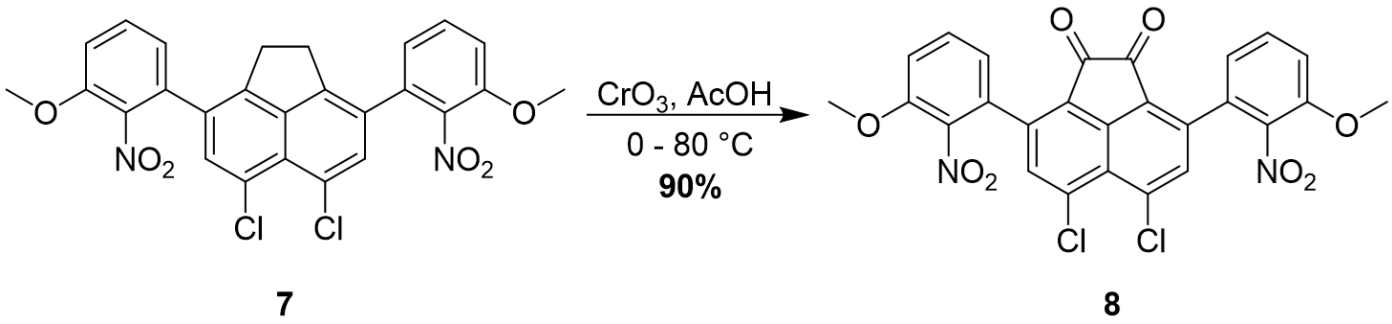

7 **8**

Chromium trioxide (1.43 g, 14.3 mmol) was added in three portions over 2 h to the vigorously stirred solution containing compound **7** (1.50 g, 2.86 mmol) and acetic anhydride (15.0 mL) at 0 ℃. After carefully heated at 80 ℃ for 30 min, the mixture was poured into 1.50 L water and stirred for 30 min. The precipitate was collected and washed with water to yield a yellow solid (1.42 g, 90 %). Mp: 338-340 ℃. ^{1}H NMR (400 MHz, $CDCl_3$) δ (ppm): 7.78 (s, 2H), 7.57 (t, *J* = 8.4 Hz, 2H), 7.23 (d, *J* = 9.2 Hz, 2H), 7.00 (d, *J* = 7.6 Hz, 2H), 3.99 (s, 6H). ^{13}C NMR (100 MHz, $CDCl_3$) δ (ppm): 184.5, 151.2, 147.0, 140.1, 134.5, 133.7, 132.9, 132.4, 129.6, 126.7, 125.0, 123.3, 115.0, 57.4; MALDI-TOF HRMS (m/z): $[M + Na]^+$ calcd. for $C_{26}H_{14}Cl_2N_2NaO_8$, 575.0025; found: 575.0025.

Synthesis of 1,14-dichloro-6,9-dimethoxyquinolino[2',3',4':3,4]indeno[2,1,7-*ghi*]phenanthridine (1)

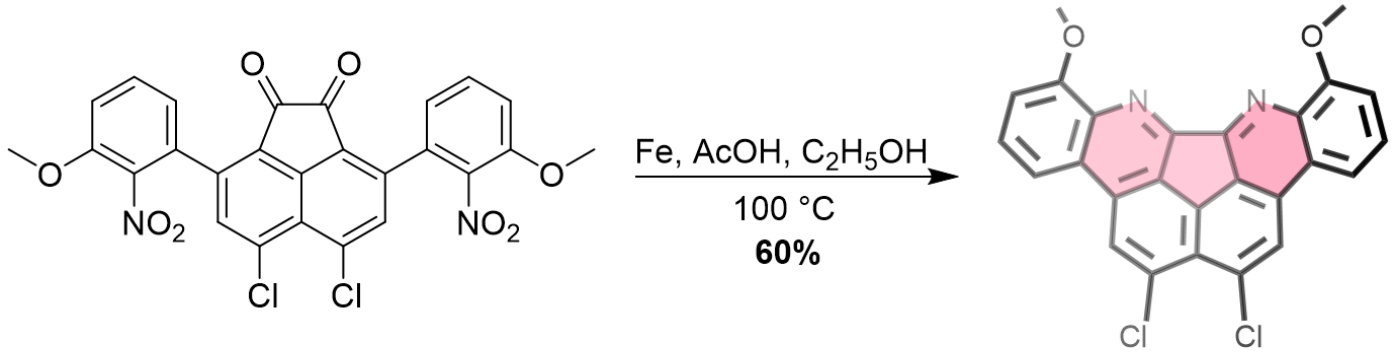

8 **1**

Under argon atmosphere, a 100 mL three-necked flask was charged with **8** (1.00 g, 1.81 mmol) and iron powder (2.00 g, 21.4 mmol). Then 10 mL ethanol and 20 mL acetic acid was added slowly with stirring. The resulting mixture was heated at 100 ℃ for 2 h. Then it was cooled to room temperature, filtered through a short celite plug. The solution was neutralized with $NaHCO_3$ aq . and extracted with CH_2Cl_2 (3 × 100 mL). Organic phases were combined and dried with Na_2SO_4. After removing the solvent with rotary evaporator. the crude product was purified with flash column chromatography (neutral alumina (200-300 mesh); elute as

CH_2Cl_2) to obtain **1** (500 mg, 60%) as a yellow powder. Mp: > 360°C. ^{1}H NMR (400 MHz, $CDCl_3$) δ (ppm): 8.65 (d, *J* = 1.6 Hz, 2H), 8.28 (s, *J* = 5.6 Hz, 2H), 8.16 (m, 2H), 7.62 (d, *J* = 5.6 Hz, 2H), 4.29 (s, 6H). ^{13}C NMR (100 MHz, $CDCl_3$/TFA-*d* (4:1, *v/v*)) δ (ppm): 154.2, 144.3, 136.7, 136.5, 134.6, 130.5, 128.3, 127.7, 127.5, 126.9, 126.1, 117.3, 114.4, 57.6. HRMS (ESI) calcd. for $C_{26}H_{14}Cl_2N_2O_2$ $[M + H]^+$: 457.0511; found: 457.0502.

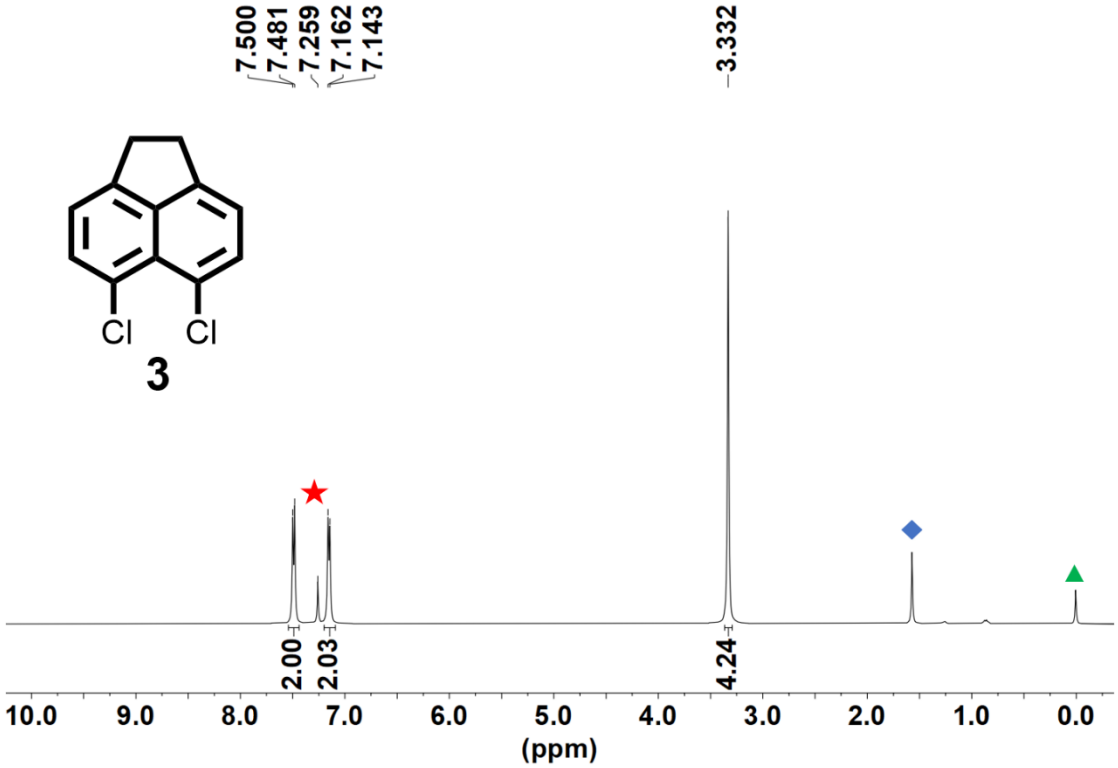

Figure S1. ^{1}H NMR spectrum of **3** in $CDCl_3$ at 298 K (400 MHz) (red "★" represents residual $CHCl_3$; blue "♦" represents H_2O; green "▲" represents TMS).

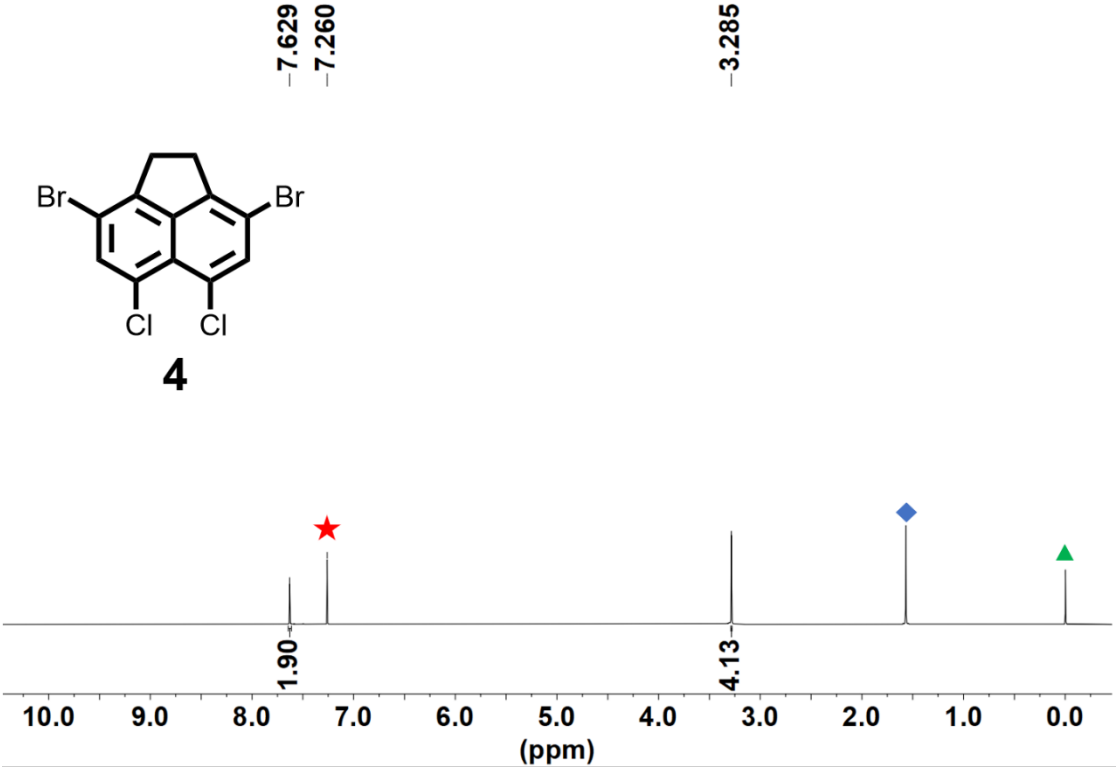

Figure S2. ^{1}H NMR spectrum of **4** in $CDCl_3$ at 298 K (400 MHz) (red "★" represents residual $CHCl_3$; blue "♦" represents H_2O; green "▲" represents TMS).

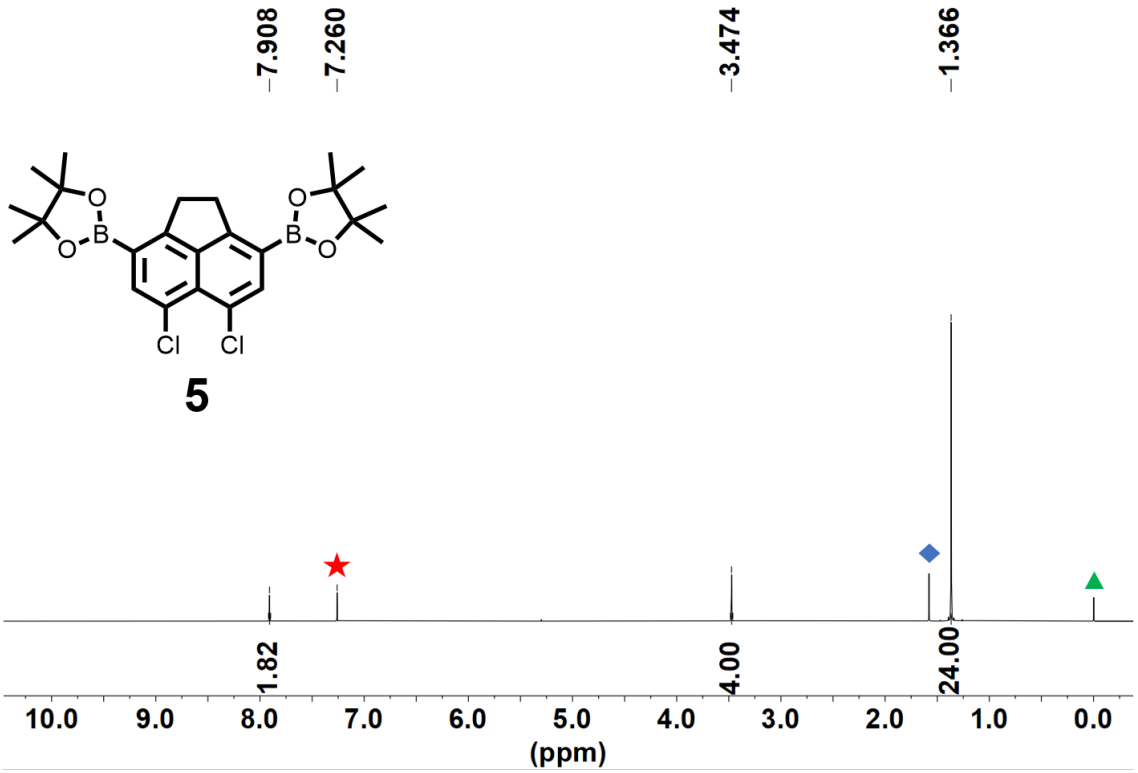

Figure S3. ^{1}H NMR spectrum of **5** in $CDCl_3$ at 298 K (400 MHz) (red "★" represents residual $CHCl_3$; blue "♦" represents H_2O; green "▲" represents TMS).

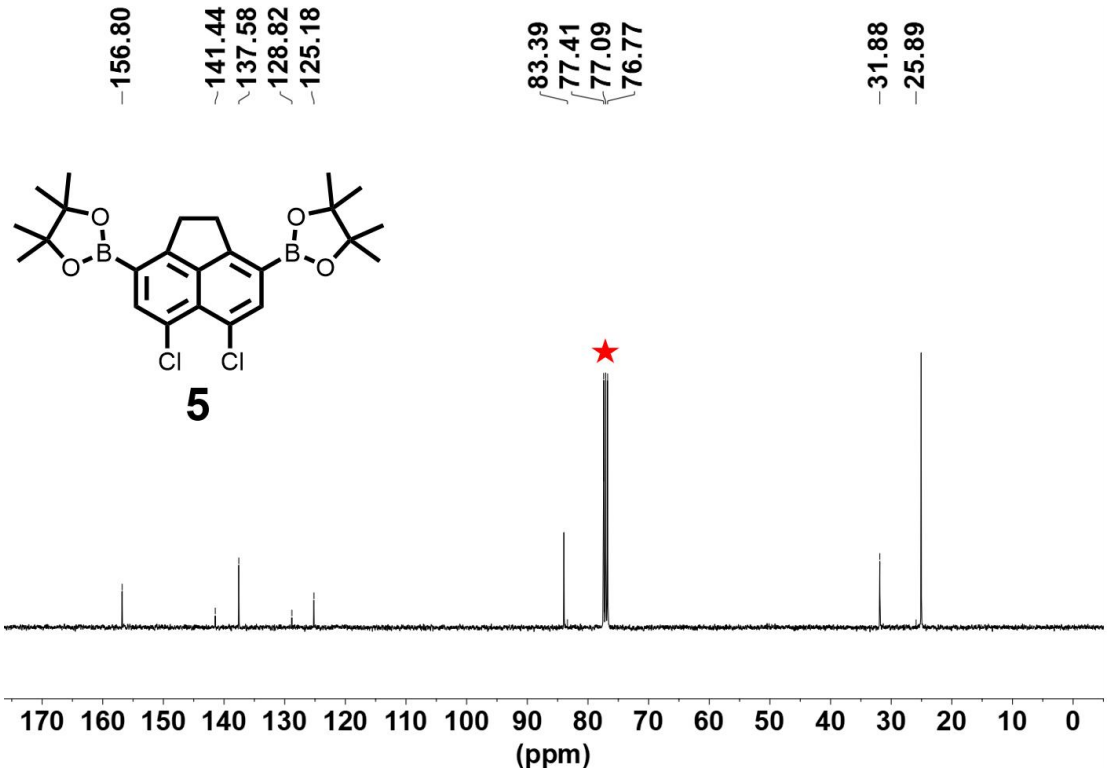

Figure S4. ^{13}C NMR spectrum of **5** in $CDCl_3$ at 298 K (100 MHz) (red "★" represents residual $CHCl_3$).

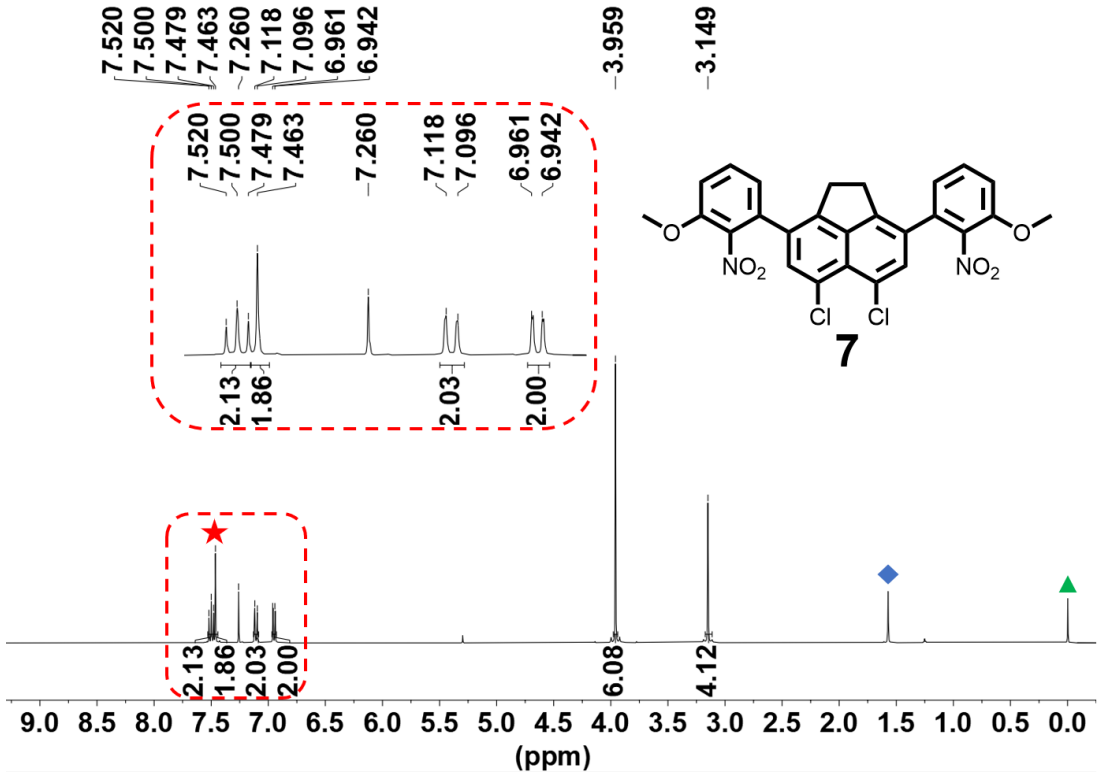

Figure S5. ^{1}H NMR spectrum of **7** in $CDCl_3$ at 298 K (400 MHz) (red "★" represents residual $CHCl_3$; blue "♦" represents H_2O; green "▲" represents TMS).

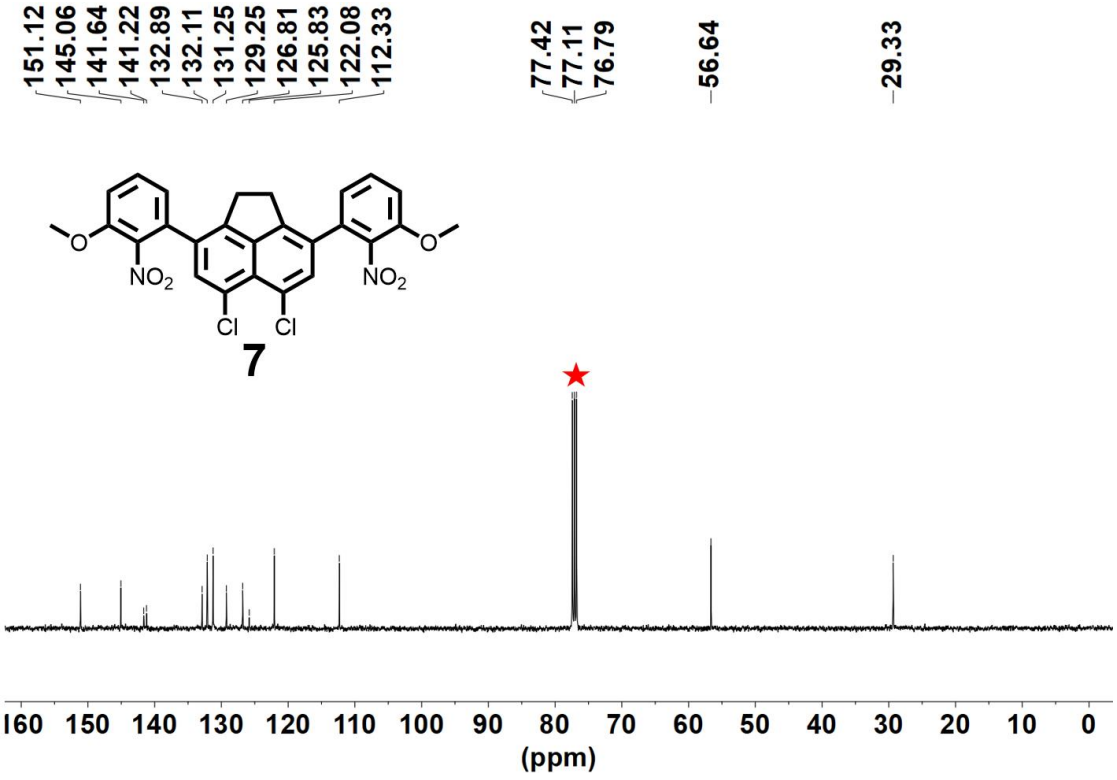

Figure S6. ^{13}C NMR spectrum of **7** in $CDCl_3$ at 298 K (100 MHz) (red "★" represents residual $CHCl_3$).

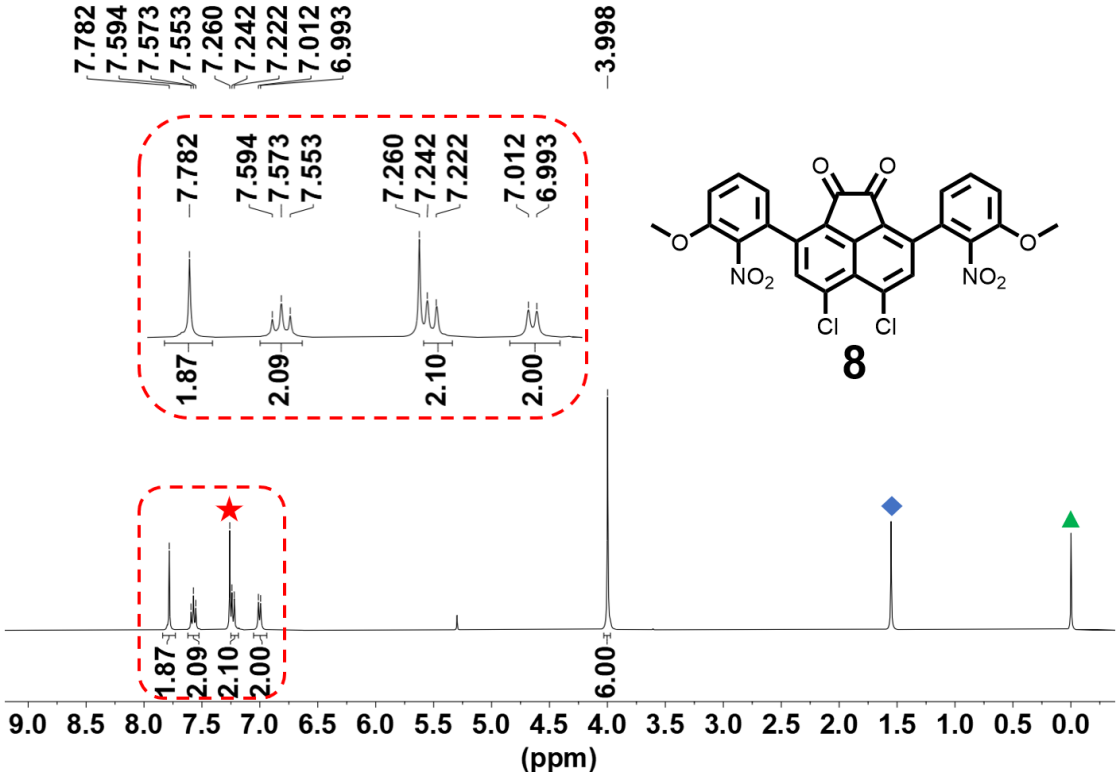

Figure S7. ^{1}H NMR spectrum of **8** in $CDCl_3$ at 298 K (400 MHz) (red "★" represents residual $CHCl_3$; blue "♦" represents H_2O; green "▲" represents TMS).

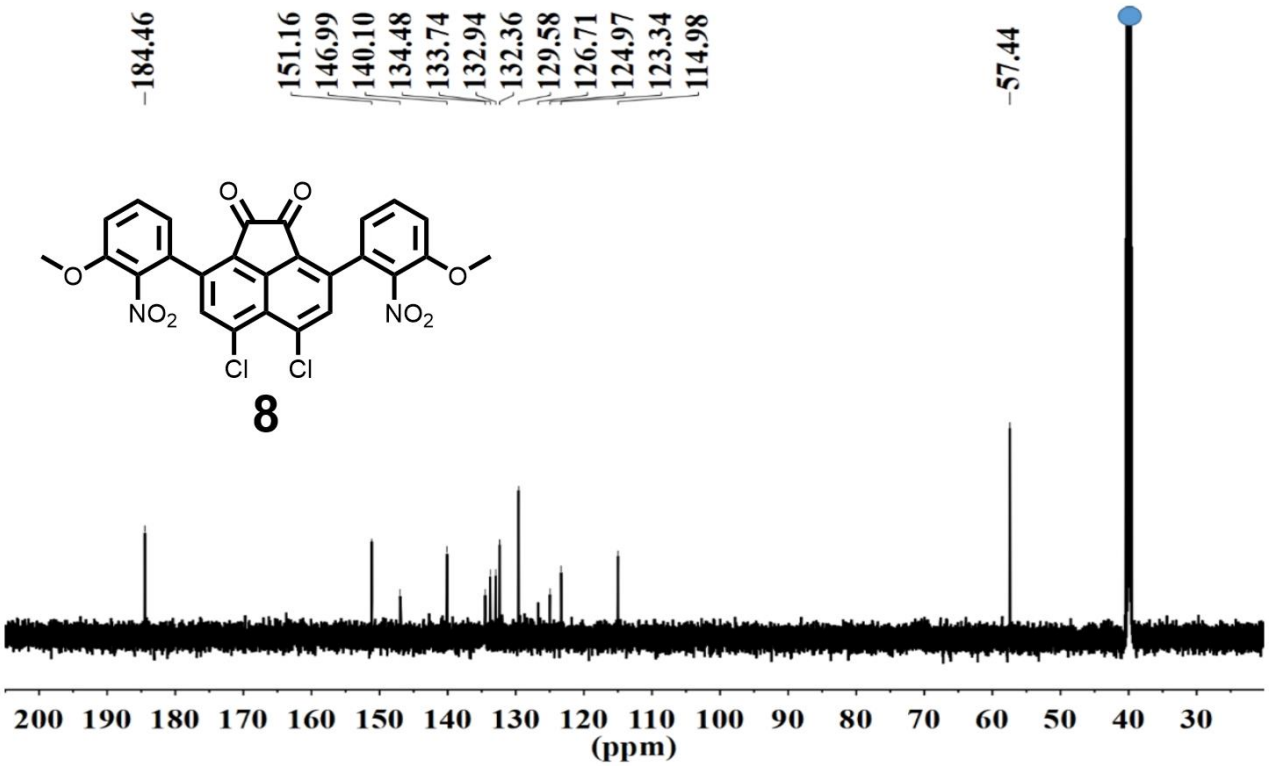

Figure S8. ^{13}C NMR spectrum of **8** in DMSO-d_6 at 298 K (100 MHz) (blue "●" represents residual DMSO).

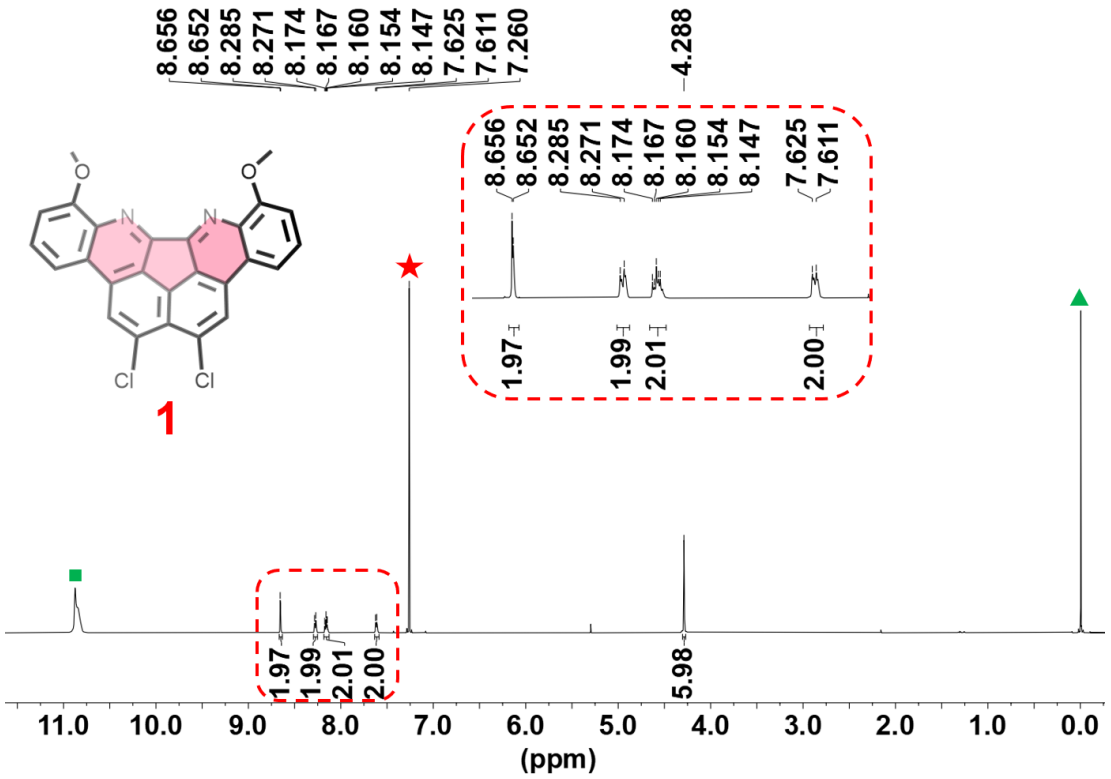

Figure S9. ^{1}H NMR spectrum of **1** in $CDCl_3$/TFA (2:1, *v/v*) at 298 K (400 MHz) (red "★" represents residual $CHCl_3$; green "▲" represents TMS ; green "■" represents TFA).

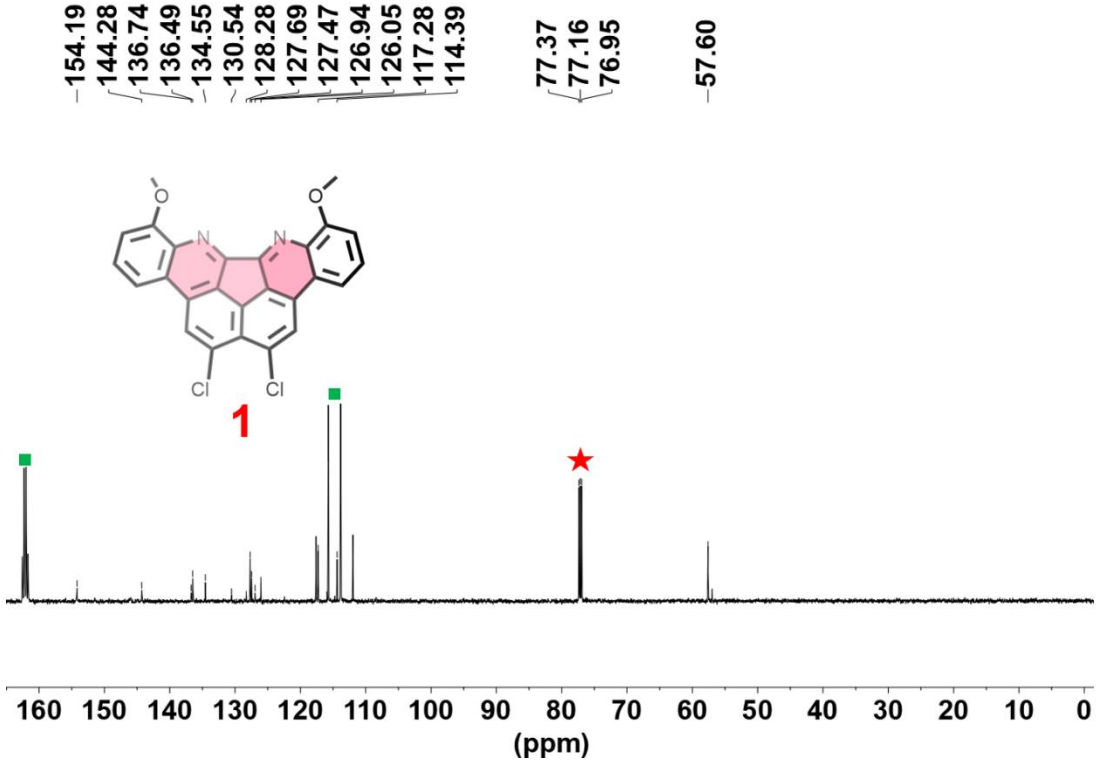

Figure S10. ^{13}C NMR spectrum of **1** in $CDCl_3$/TFA-*d* (2:1, *v/v*) at 298 K (100 MHz) (red "★" represents residual $CHCl_3$, green "■" represents TFA).

Mass Spectra

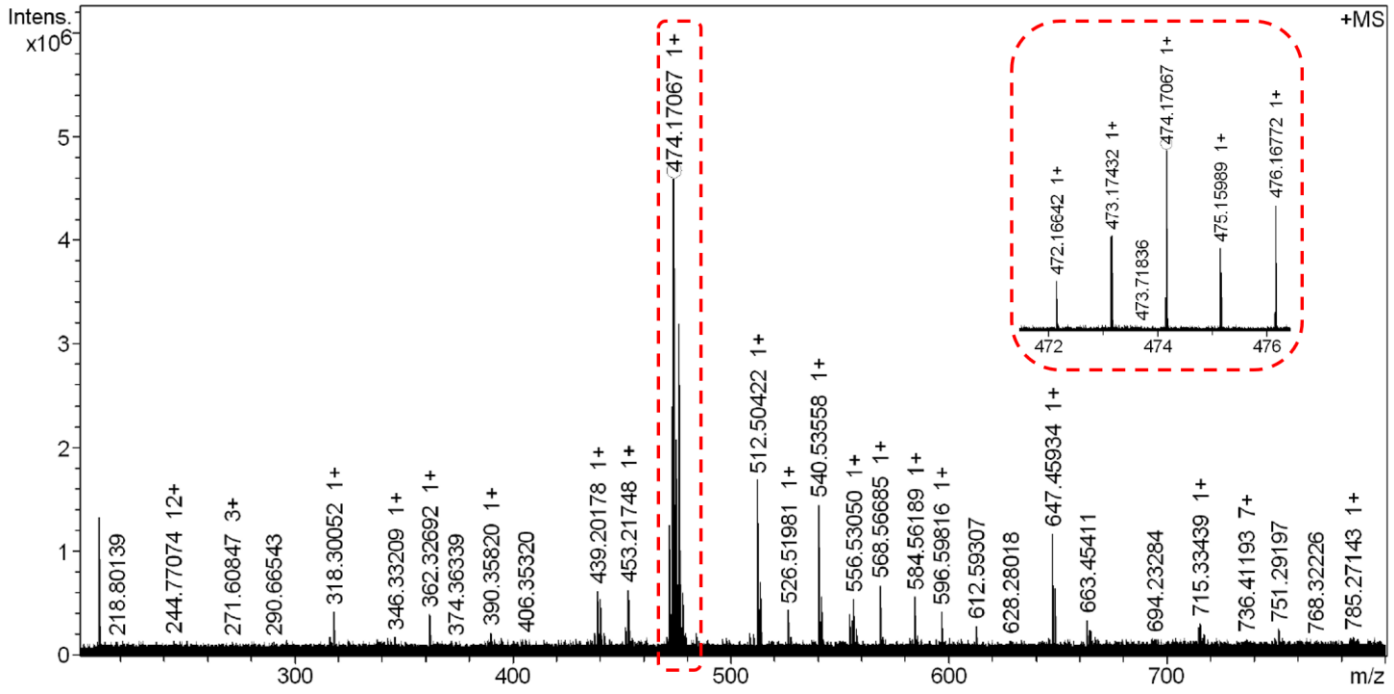

Figure S11. Positive MALDI-TOF HRMS spectrum of **4.** MALDI-TOF HRMS (*m/z*): $[M]^{+\bullet}$ calcd. for $C_{24}H_{30}B_2Cl_2O_4$, 474.1707; found: 474.1707.

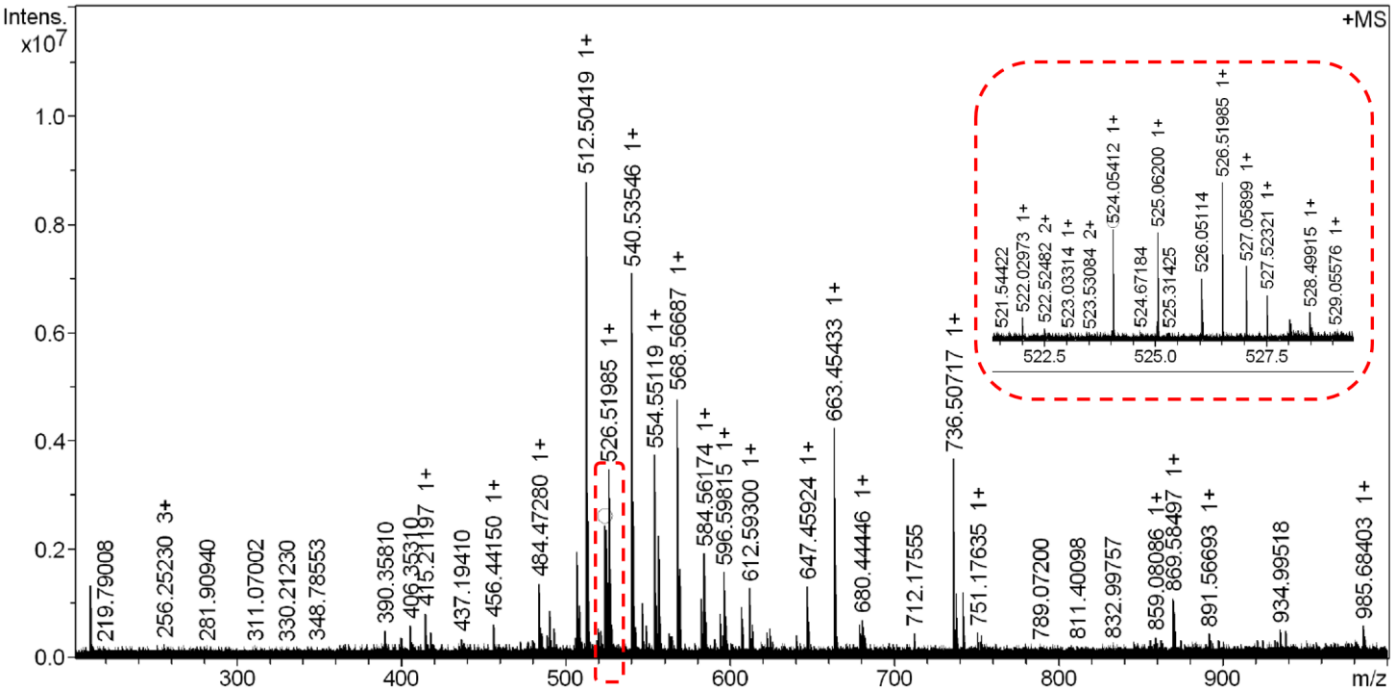

Figure S12. Positive MALDI-TOF HRMS spectrum of **6.** MALDI-TOF HRMS (*m/z*): $[M]^{+\bullet}$ calcd. for $C_{26}H_{18}Cl_2N_2O_6$, 524.0542; found: 524.0541.

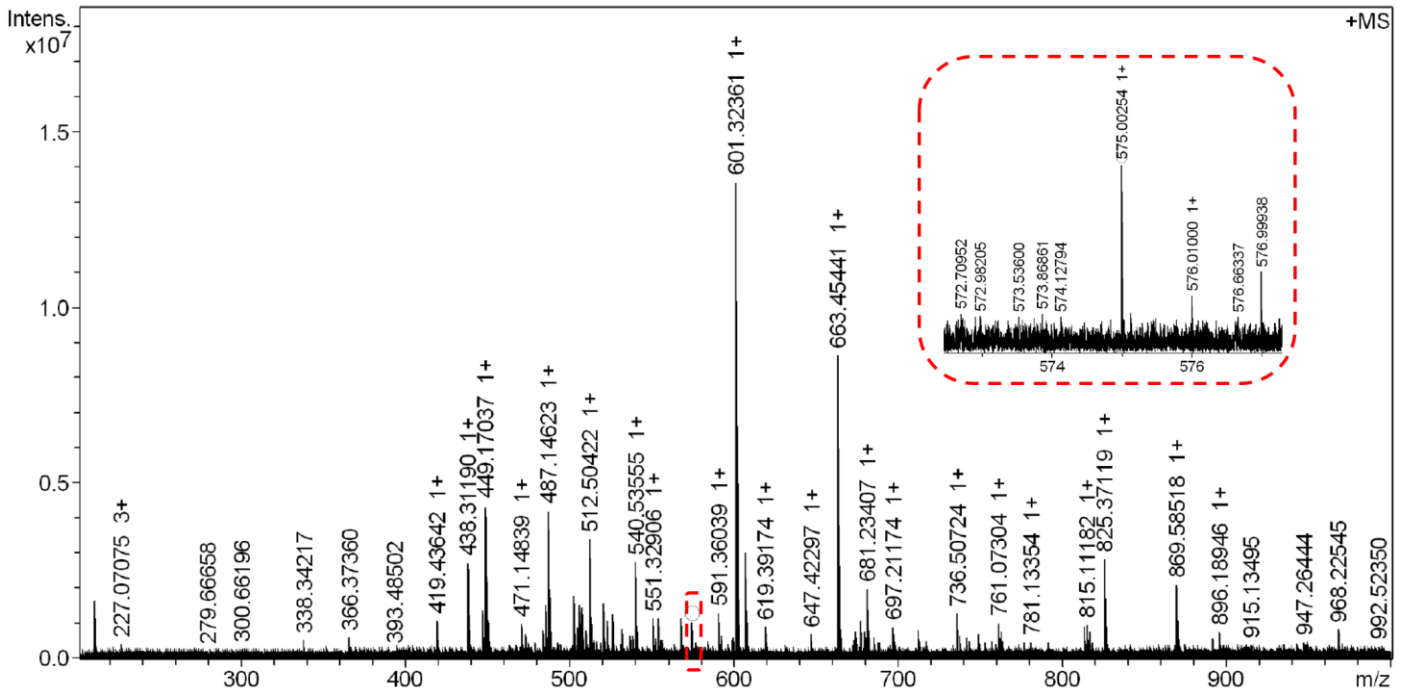

Figure S13. Positive MALDI-TOF HRMS spectrum of **7.** MALDI-TOF HRMS (m/z): $[M + Na]^+$ calcd. for $C_{26}H_{14}Cl_2N_2NaO_8$, 575.0025; found: 575.0025.

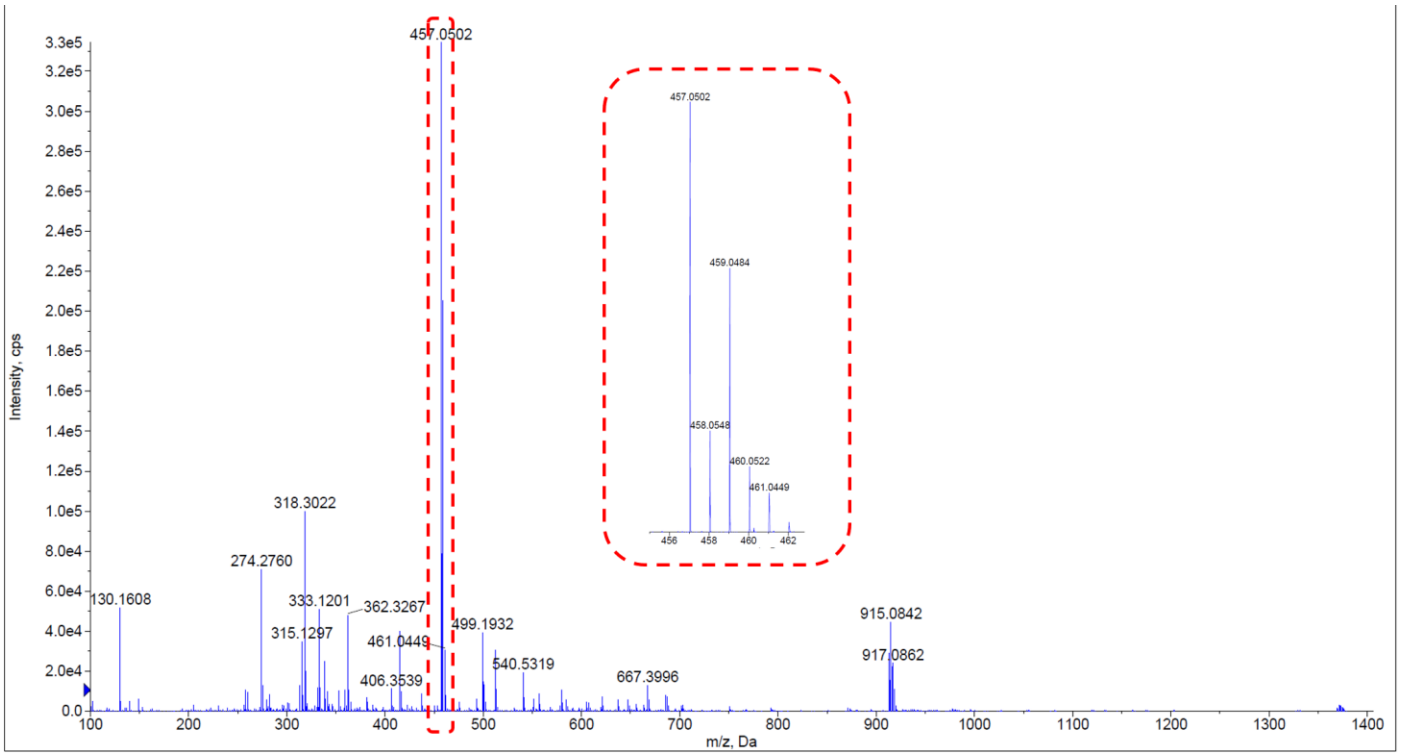

Figure S14. Positive ESI HRMS spectrum of **1.** HRMS-ESI (m/z): $[M + H]^+$ calcd. for $C_{26}H_{14}Cl_2N_2O_2$: 457.0511; found: 457.0502.

Single crystal of **1**•C_2H_5OH was grown via slow evaporation of the solution containing **1** (5 mg) in 6 mL CH_2Cl_2/C_2H_5OH (2:1, *v/v*).

Table S1. Crystal data and structure refinement for [**1**·C_2H_5OH]**.**

Identification code	2305337
Empirical formula	$C_{28}H_{20}Cl_2N_2O_3$
Formula weight	503.36
Temperature/K	169.98(11)
Crystal system	monoclinic
Space group	I2
a/Å	23.523(2)
b/Å	3.9699(5)
c/Å	25.723(3)
α/°	90
β/°	113.829(12)
γ/°	90
Volume/Å^3	2197.3(5)
Z	4
ρ_{calc}g/cm^3	1.522
μ/mm^{-1}	2.962
F(000)	1040.0
Crystal size/mm^3	0.16 × 0.05 × 0.02
Radiation	CuK_α (λ = 1.54184)
2θ range for data collection/°	4.302 to 124.986
Index ranges	$-27 \le h \le 26$, $-4 \le k \le 4$, $-29 \le l \le 28$
Reflections collected	8035
Independent reflections	3057 [R_{int} = 0.0856, R_{sigma} = 0.0774]
Data/restraints/parameters	3057/43/319
Goodness-of-fit on F^2	1.002
Final R indexes [I>=2σ (I)]	R_1 = 0.1025, wR_2 = 0.2495
Final R indexes [all data]	R_1 = 0.1227, wR_2 = 0.2706
Largest diff. peak/hole / e Å^{-3}	1.25/-0.40
Flack parameter	0.07(5)

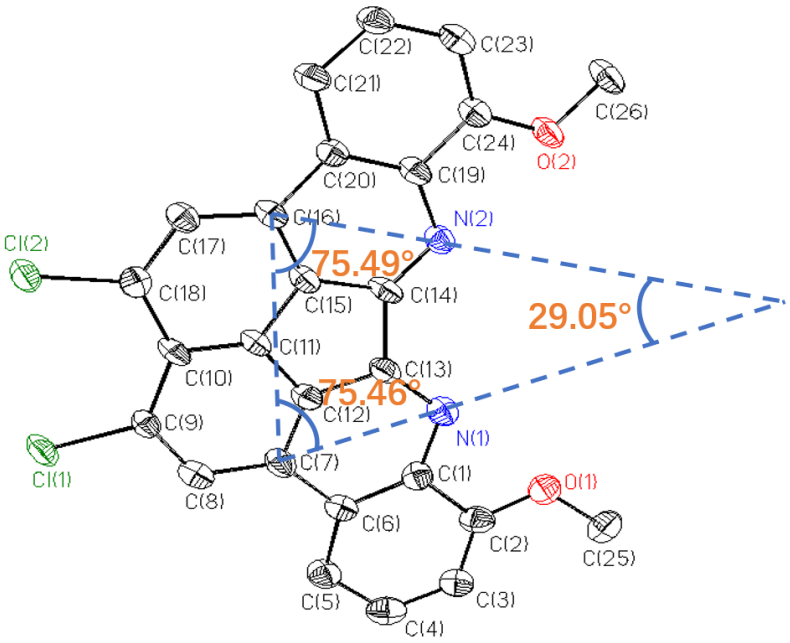

Figure S15. 1 in the single crystal of [**1**·C_2H_5OH] was shown in ellipsoid form. Displacement ellipsoids are scaled to the 50% probability level. Selected interatomic distance (Å): N(1)…N(2) 3.34(1). Selected interatomic angle: ∠N(2) …C(16) …C(7) 75.46(1)°. ∠N(1) …C(7) …C(16) 75.49(1)°.

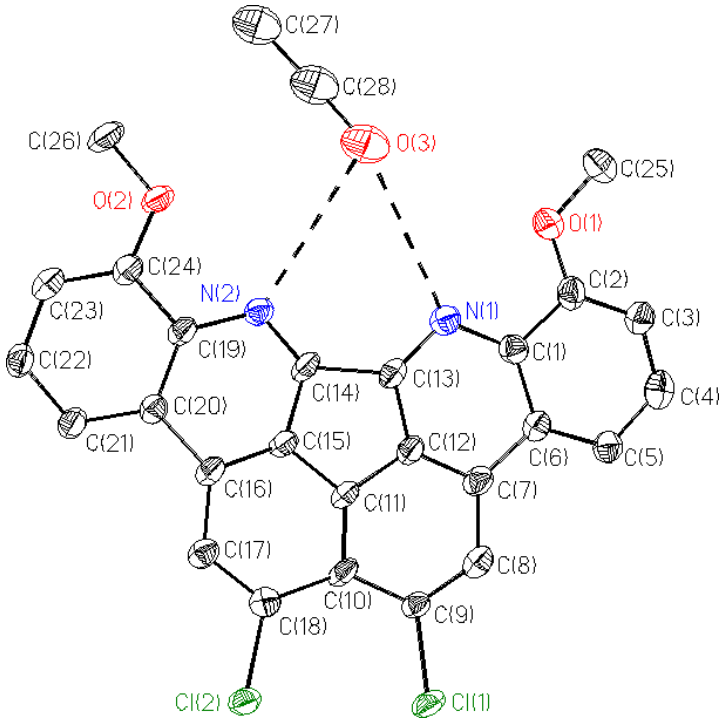

Figure S16. The interaction between ethanol and neighboring **1** in the single crystal structure of [**1**·C_2H_5OH] was shown in ellipsoid form showing. Displacement ellipsoids are scaled to the 50% probability level. Selected interatomic lengths (Å): N(1)…O(3) 3.42(7); N(2)…O(3) 3.46(7).

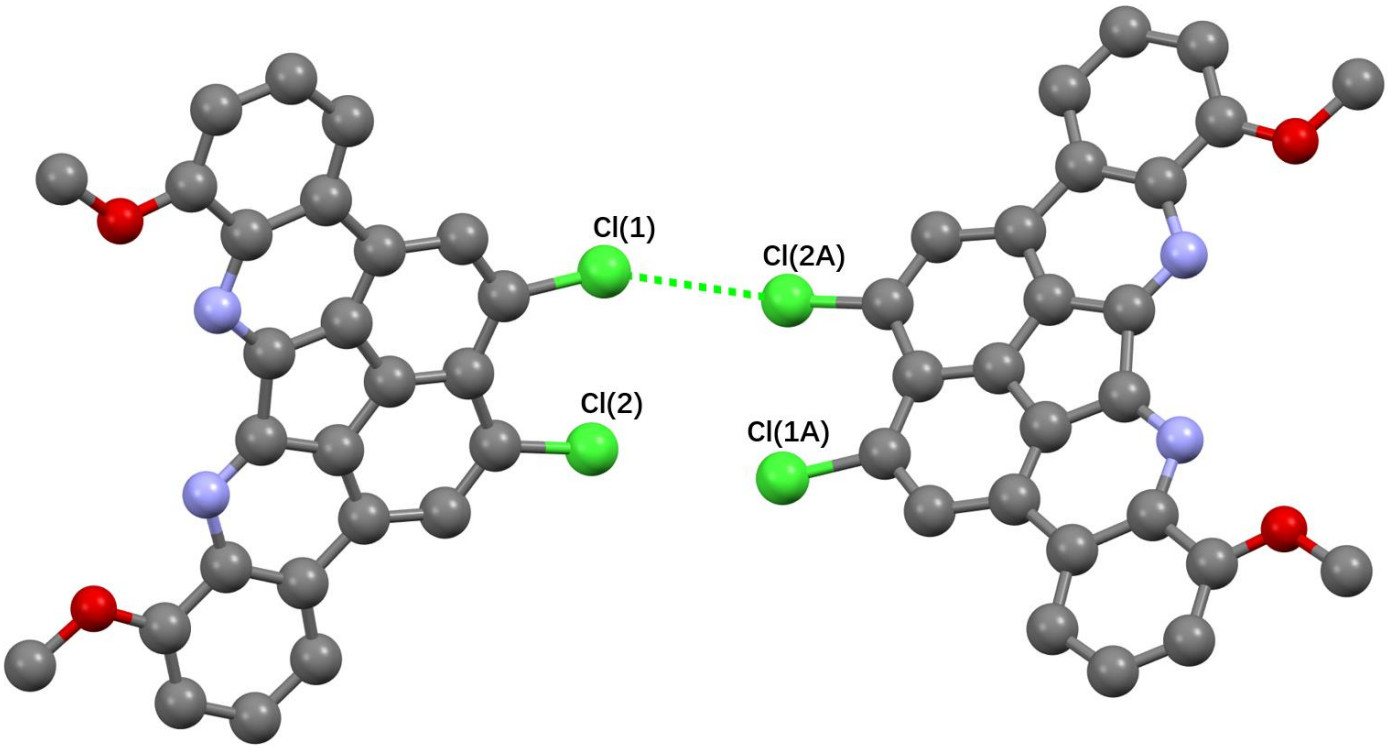

Figure S17. The Cl-Cl halogen bonding between neighboring **1** shown in the single crystal of [**1**·C_2H_5OH] Selected interatomic distance (Å): Cl(1)…Cl(2A) 3.42(2).

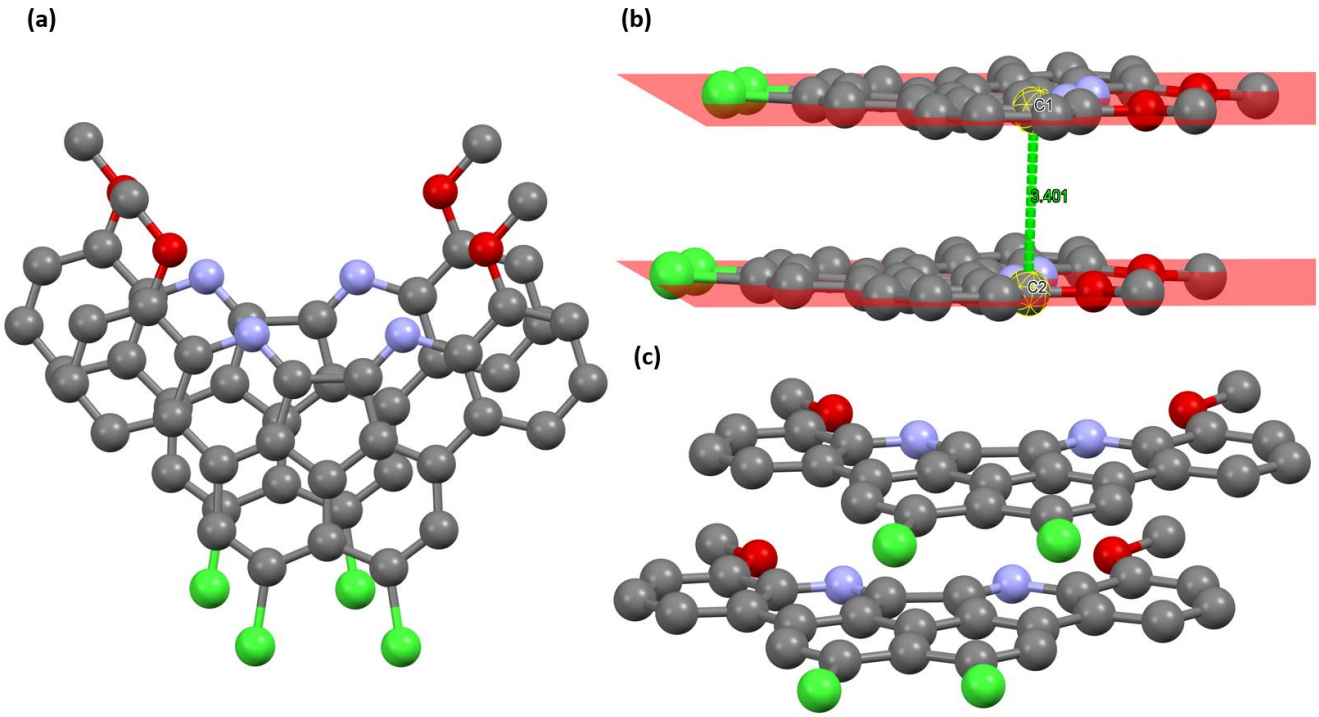

Figure S18. Top (a), side (b) and front (c) views of dimeric structure containing two neighbor **1** shown in the single crystal X-ray diffraction structure of [**1**·C_2H_5OH]. The π-π donor acceptor interaction was suggested with selected interatomic distance (Å): C(1)…C(2A) 3.40(1).

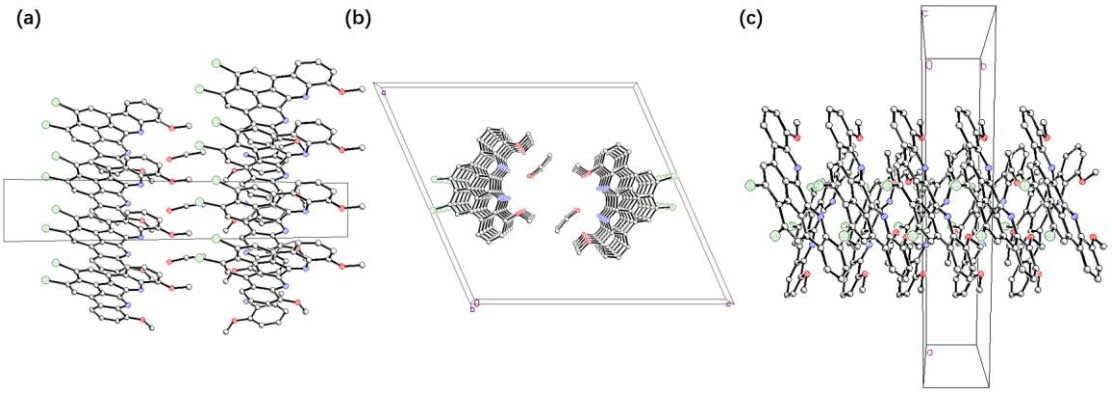

Figure S19. Packing diagram of the single crystal [**1**·C_2H_5OH] along with *a* (a), *b* (b), or *c* (c) cell axis.

Section S3: *Metal cation coordination study of* ***1*** *and* ***TB(phen)*** *in CH_2Cl_2/CH_3OH (4:1, v/v)*

Uv-vis spectroscopic studies

(1) General procedure for the Uv-vis spectral studies

All Uv-vis spectra in this study were performed using a Shimadzu UV-2450 spectrophotometer at 298 K. In all titration experiments, 2000 μL of **1** or **TB(phen)** solution (2.00×10^{-5} M in CH_2Cl_2/CH_3OH (4:1, *v/v*)) was added to the quartz cell. Each tested metal cation solution with a much higher concentration (1.00×10^{-2} M or 1.00×10^{-3} M in CH_2Cl_2/ CH_3OH (4:1, *v/v*)) was dropwise added. Data was collected after each aliquot was added and mixed. The concentration of **1** or **TB(phen)** was subject to slight dilution; this was accounted for mathematically the Hyperquad Programme 2003.

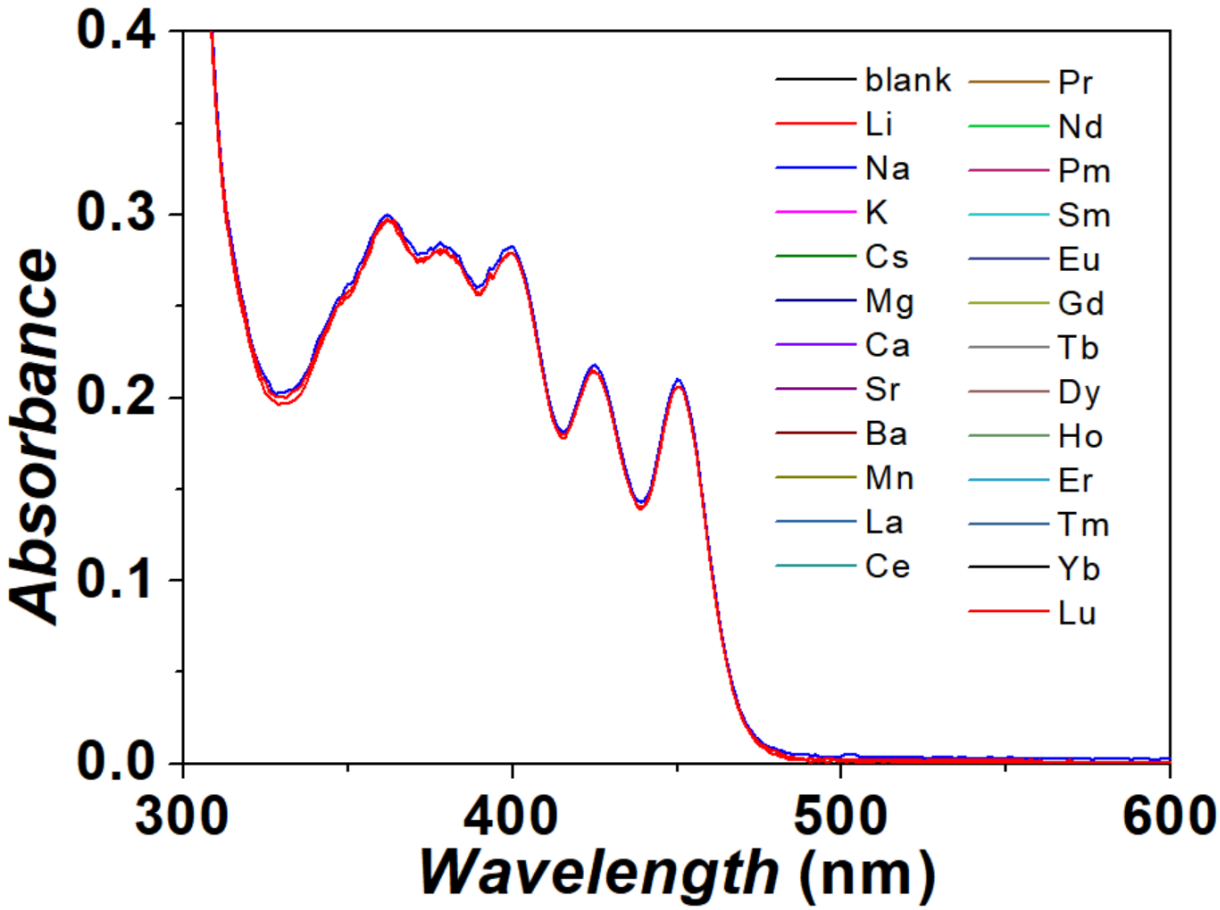

Figure S20. Uv-vis spectra of **1** (2.00×10^{-5} M in CH_2Cl_2/CH_3OH (4:1, *v/v*)) in the absence and presence of 100 molar equiv. of each tested metal cations, including alkali (*i.e.*, Li^+, Na^+, K^+ or Cs^+), alkaline earth (*i.e.*, Mg^{2+}, Ca^{2+}, Sr^{2+} or Ba^{2+}), Mn^{2+} or lanthanide (*i.e.*, La^{3+}, Ce^{3+}, Pr^{3+}, Nd^{3+}, Sm^{3+}, Eu^{3+}, Gd^{3+}, Tb^{3+}, Dy^{3+}, Ho^{3+}, Er^{3+}, Tm^{3+}, Yb^{3+} or Lu^{3+}) cation.

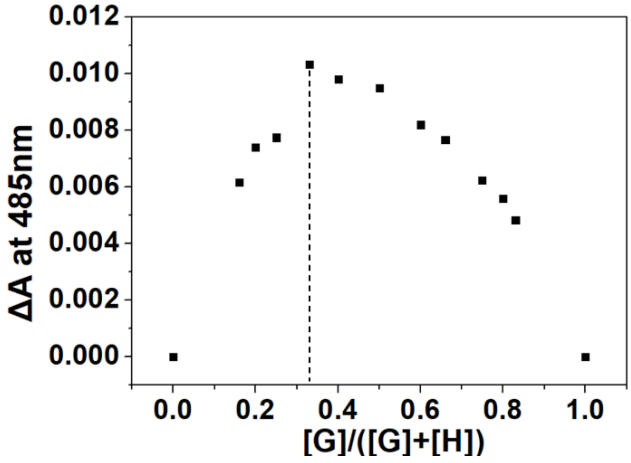

Figure S21. Job plot corresponding to the interactions between **1** and Co^{2+} in CH_2Cl_2/CH_3OH (4:1, *v/v*) at 298 K as monitored via Uv-vis spectroscopy. [Ligand] + [Metal] = 0.10 mM. Maximum value was seen at 0.33 in the case of Co^{2+}, this supports the 2:1 (ligand/metal) stoichiometry as suggested in the main text.

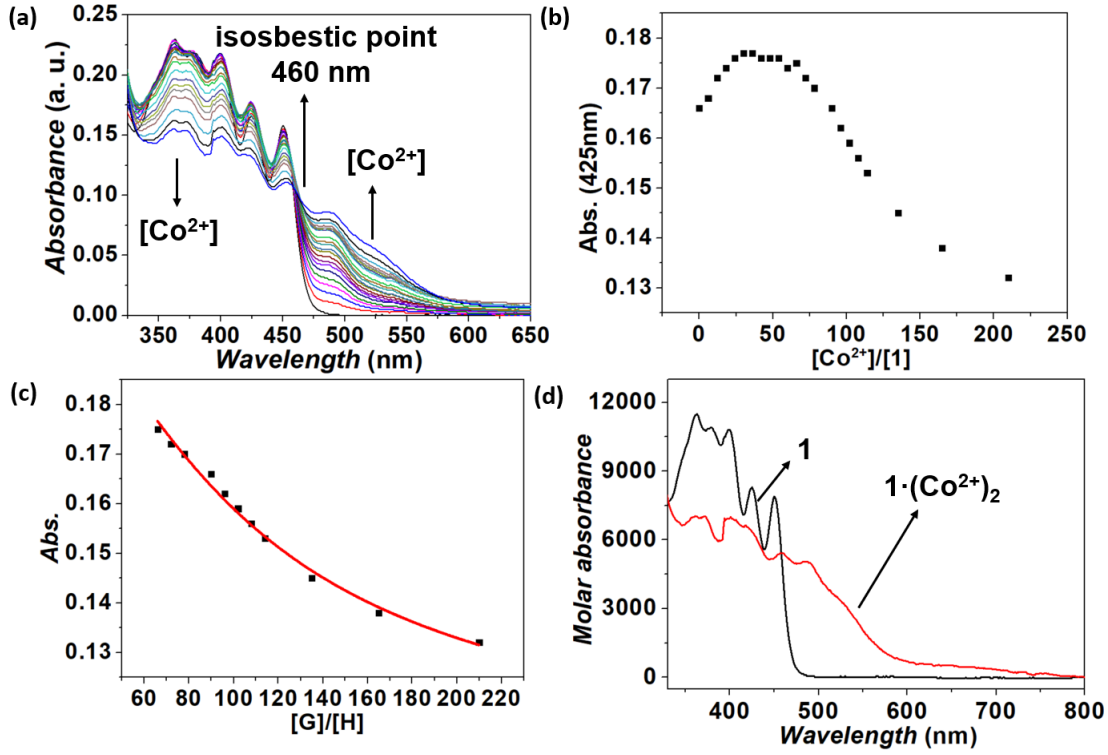

Figure S22. (a) Uv-vis spectra corresponding to **1** (2.00×10^{-5} M in CH_2Cl_2/CH_3OH (4:1, *v/v*)) with increasing [Co^{2+}] (from 0 to 210.0 molar equiv.) at 298 K. (b) The absorbance changes at 425 nm ("■"). And (c) the results of the corresponding nonlinear curve fitting according calculated model (red line) using Hyperquad 2003. (d) The calculated molar absorbance of **1** and **1**·(Co^{2+})$_2$ in CH_2Cl_2/CH_3OH (4:1, *v/v*). It is noted that the data with [Co^{2+}]/[**1**] less than 66 were ignored in K_a calculation due to the complexity (including possible solvent competition and/or 1:1 complexation, *etc.*), which was weaken and could be ignored with [Co^{2+}]/[**1**] larger than 66. The equilibriums and related K_a calculation results as shown: $2M + L \overset{K_2}{\rightleftarrows} M_2{\cdot}L$; log K_2 = 5.5(3).

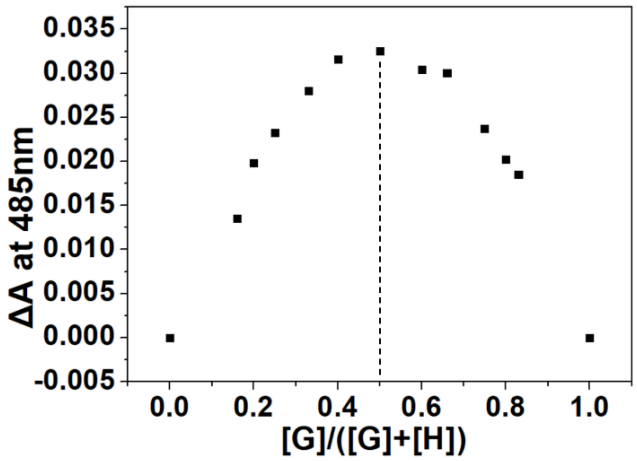

Figure S23. Job plot corresponding to the interactions between **1** and Ni^{2+} in CH_2Cl_2/CH_3OH (4:1, *v/v*) at 298 K as monitored via Uv-vis spectroscopy. [Ligand] + [Metal] = 0.10 mM. Maximum value was seen at 0.50, this supports 1:1 (ligand/metal) stoichiometry as suggested in the main text.

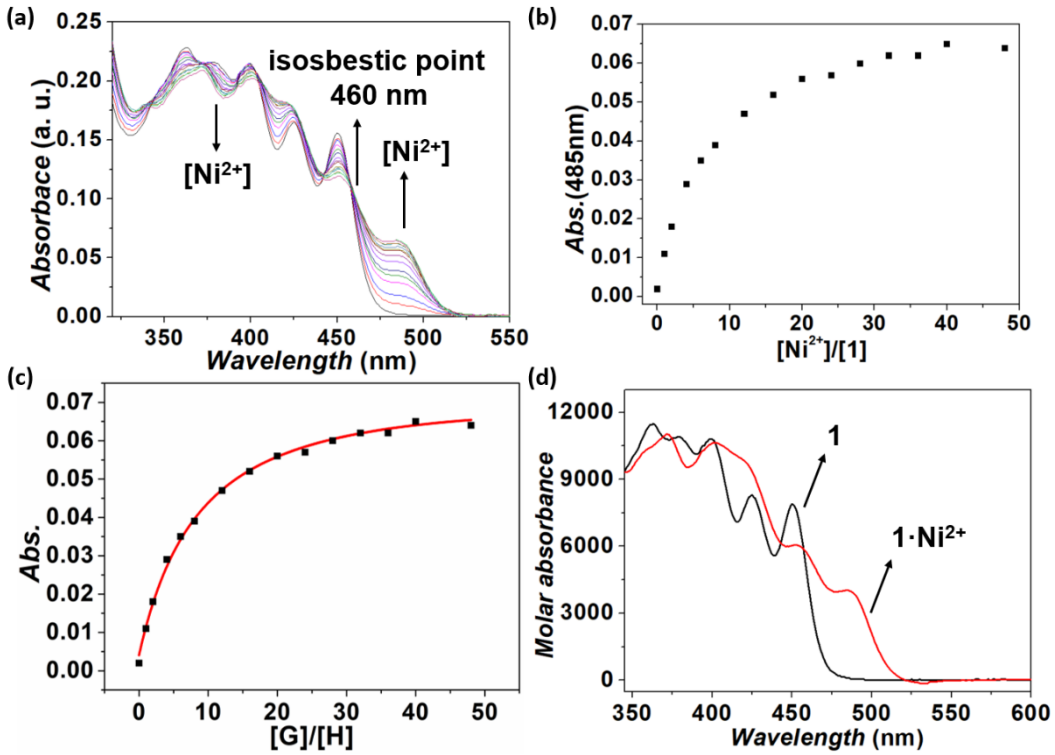

Figure S24. (a) Uv-vis spectra recorded corresponding to **1** (2.00×10^{-5} M in CH_2Cl_2/CH_3OH (4:1, *v/v*)) with increasing [Ni^{2+}] (from 0 to 48.0 molar equiv.) at 298 K. (b) The absorbance changes at 485 nm ("■"). And (c) the results of the corresponding nonlinear curve fitting according calculated model (red line) using Hyperquad 2003. (d) The calculated molar absorbance of **1** and **1**·Ni^{2+} in CH_2Cl_2/CH_3OH (4:1, *v/v*). The equilibriums and related K_a calculation results as shown: $M + L \overset{K_1}{\rightleftarrows} M{\cdot}L$, $\log K_1 = 3.7(2)$.

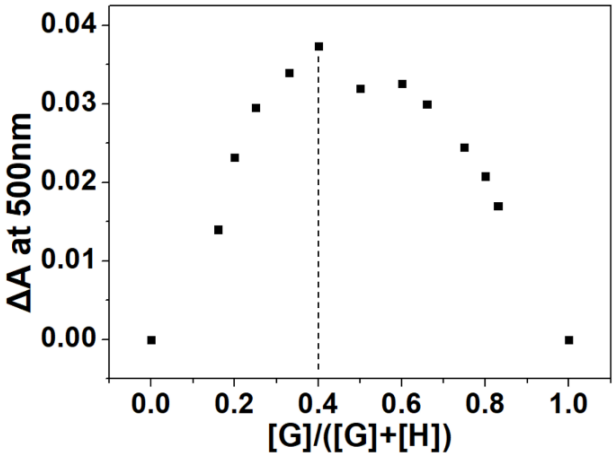

Figure S25. Job plot corresponding to the interactions between **1** and Cu^{2+} in CH_2Cl_2/CH_3OH (4:1, *v/v*) at 298 K as monitored via Uv-vis spectroscopy. [Ligand] + [Metal] = 0.10 mM. Maximum value was seen at 0.4, this supports 2:1 and 1:1 (ligand/metal) stoichiometry as suggested in the main text.

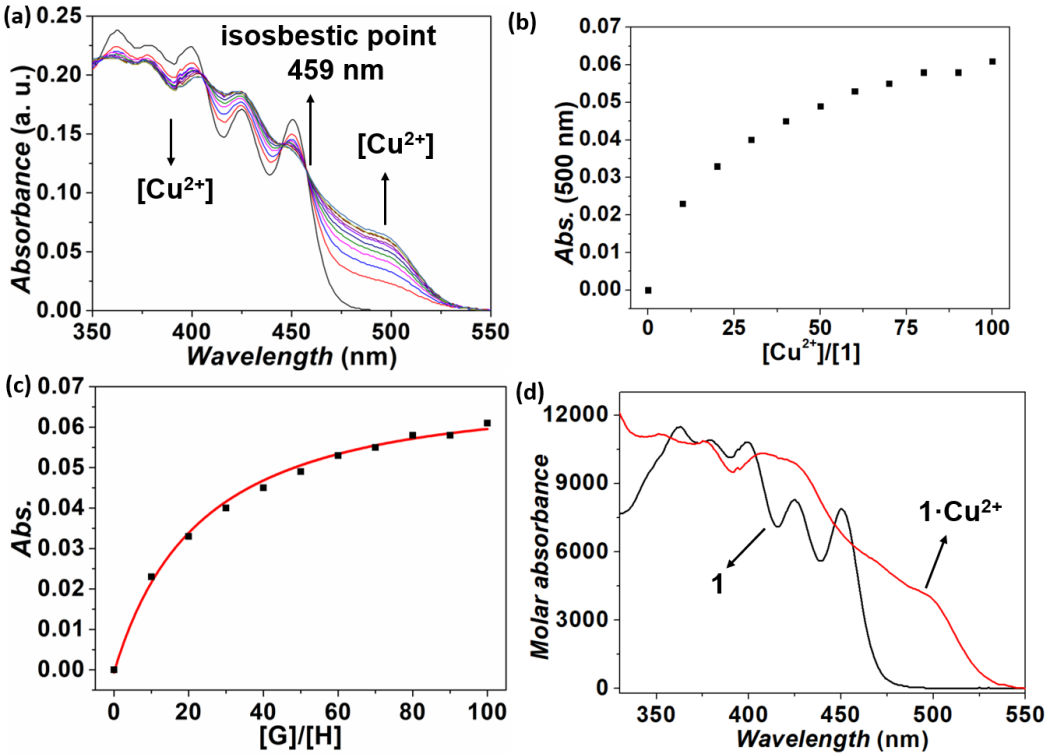

Figure S26. (a) Uv-vis spectra recorded corresponding to **1** (2.00×10^{-5} M in CH_2Cl_2/CH_3OH (4:1, *v/v*)) with increasing [Cu^{2+}] (from 0 to 100.0 molar equiv.) at 298 K. (b) The absorbance changes at 500 nm ("■"). And (c) the results of the corresponding nonlinear curve fitting according calculated model (red line) using Hyperquad 2003. (d) The calculated molar absorbance of **1** and **1**·Cu^{2+} in CH_2Cl_2/CH_3OH (4:1, *v/v*). The equilibriums and related K_a calculation results as shown: $M + L \overset{K_1}{\rightleftarrows} M{\cdot}L$; $\log K_1 = 3.3(2)$.

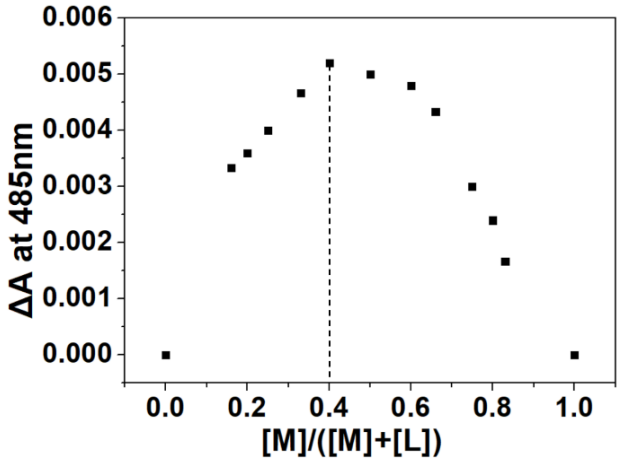

Figure S27. Job plot corresponding to the interactions between **1** and Zn^{2+} in CH_2Cl_2/CH_3OH (4:1, *v/v*) at 298 K as monitored via Uv-vis spectroscopy. [Ligand] + [Metal] = 0.10 mM. Maximum value was seen at 0.4, this supports mixing 2:1 and 1:1 (ligand/metal) stoichiometry as suggested in the main text.

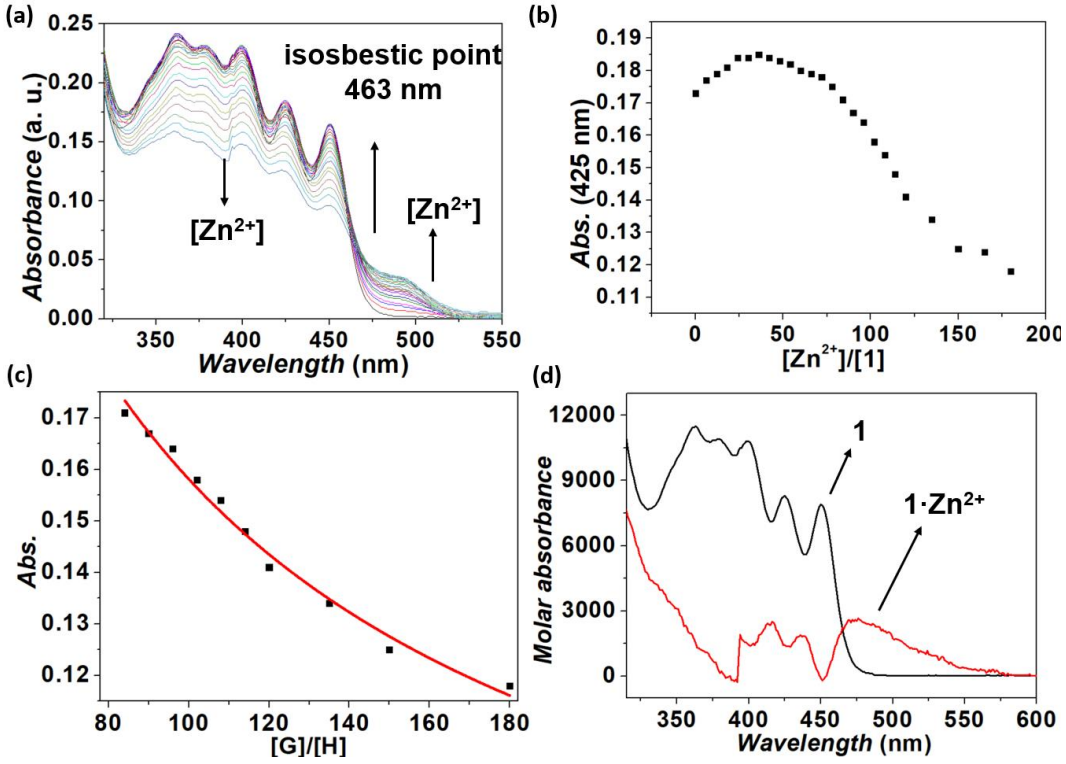

Figure S28. (a) Uv-vis spectra recorded corresponding to **1** (2.00×10^{-5} M in CH_2Cl_2/CH_3OH (4:1, *v/v*)) with increasing [Zn^{2+}] (from 0 to 180.0 molar equiv.) at 298 K. (b) The absorbance changes at 425 nm ("■"). And (c) the results of the corresponding nonlinear curve fitting according calculated model (red line) using Hyperquad 2003. (d) The calculated molar absorbance of **1** and **1**·Zn^{2+} in CH_2Cl_2/CH_3OH (4:1, *v/v*). It is noted that the data with [Zn^{2+}]/[**1**] less than 84 were ignored in K_a calculation due to the complexity (including possible solvent competition and/or 2:1 complexation, etc.), which was weaken and could be ignored with [Zn^{2+}]/[L] larger than 84. The equilibriums and related K_a calculation results as shown: $M + L \overset{K_1}{\rightleftarrows} M{\cdot}L$; log K_1 =3.2(2).

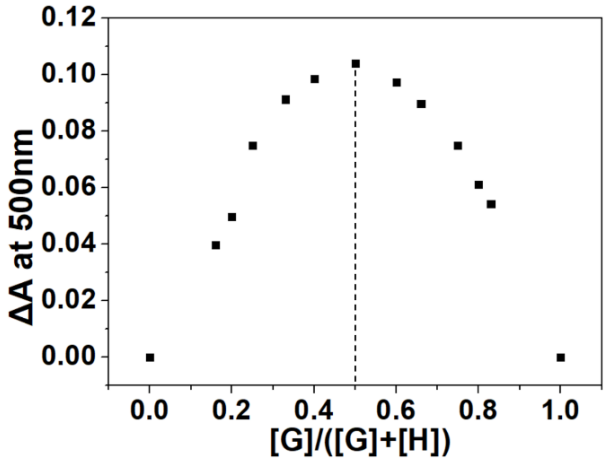

Figure S29. Job plot corresponding to the interactions between **1** and Zr^{4+} in CH_2Cl_2/CH_3OH (4:1, *v/v*) at 298 K as monitored via Uv-vis spectroscopy. [Ligand] + [Metal] = 0.10 mM. Maximum value was seen at 0.5, this supports 1:1 (ligand/metal) stoichiometry as suggested in the main text.

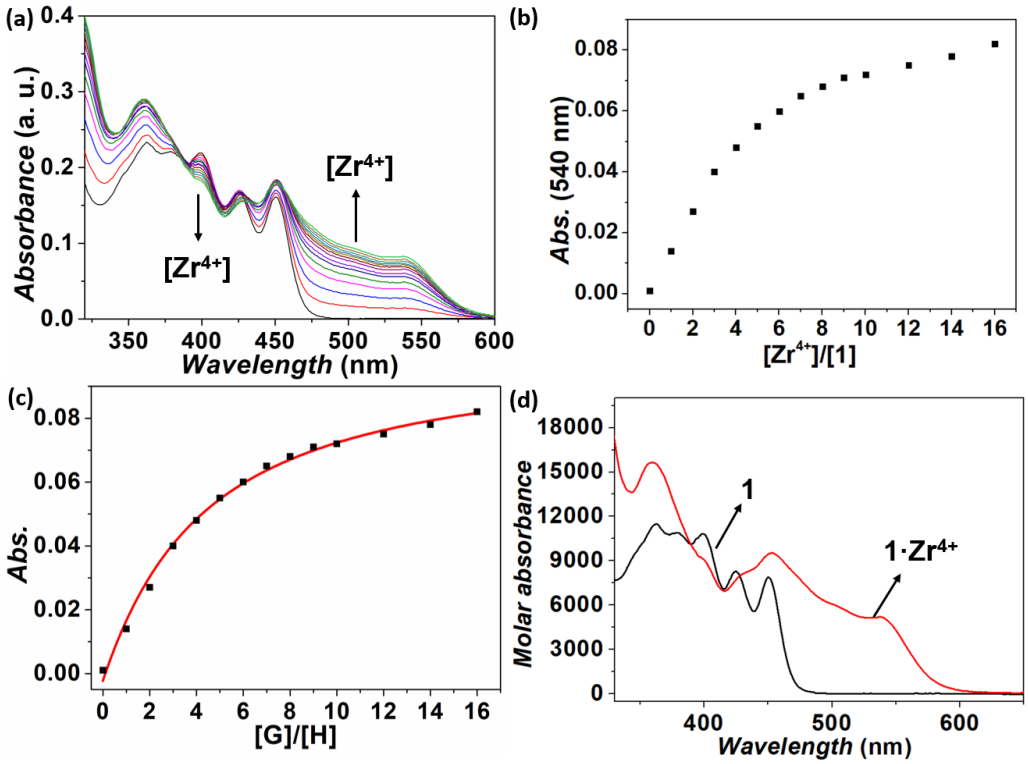

Figure S30. (a) Uv-vis spectra recorded corresponding to **1** (2.00×10^{-5} M in CH_2Cl_2/CH_3OH (4:1, *v/v*)) with increasing [Zr^{4+}] (from 0 to 16.0 molar equiv.) at 298 K. (b) The absorbance changes at 540 nm ("■"). And (c) the results of the corresponding nonlinear curve fitting according calculated model (red line) using Hyperquad 2003. (d) The calculated molar absorbance of **1** and **1**·Zr^{4+} in CH_2Cl_2/CH_3OH (4:1, *v/v*). The equilibriums and related K_a calculation results as shown: $M + L \overset{K_1}{\rightleftarrows} M{\cdot}L$; $\log K_1 = 4.1(2)$.

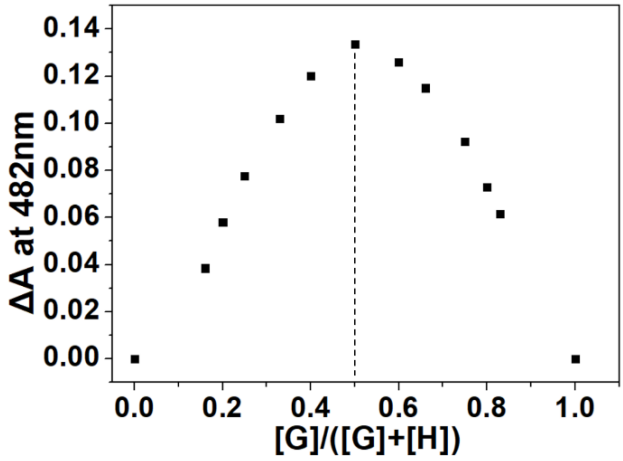

Figure S31. Job plot corresponding to the interactions between **1** and Ag^+ in CH_2Cl_2/CH_3OH (4:1, *v/v*) at 298 K as monitored via Uv-vis spectroscopy. [Ligand] + [Metal] = 0.10 mM. Maximum value was seen at 0.5, this supports 1:1 (ligand/metal) stoichiometry as suggested in the main text.

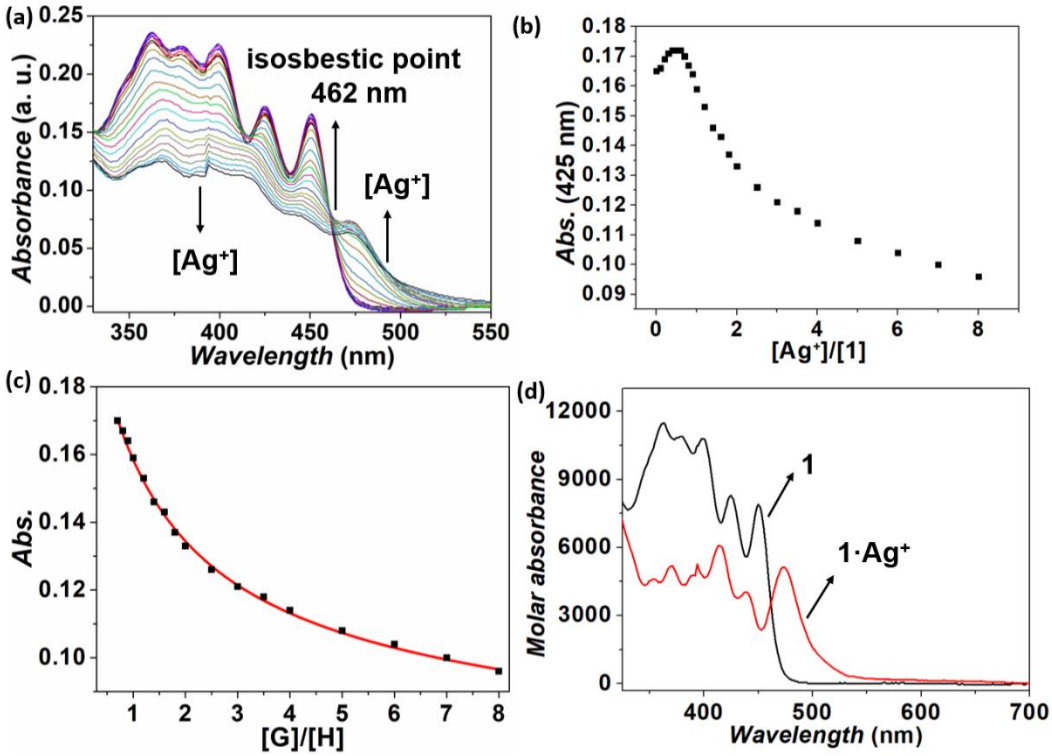

Figure S32. (a) Uv-vis spectra recorded corresponding to **1** (2.00×10^{-5} M in CH_2Cl_2/CH_3OH (4:1, *v/v*)) with increasing [Ag^+] (from 0 to 8.0 molar equiv.) at 298 K. (b) The absorbance changes at 425 nm ("■"). And (c) the results of the corresponding nonlinear curve fitting according calculated model (red line) using Hyperquad 2003. (d) The calculated molar absorbance of **1** and **1**•Ag^+ in CH_2Cl_2/CH_3OH (4:1, *v/v*). The equilibriums and related K_a calculation results as shown: $M + L \overset{K_1}{\rightleftarrows} M{\cdot}L$; $\log K_1 = 3.6(2)$.

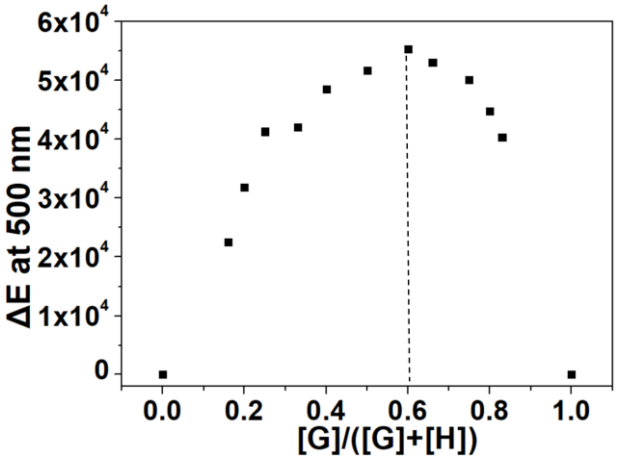

Figure S33. Job plot corresponding to the interactions between **1** and Cd^{2+} in CH_2Cl_2/CH_3OH (4:1, *v/v*) at 298 K as monitored via Uv-vis spectroscopy. [Ligand] + [Metal] = 0.10 mM. Maximum value was seen at 0.6, this supports 2:1 (ligand/metal) stoichiometry as suggested in the main text.

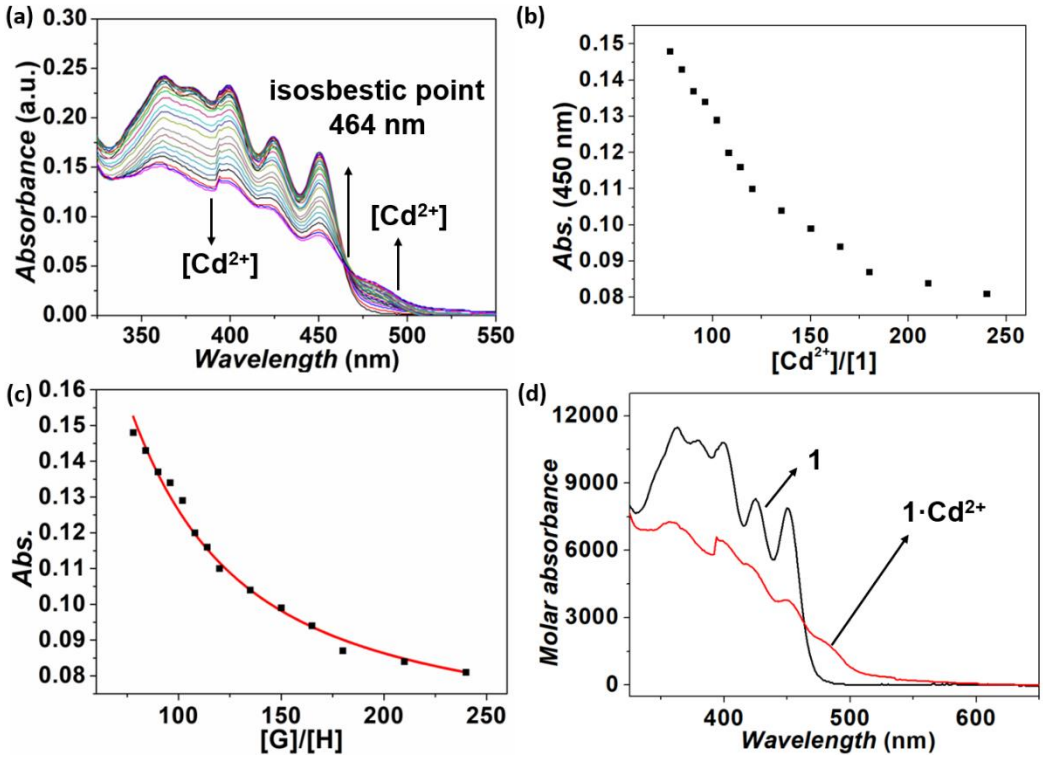

Figure S34. (a) Uv-vis spectra recorded corresponding to **1** (2.00×10^{-5} M) in CH_2Cl_2/CH_3OH (4:1, *v/v*)) as a function of increasing [Cd^{2+}] (from 0 to 240.0 molar equiv.) at 298 K. (b) The absorbance changes at 450 nm ("■"). (c) The results of the corresponding nonlinear curve fitting according calculated model (red line) using Hyperquad 2003. (d) The calculated molar absorbance of **1** and **1**·Cd^{2+} in CH_2Cl_2/CH_3OH (4:1, *v/v*). It is noted that the data with [Cd^{2+}]/[**1**] less than 84 were ignored in K_a calculation due to the complexity (including possible solvent competition and/or 2:1 complexation, etc.), which was weaken. The equilibriums and related K_a calculation results as shown: $2M + L \overset{K_2}{\rightleftarrows} M_2L$; $\log K_2 = 6.1(3)$.

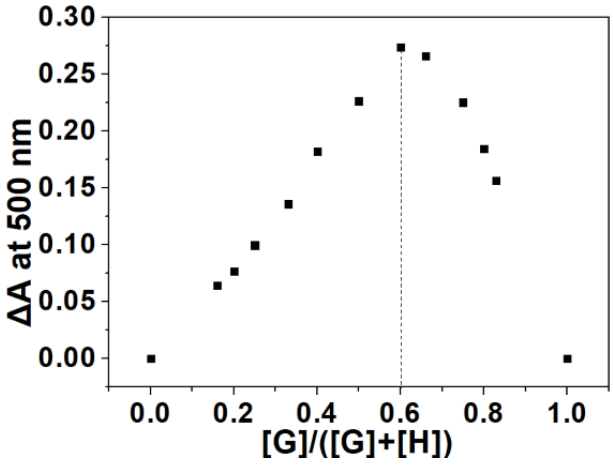

Figure S35. Job plot corresponding to the interactions between **TB(phen)** and Co^{2+} in CH_2Cl_2/CH_3OH (4:1, *v/v*) at 298 K as monitored via Uv-vis spectroscopy. [Ligand] + [Metal] = 0.40 mM. Maximum value was seen at 0.6 in the case of Co^{2+}, this supports mixing 1:1 and 1:2 (ligand/metal) stoichiometry as suggested in the main text.

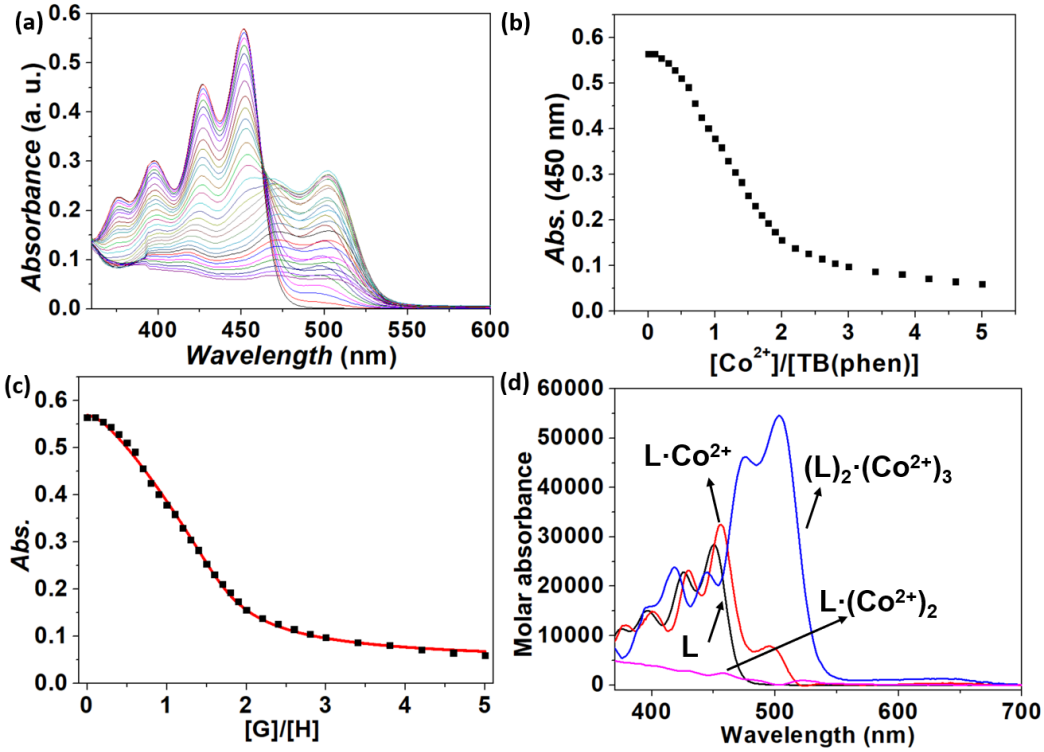

Figure S36. (a) Uv-vis spectra recorded corresponding to **TB(phen)** (**L**: 2.00×10^{-5} M in CH_2Cl_2/CH_3OH (4:1, *v/v*)) with increasing [Co^{2+}] (from 0 to 5.0 molar equiv.) at 298 K. (b) The absorbance changes at 450 nm ("■"). And (c) the results of the corresponding nonlinear curve fitting according calculated model (red line) using Hyperquad 2003. (d) The calculated molar absorbance of **TB(phen)** and its complexes. The equilibriums and related K_a calculation results as shown: $2M + L \overset{K_2}{\rightleftarrows} M_2L$; $\log K_2 = 12.3(3)$; $3M + 2L \overset{K_3}{\rightleftarrows} M_3L_2$; $\log K_3 = 23.9(2)$; $M + L \overset{K_1}{\rightleftarrows} ML$; $\log K_1 = 6.3(6)$.

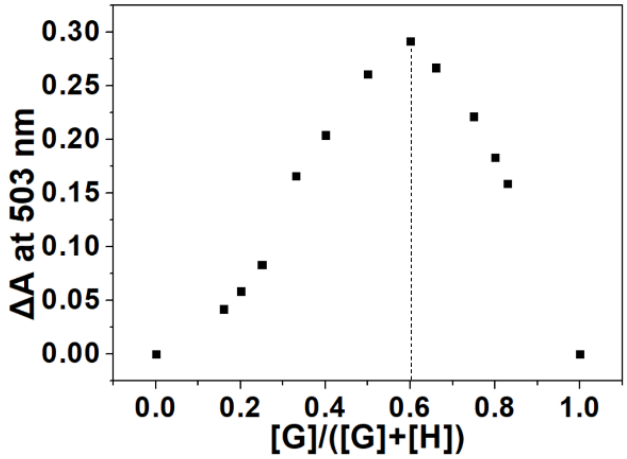

Figure S37. Job plot corresponding to the interactions between **TB(phen)** and Ni^{2+} in CH_2Cl_2/CH_3OH (4:1, *v/v*) at 298 K as monitored via Uv-vis spectroscopy. [Ligand] + [Metal] = 0.40 mM. Maximum value was seen at 0.6 in the case of Ni^{2+}, this supports mixing 1:1 and 1:2 (ligand/metal) stoichiometry as suggested in the main text.

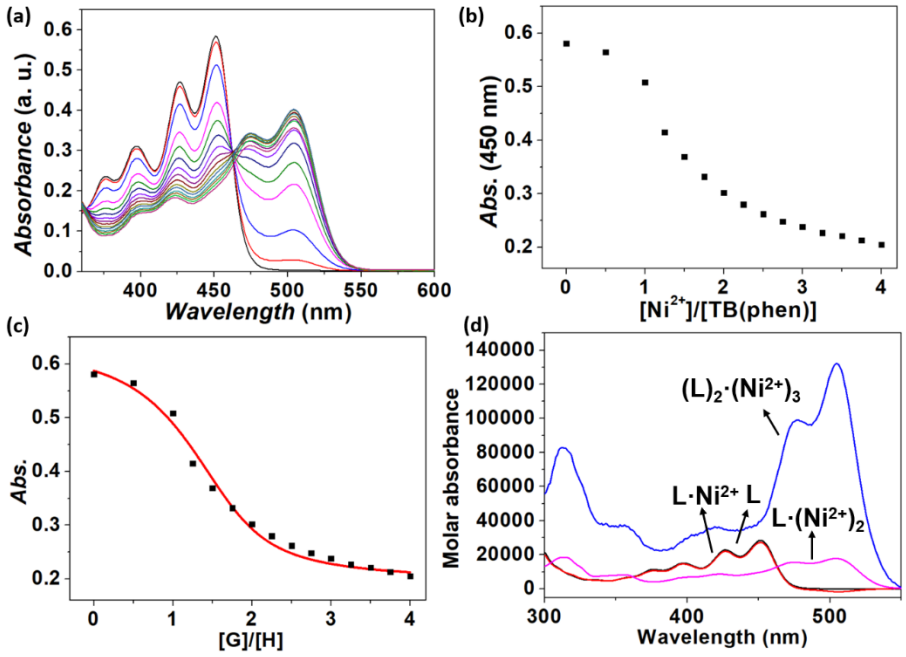

Figure S38. (a) Uv-vis spectra recorded corresponding to **TB(phen)** (**L**: 2.00×10^{-5} M in CH_2Cl_2/CH_3OH (4:1, *v/v*)) with increasing [Ni^{2+}] (from 0 to 6.0 molar equiv.) at 298 K. (b) The absorbance changes at 450 nm ("■"). And (c) the results of the corresponding nonlinear curve fitting according calculated model (red line) using Hyperquad 2003. (d) The calculated molar absorbance of **TB(phen)** and its complexes. The equilibriums and related K_a calculation results as shown: $2M + L \overset{K_2}{\rightleftarrows} M_2L$; $\log K_2 = 12.5(3)$; $3M + 2L \overset{K_3}{\rightleftarrows} M_3L_2$; $\log K_3 = 23.5(2)$; $M + L \overset{K_1}{\rightleftarrows} ML$; $\log K_1 = 6.8(3)$.

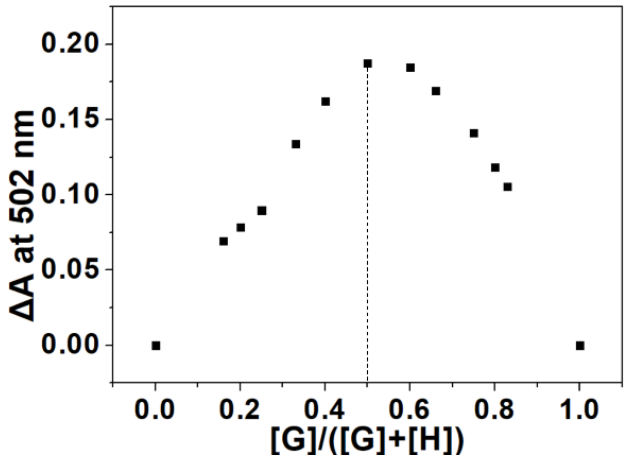

Figure S39. Job plot corresponding to the interactions between **TB(phen)** and Cd^{2+} in CH_2Cl_2/CH_3OH (4:1, *v/v*) at 298 K as monitored via Uv-vis spectroscopy. [Ligand] + [Metal] = 0.40 mM. Maximum value was seen at 0.5 in the case of Cd^{2+}, this supports the 1:1 (ligand/metal) stoichiometry as suggested in the main text.

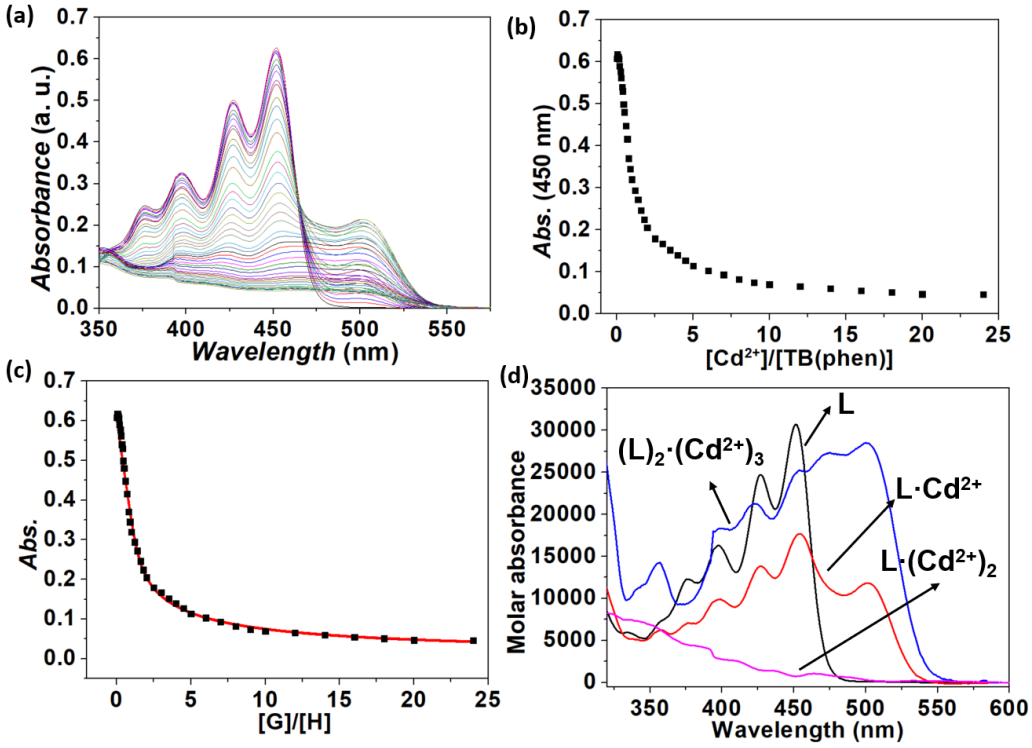

Figure S40. (a) Uv-vis spectra recorded corresponding to **TB(phen)** (**L**: 2.00×10^{-5} M in CH_2Cl_2/CH_3OH (4:1, *v/v*)) with increasing [Cd^{2+}] (from 0 to 24.0 molar equiv.) at 298 K. (b) The absorbance changes at 450 nm ("■"). And (c) the results of the corresponding nonlinear curve fitting according calculated model (red line) using Hyperquad 2003. (d) The calculated molar absorbance of **TB(phen)** and its complexes. The equilibriums and related K_a calculation results as shown: $2M + L \overset{K_2}{\rightleftarrows} M_2L$; $\log K_2 = 12.3(5)$; $3M + 2L \overset{K_3}{\rightleftarrows} M_3L_2$; $\log K_3 = 24.9(4)$; $M + L \overset{K_1}{\rightleftarrows} ML$; $\log K_1 = 7.3(2)$.

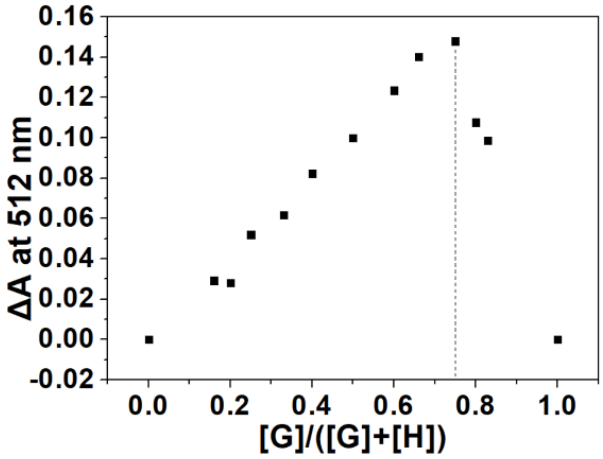

Figure S41. Job plot corresponding to the interactions between **TB(phen)** and Zn^{2+} in CH_2Cl_2/CH_3OH (4:1, *v/v*) at 298 K as monitored via Uv-vis spectroscopy. [Ligand] + [Metal] = 0.40 mM. Maximum value was seen at 0.75 in the case of Zn^{2+}, this supports the 1:3 (ligand/metal) stoichiometry as suggested in the main text.

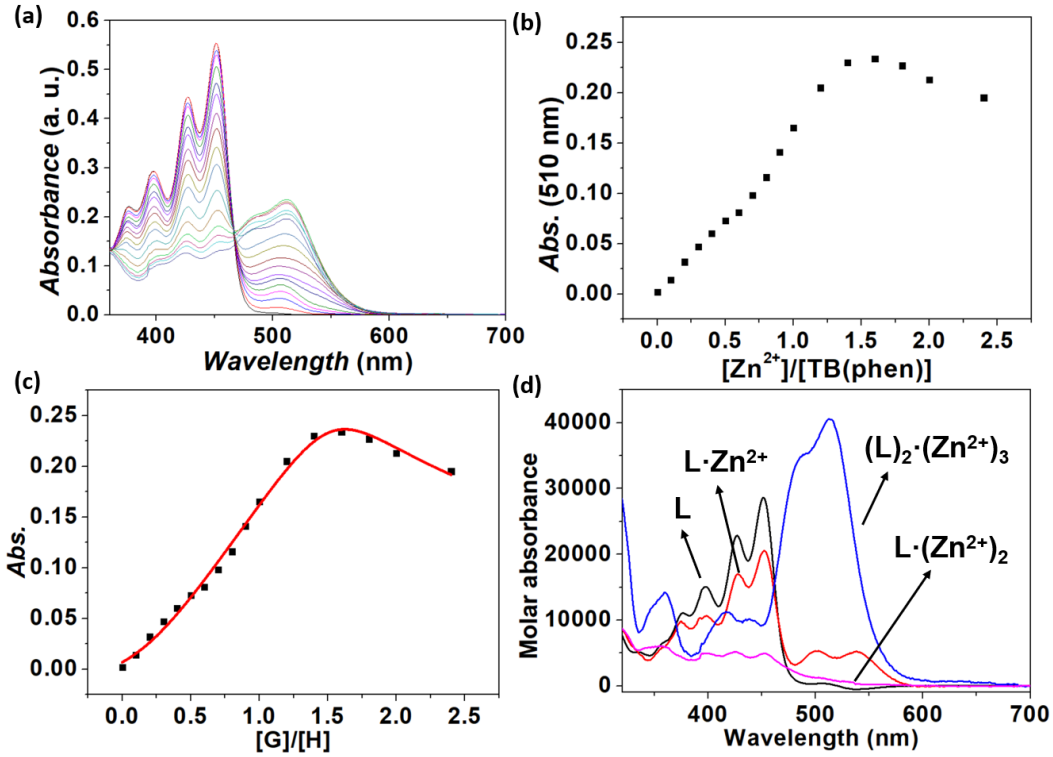

Figure S42. (a) Uv-vis spectra recorded corresponding to **TB(phen)** (**L**: 2.00×10^{-5} M in CH_2Cl_2/CH_3OH (4:1, *v/v*)) with increasing [Zn^{2+}] (from 0 to 4.0 molar equiv.) at 298 K. (b) The absorbance changes at 450 nm ("■"). And (c) the results of the corresponding nonlinear curve fitting according calculated model (red line) using Hyperquad 2003. (d) The calculated molar absorbance of **TB(phen)** and its complexes. The equilibriums and related K_a calculation results as shown: $2M + L \overset{K_2}{\rightleftarrows} M_2L$; $\log K_2 = 11.9(2)$; $3M + 2L \overset{K_3}{\rightleftarrows} M_3L_2$; $\log K_3 = 23.6(4)$; $M + L \overset{K_1}{\rightleftarrows} ML$; $\log K_1 = 6.3(5)$.

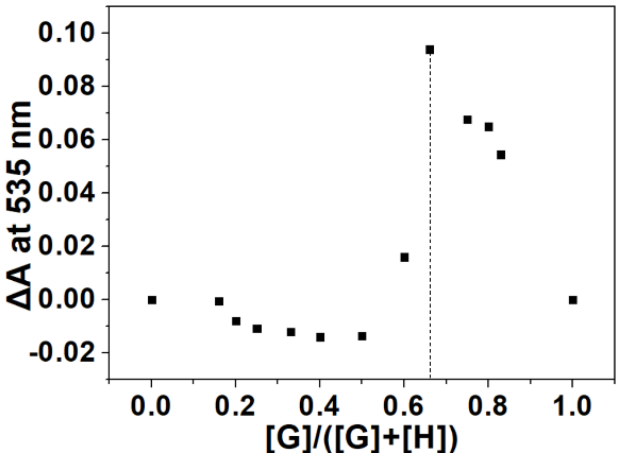

Figure S43. Job plot corresponding to the interactions between **TB(phen)** and Zr^{4+} in CH_2Cl_2/CH_3OH (4:1, *v/v*) at 298 K as monitored via Uv-vis spectroscopy. [Ligand] + [Metal] = 0.40 mM. Maximum value was seen at 0.66 in the case of Zr^{4+}, this supports the 1:2 (ligand/metal) stoichiometry as suggested in the main text.

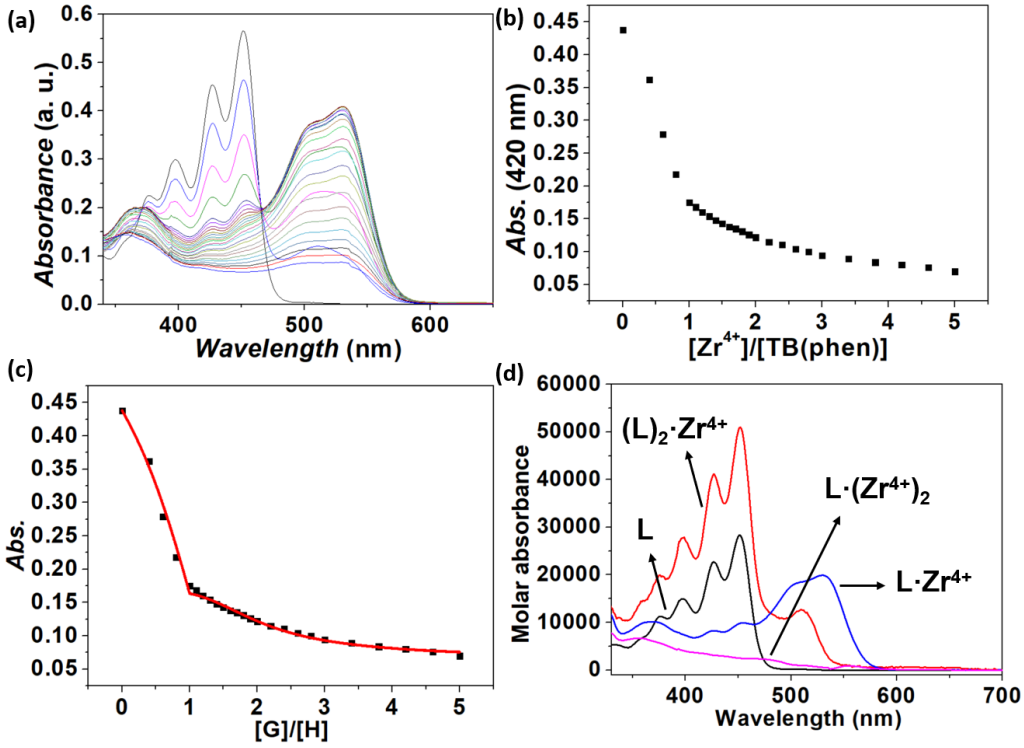

Figure S44. (a) Uv-vis spectra recorded corresponding to **TB(phen)** (**L**: 2.00×10^{-5} M in CH_2Cl_2/CH_3OH (4:1, *v/v*)) with increasing [Zr^{4+}] (from 0 to 5.0 molar equiv.) at 298 K. (b) The absorbance changes at 420 nm ("■"). And (c) the results of the corresponding nonlinear curve fitting according calculated model (red line) using Hyperquad 2003. (d) The calculated molar absorbance of **TB(phen)** and its complexes. The equilibriums and related K_a calculation results as shown: $2M + L \overset{K_2}{\rightleftarrows} M_2L$; $\log K_2 = 16.9(8)$; $M + L \overset{K_1}{\rightleftarrows} ML$; $\log K_1 = 11.7(5)$; $M + 2L \overset{K_{2'}}{\rightleftarrows} ML_2$; $\log K_{2'} = 16.5(5)$.

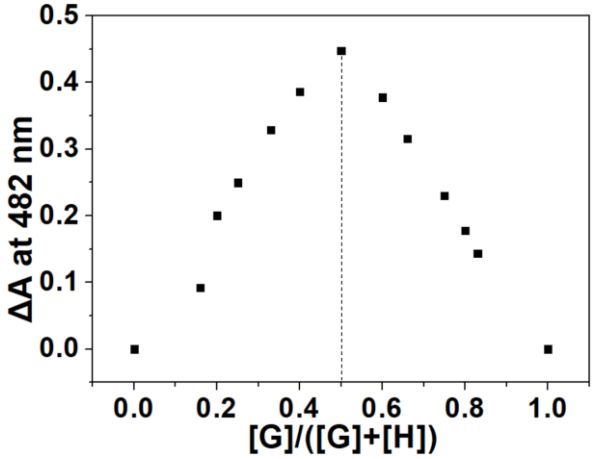

Figure S45. Job plot corresponding to the interactions between **TB(phen)** and Ag^+ in CH_2Cl_2/CH_3OH (4:1, *v/v*) at 298 K as monitored via Uv-vis spectroscopy. [Ligand] + [Metal] = 0.40 mM. Maximum value was seen at 0.50 in the case of Ag^+, this supports the 1:1 (ligand/metal) stoichiometry as suggested in the main text.

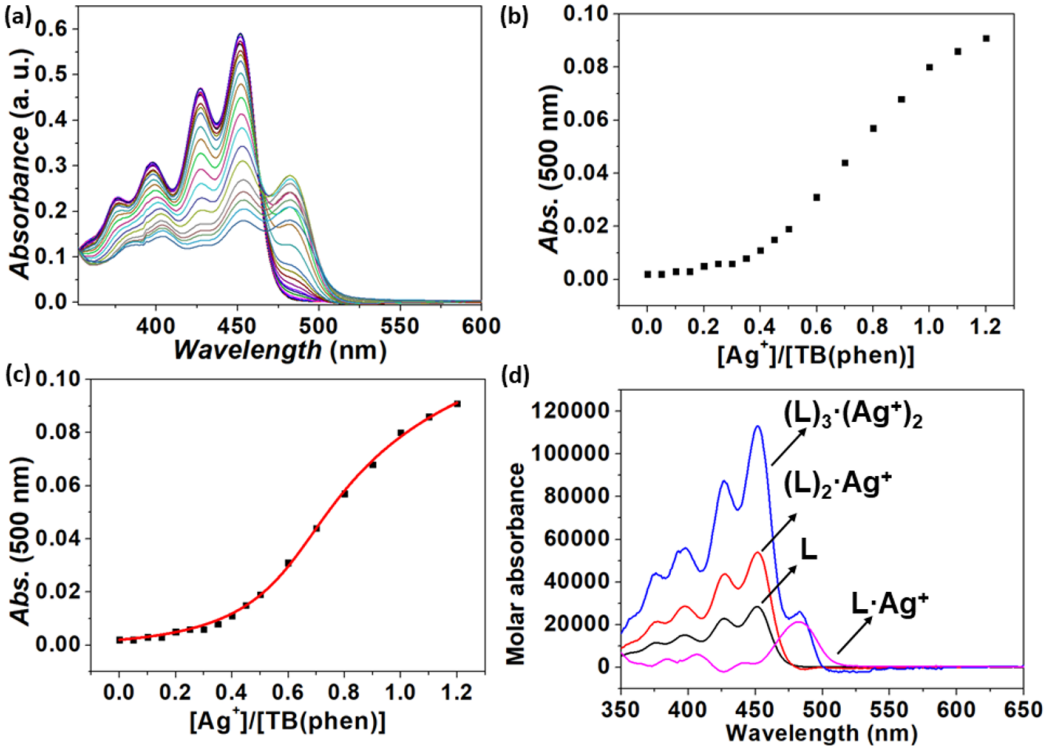

Figure S46. (a) Uv-vis spectra recorded corresponding to **TB(phen)** (**L**: 2.00×10^{-5} M in CH_2Cl_2/CH_3OH (4:1, *v/v*)) with increasing [Ag^+] (from 0 to 1.2 molar equiv.) at 298 K. (b) The absorbance changes at 500 nm ("■"). And (c) the results of the corresponding nonlinear curve fitting according calculated model (red line) using Hyperquad 2003. (d) The calculated molar absorbance of **TB(phen)** and its complexes. The equilibriums and related K_a calculation results as shown: $M + 2L \overset{K_{2'}}{\rightleftarrows} ML_2$; $\log K_{2'} = 12.6(3)$; $3M + 3L \overset{K_{3'}}{\rightleftarrows} M_3L_2$; $\log K_{3'} = 24.6(3)$; $M + L \overset{K_1}{\rightleftarrows} ML$; $\log K_1 = 6.8(6)$.

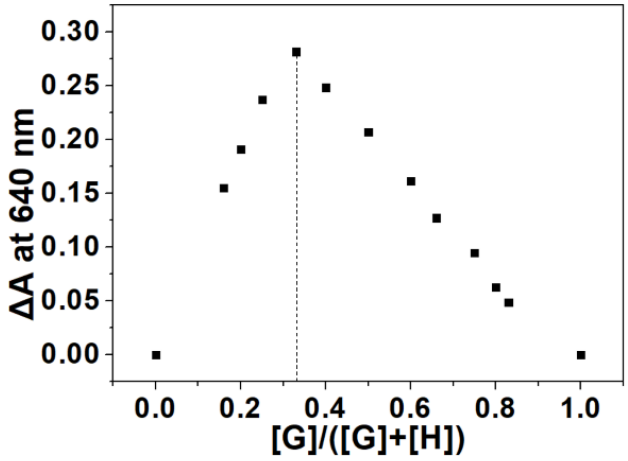

Figure S47. Job plot corresponding to the interactions between **TB(phen)** and Cu^{2+} in CH_2Cl_2/CH_3OH (4:1, *v/v*) at 298 K as monitored via Uv-vis spectroscopy. [Ligand] + [Metal] = 0.40 mM. Maximum value was seen at 0.33 in the case of Cu^{2+}, this supports the 2:1 (ligand/metal) stoichiometry as suggested in the main text.

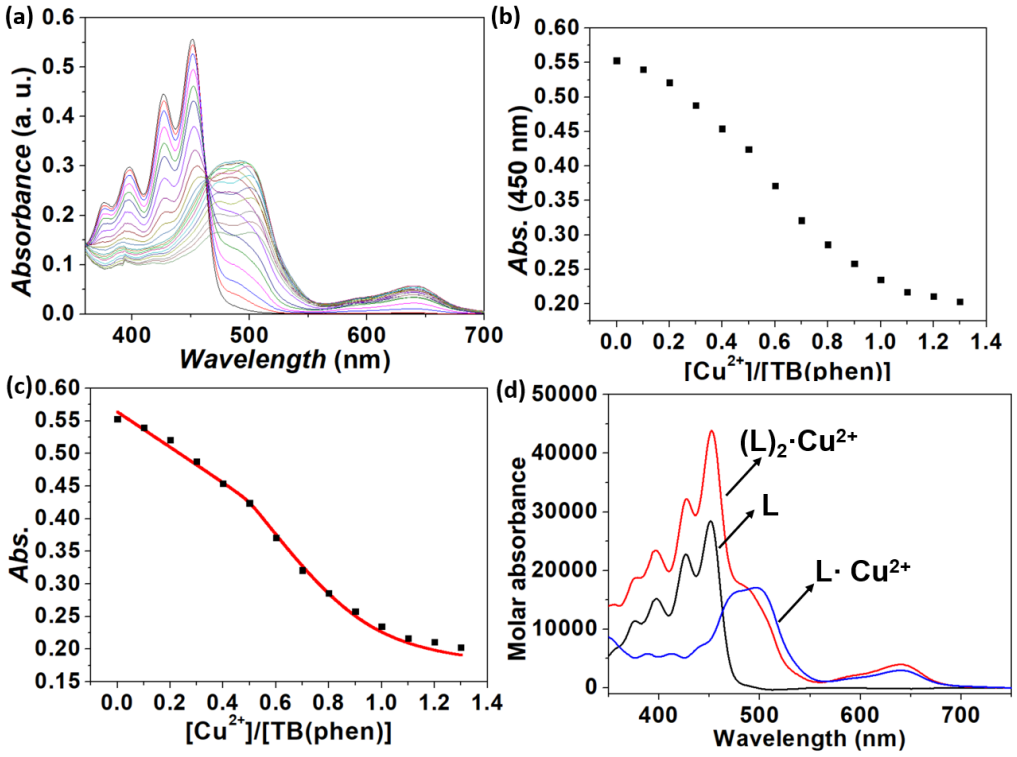

Figure S48. (a) Uv-vis spectra recorded corresponding to **TB(phen)** (**L**: 2.00×10^{-5} M in CH_2Cl_2/CH_3OH (4:1, *v/v*)) with increasing [Cu^{2+}] (from 0 to 1.3 molar equiv.) at 298 K. (b) The absorbance changes at 450 nm ("■"). And (c) the results of the corresponding nonlinear curve fitting according calculated model (red line) using Hyperquad 2003. (d) The calculated molar absorbance of **TB(phen)** and its complexes. The equilibriums and related K_a calculation results as shown: M + 2L $\overset{K_{2'}}{\rightleftarrows}$ ML_2; log $K_{2'}$ = 16.2(2); M + L $\overset{K_1}{\rightleftarrows}$ ML; log K_1 = 8.9(3).

Fluorescence spectroscopic studies

Fluorescence spectra were detected using an Edinburgh Instruments FS5 spectrometer. A 2000 μL solution of **1** (2.00×10^{-5} M in CH_2Cl_2/CH_3OH (4:1, *v/v*)) was added to a sample cell. Specific metal ion solution with much higher concentrations ($1.00 - 8.00 \times 10^{-2}$ M in CH_2Cl_2/CH_3OH (4:1, *v/v*)) were then added gradually. Data were collected after each addition and subsequent mixing.

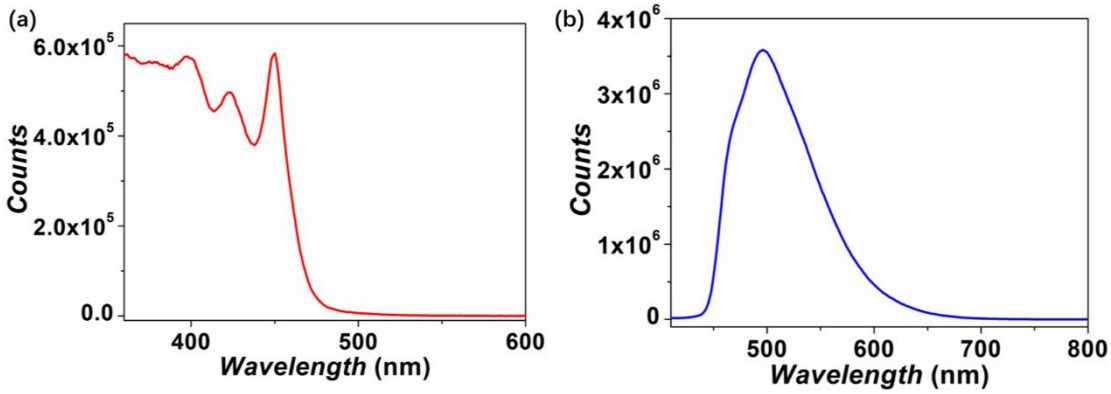

Figure S49. Excitation (a) and emission (b) spectra of **1** (2.00×10^{-5} M in CH_2Cl_2/CH_3OH (4:1, *v/v*), λ_{em} = 450 nm (voltage = 400 V, entrance slit width = 5 nm, exit slit width = 5 nm).

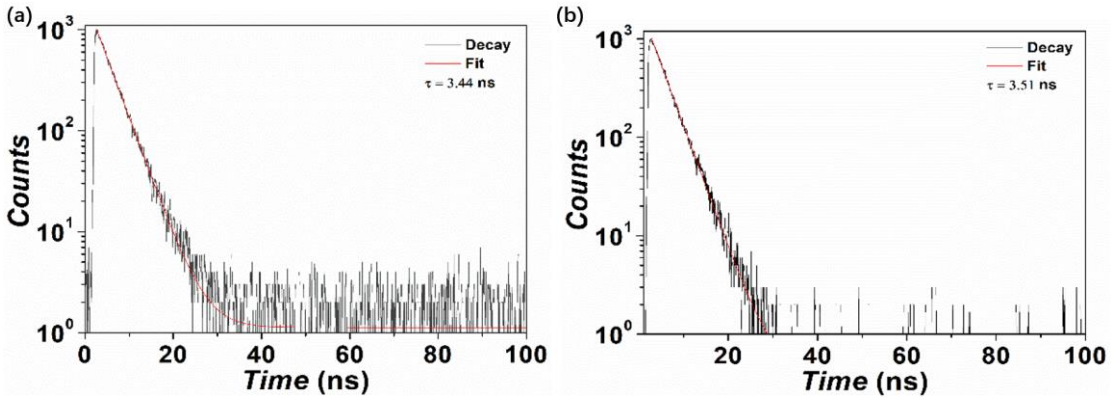

Figure S50. The fluorescence lifetime analysis of **1** (a) and **TB(phen)** (b) (each concentration as 2.00×10^{-5} M in CH_2Cl_2/CH_3OH (4:1, *v/v*) with excitation wavelength as 450 nm.

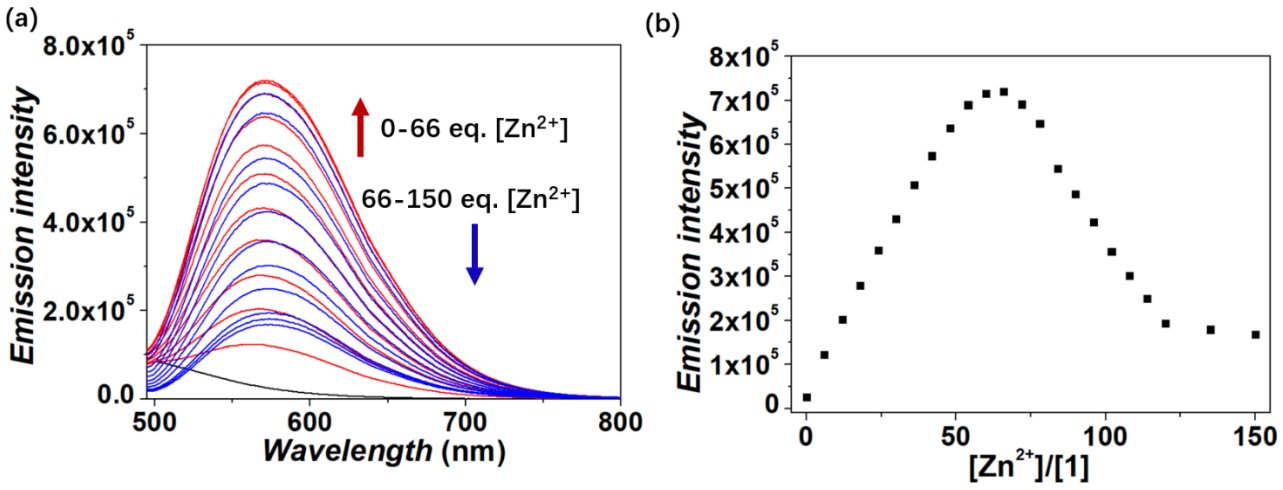

Figure S51. (a) Fluorescent emission spectra corresponding to **1** (2.00×10^{-5} M in CH_2Cl_2/CH_3OH (4:1, *v/v*) with increasing [Zn^{2+}] (from 0 to 150.0 molar equiv.) at 298 K (λ_{ex} = 485 nm, voltage = 400 V, entrance slit width = 4 nm, exit slit width = 4 nm). (b) The fluorescence intensity changes at 570 nm ("■"). It is noted that the emission increasing with [Zn^{2+}]/[**1**] from 0 to 66.0 equiv., and then decreasing with [Zn^{2+}]/[**1**] from 66.0 to 150.0 equiv. The change trends are consistent with the corresponding case of Uv-vis titration. The possible reason is suggested as the binding complexity.

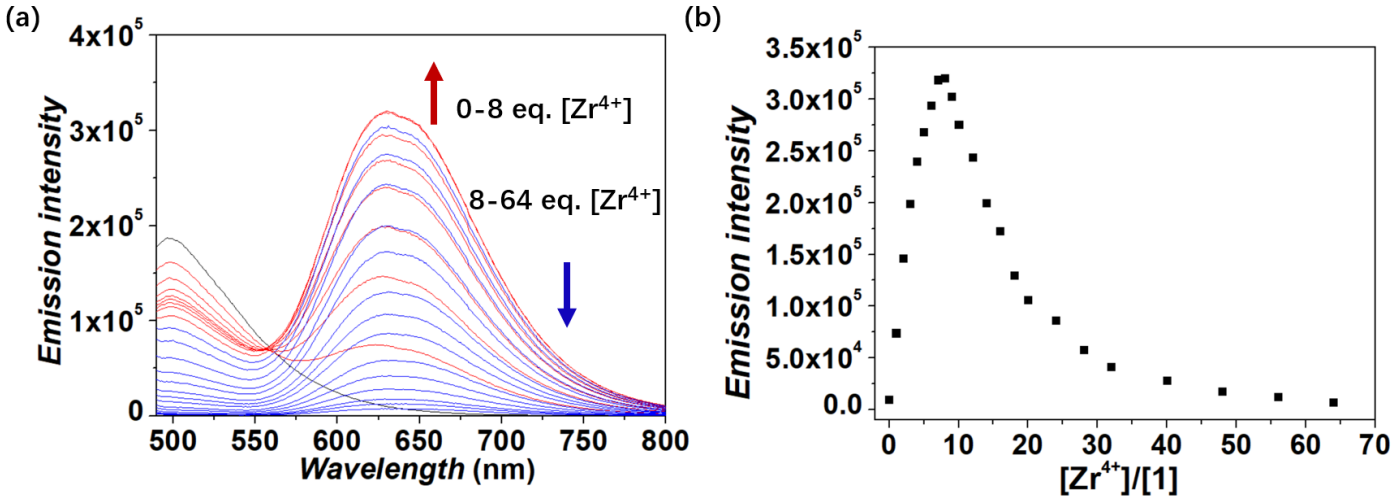

Figure S52. (a) Fluorescent emission spectra corresponding to **1** (2.00×10^{-5} M in CH_2Cl_2/CH_3OH (4:1, *v/v*)) with increasing [Zr^{4+}] (from 0 to 64.0 molar equiv.) at 298 K. (λ_{ex} = 480 nm, Voltage = 400 V, entrance slit width = 4.0 nm, exit slit width = 4.0 nm). (b) The fluorescence intensity changes at 630 nm ("■").

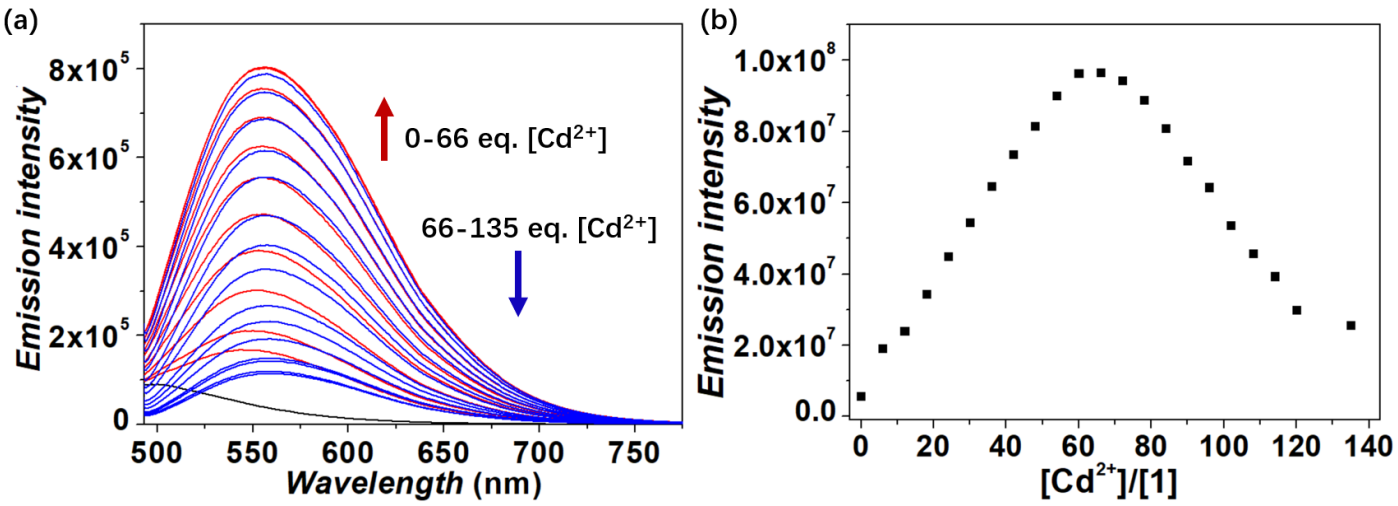

Figure S53. (a) Fluorescent emission spectra corresponding to **1** (2.00×10^{-5} M in CH_2Cl_2/CH_3OH (4:1, *v/v*)) with increasing [Cd^{2+}] (from 0 to 135.0 molar equiv.) at 298 K. (λ_{ex} = 485 nm, Voltage = 400 V, entrance slit width = 4 nm, exit slit width = 4 nm). (b) The fluorescence intensity changes at 555 nm ("■").

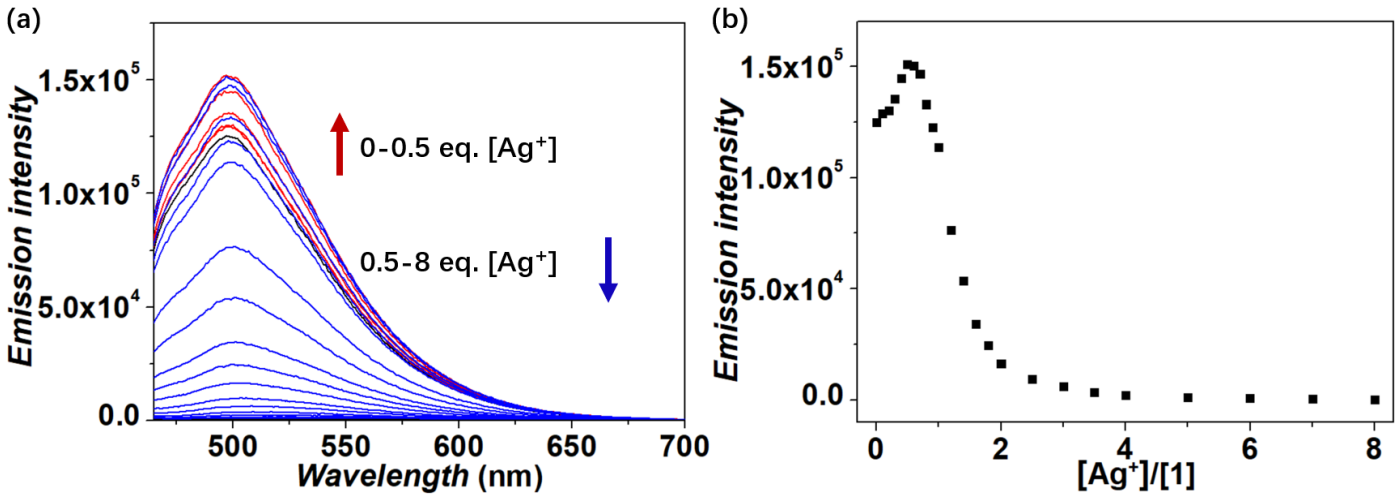

Figure S54. (a) Fluorescent emission spectra corresponding to **1** (2.00×10^{-5} M in CH_2Cl_2/CH_3OH (4:1, *v/v*)) with increasing [Ag^{+}] (from 0 to 8.0 molar equiv.) at 298 K. (λ_{ex} = 460 nm, Voltage = 400 V, entrance slit width = 1.7 nm, exit slit width = 1.7 nm). (b)The fluorescence intensity changes at 500 nm ("■").

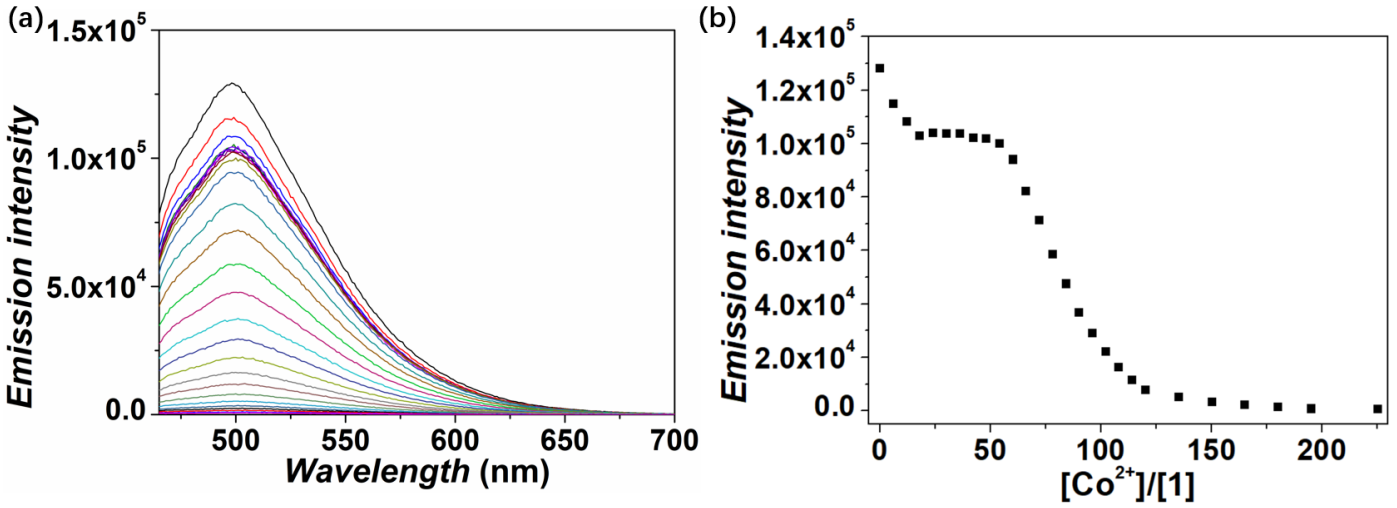

Figure S55. (a) Fluorescent emission spectra corresponding to **1** (2.00×10^{-5} M in CH_2Cl_2/CH_3OH (4:1, *v/v*)) with increasing [Co^{2+}] (from 0 to 225.0 molar equiv.) at 298 K. (λ_{ex} = 460 nm, Voltage = 400 V, entrance slit width = 1.7 nm, exit slit width = 1.7 nm). (b)The fluorescence intensity changes at 500 nm ("■").

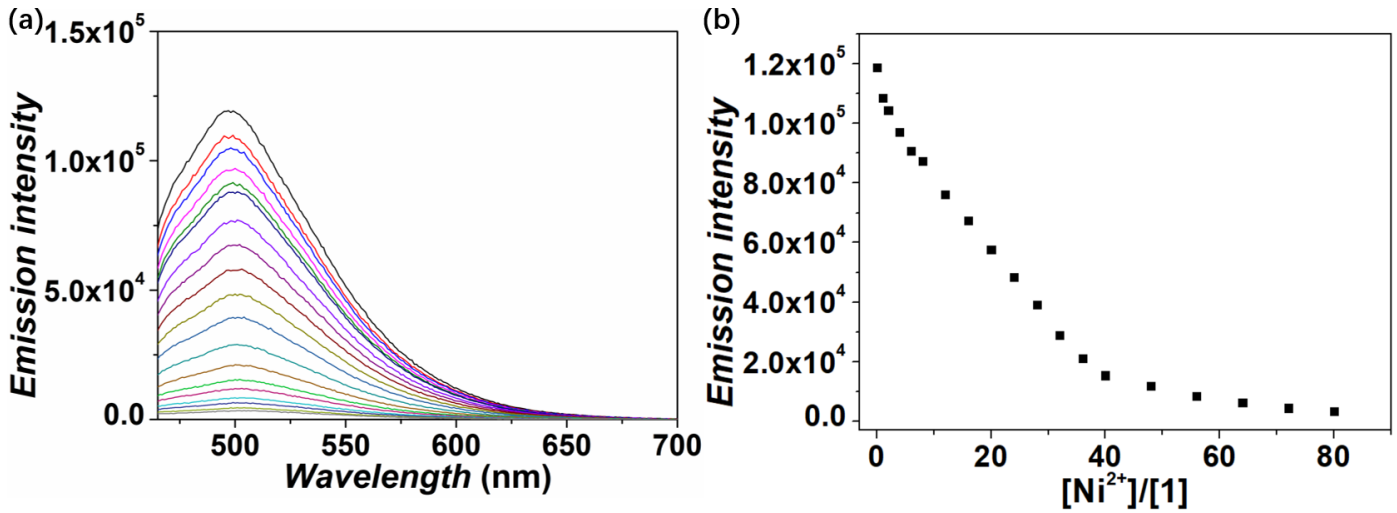

Figure S56. (a) Fluorescent emission spectra corresponding to **1** (2.00×10^{-5} M in CH_2Cl_2/CH_3OH (4:1, *v/v*)) with increasing [Ni^{2+}] (from 0 to 80.0 molar equiv.) at 298 K. (λ_{ex} = 460 nm, Voltage = 400 V, entrance slit width = 1.7 nm, exit slit width = 1.7 nm). (b)The fluorescence intensity changes at 500 nm ("■").

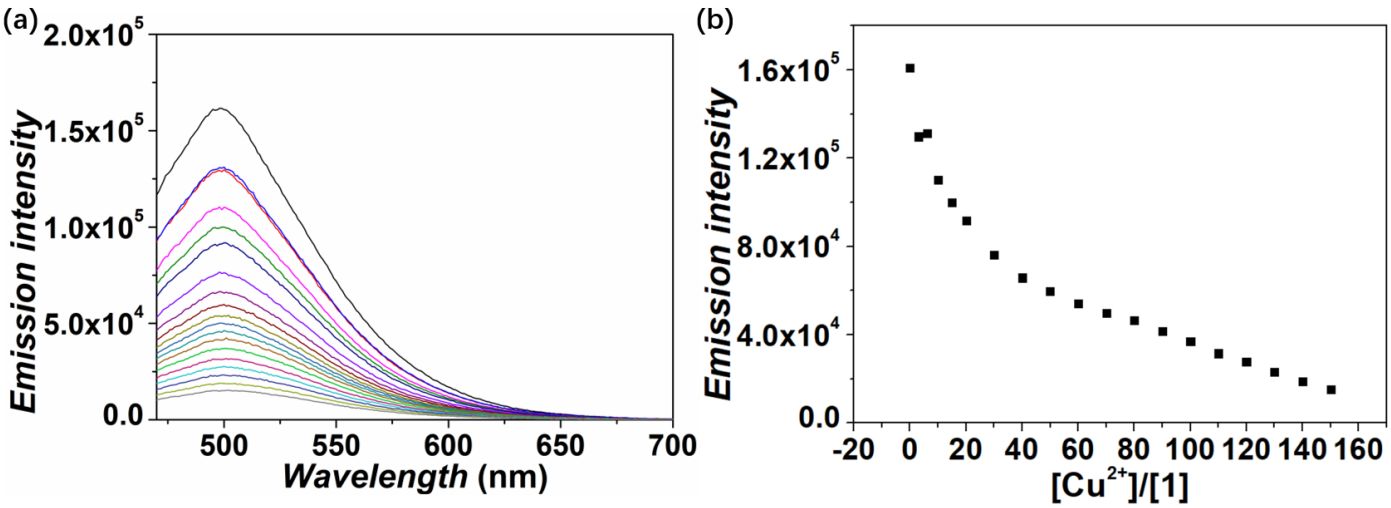

Figure S57. (a) Fluorescent emission spectra corresponding to **1** (2.00×10^{-5} M in CH_2Cl_2/CH_3OH (4:1, *v/v*)) with increasing [Cu^{2+}] (from 0 to 150.0 molar equiv.) at 298 K. (λ_{ex} = 460 nm, Voltage = 400 V, entrance slit width = 1.7 nm, exit slit width = 1.8 nm). (b)The fluorescence intensity changes at 500 nm ("■").

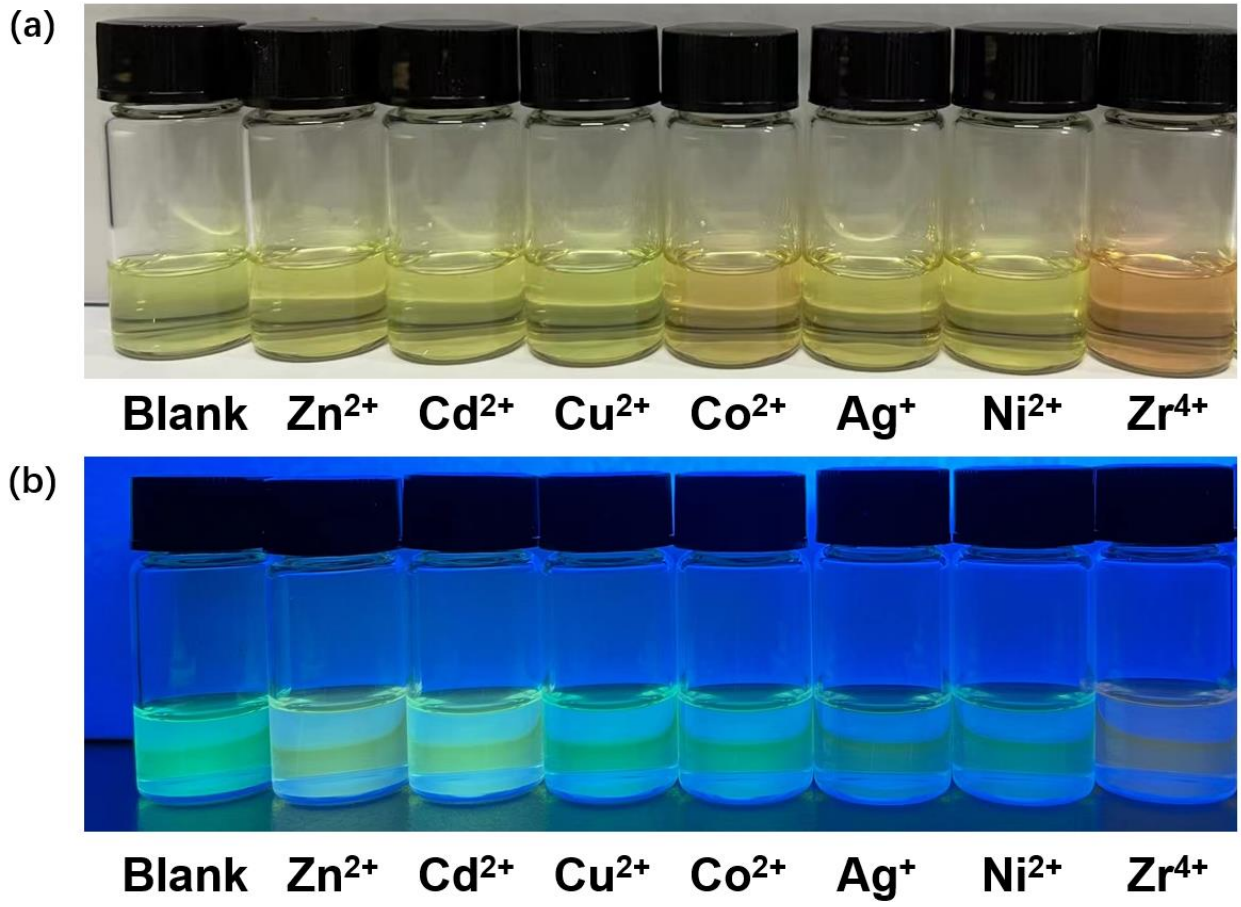

Figure S58. Photographs of **1** (2.00×10^{-5} M) coordination with each transition metal cation (20 molar equiv.) in CH_2Cl_2/CH_3OH (4:1, *v/v*) under (a) visible light and (b) 365 nm UV light, respectively.

Mass spectra studies of the complexes formed between 1 (L) and metal cations.

Adding 20 molar equiv. of metal cations into the solution of **1** in CH_2Cl_2/CH_3OH (4:1, *v/v*). The mixture was used for electrospray high resolution mass spectra (ESI-HRMS) analysis with a Bruker Solarix XR FTMS operating in the positive ion model. The signals corresponding to the complexation between **1** and metal cation were observed as below.

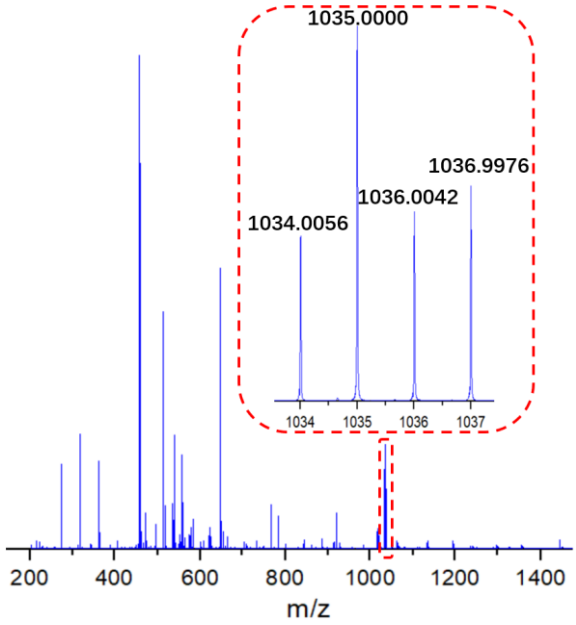

Figure **S59**. ESI high resolution mass spectrum of the mixture containing **1** and 20 molar equiv. of Co^{2+} in CH_2Cl_2/CH_3OH (4:1, v/v). ESI-HRMS (m/z) $\mathbf{L_2}\cdot Co^{2+}$, calcd. for $[\mathbf{2L}+Co^{2+}+NO_3^-]^+$ 1035.0045; found: 1035.0000.

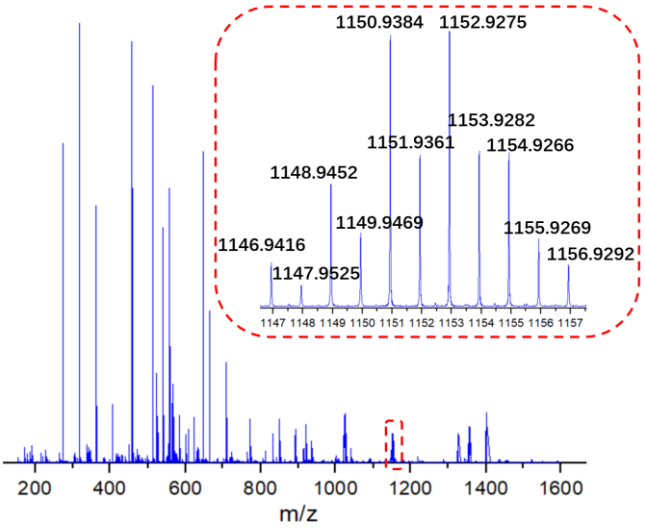

Figure **S60**. ESI high resolution mass spectrum of the mixture containing **1** and 20 molar equiv. of Zn^{2+} in CH_2Cl_2/CH_3OH (4:1, v/v). ESI-HRMS (m/z) $\mathbf{L_2}\cdot Zn^{2+}$, calcd. for $[\mathbf{2L}+Zn^{2+}+2NO_3^-+2Na^+-H^+]^+$ 1146.9600; found: 1146.9416.

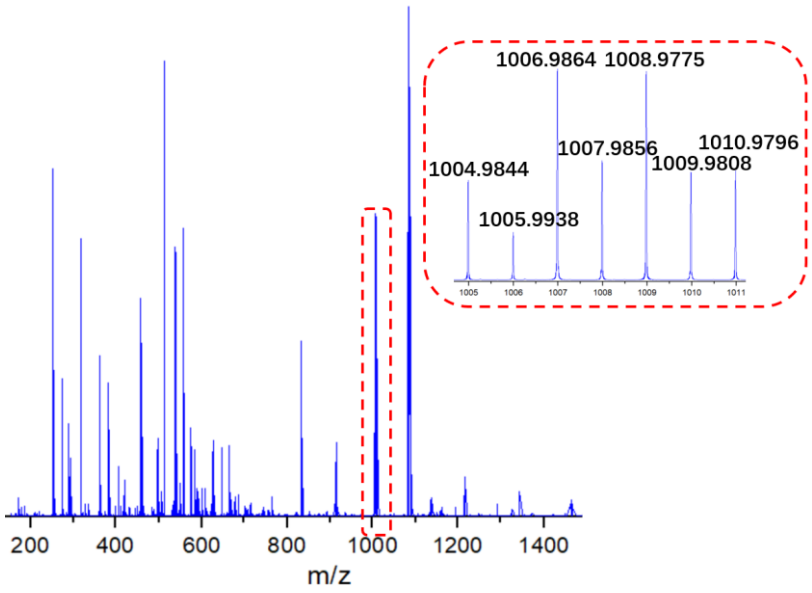

Figure **S61**. ESI high resolution mass spectrum of the mixture containing **1** and 20 molar equiv. of Ni^{2+} in CH_2Cl_2/CH_3OH (4:1, v/v). ESI-HRMS (m/z) $\mathbf{L_2}\cdot Ni^{2+}$, calcd. for $[\mathbf{2L}+Ni^{2+}+K^{+}-2H^{+}]^{+}$ 1008.9670; found: 1008.9775.

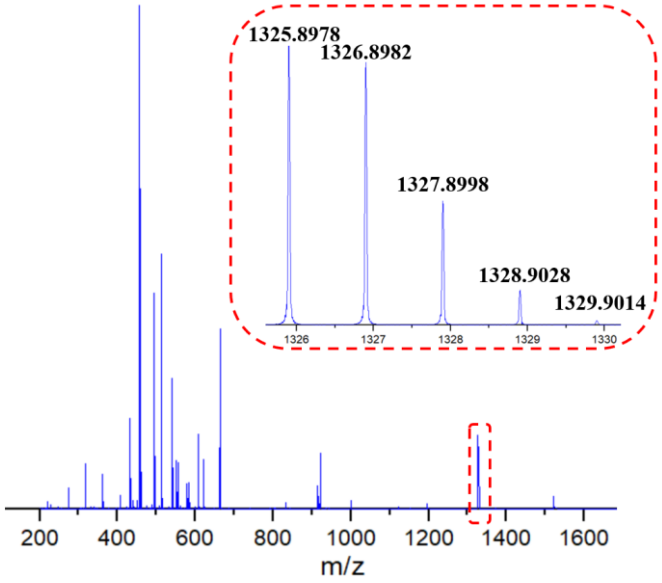

Figure **S62**. ESI high resolution mass spectrum of the mixture containing **1** and 20 molar equiv. of Zr^{4+} in CH_2Cl_2/CH_3OH (4:1, v/v). ESI-HRMS (m/z)$\mathbf{L_2}\cdot Zr^{4+}$, calcd. for $[\mathbf{2L}+Zr^{4+}+5Cl^{-}+2H_2O+2CH_3OH+2Na^{+}]^{+}$ 1326.8826; found: 1326.8982.

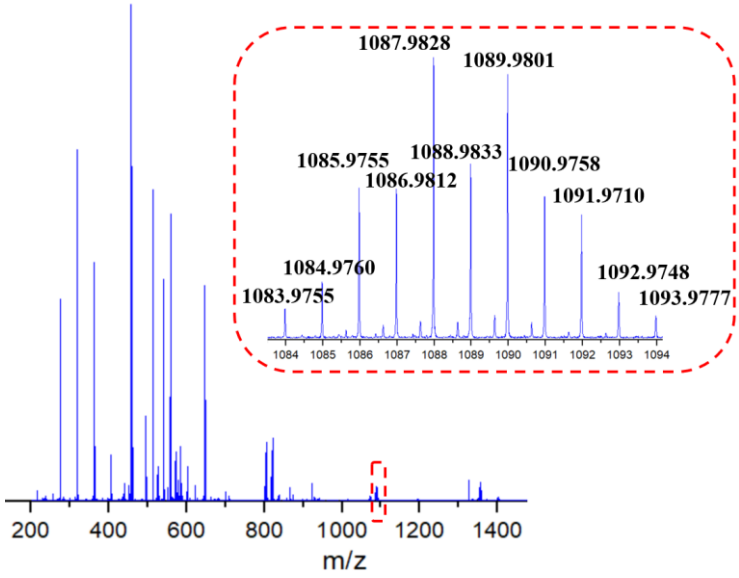

Figure **S63**. ESI high resolution mass spectrum of the mixture containing **1** and 20 molar equiv. of Cd^{2+} in CH_2Cl_2/CH_3OH (4:1, v/v). ESI-HRMS (m/z) $\mathbf{L_2}\cdot Cd^{2+}$, calcd. for $[\mathbf{2L}+Cd^{2+}+H_2O+2Na^{+}-2H]^{+}$ 1089.9613; found: 1089.9801.

Table S2. Summary of ESI-HRMS Results

Presumed Complex	Peak Assignment	Calculated m/z	Observed m/z
$[L_2\cdot Co^{2+}]$	$[2L+Co^{2+}+NO_3^{-}]^{+}$	1035.0045	1035.0000
$[L_2\cdot Zn^{2+}]$	$[2L+Zn^{2+}+2NO_3^{-}+2Na^{+}-H^{+}]^{+}$	1146.9600	1146.9416
$[L_2\cdot Ni^{2+}]$	$[2L+Ni^{2+}+K^{+}-2H^{+}]^{+}$	1008.9670	1008.9775
$[L_2\cdot Zr^{4+}]$	$[\mathbf{2L}+Zr^{4+}+5Cl^{-}+2H_2O+2CH_3OH+2Na^{+}]^{+}$	1326.8826	1326.8982
$[L_2\cdot Cd^{2+}]$	$[2L+Cd^{2+}+H_2O+2Na^{+}-2H^{+}]^{+}$	1089.9613	1089.9801

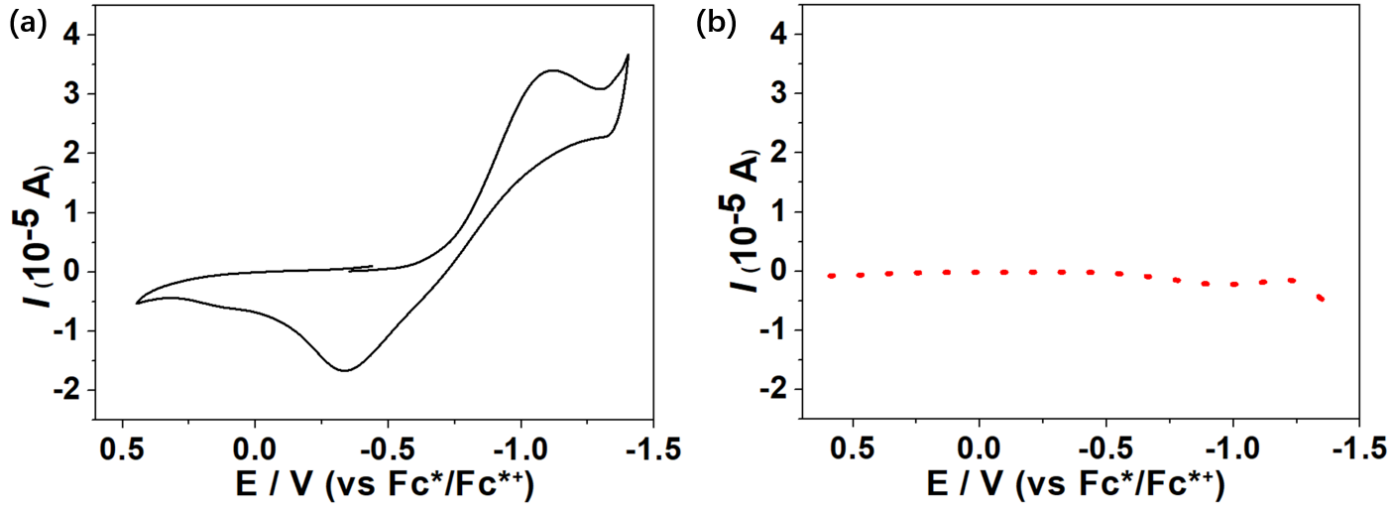

Figure S64. CV (black solid lines) (a) and DPV (red dashed lines) (b) curves of **1**.

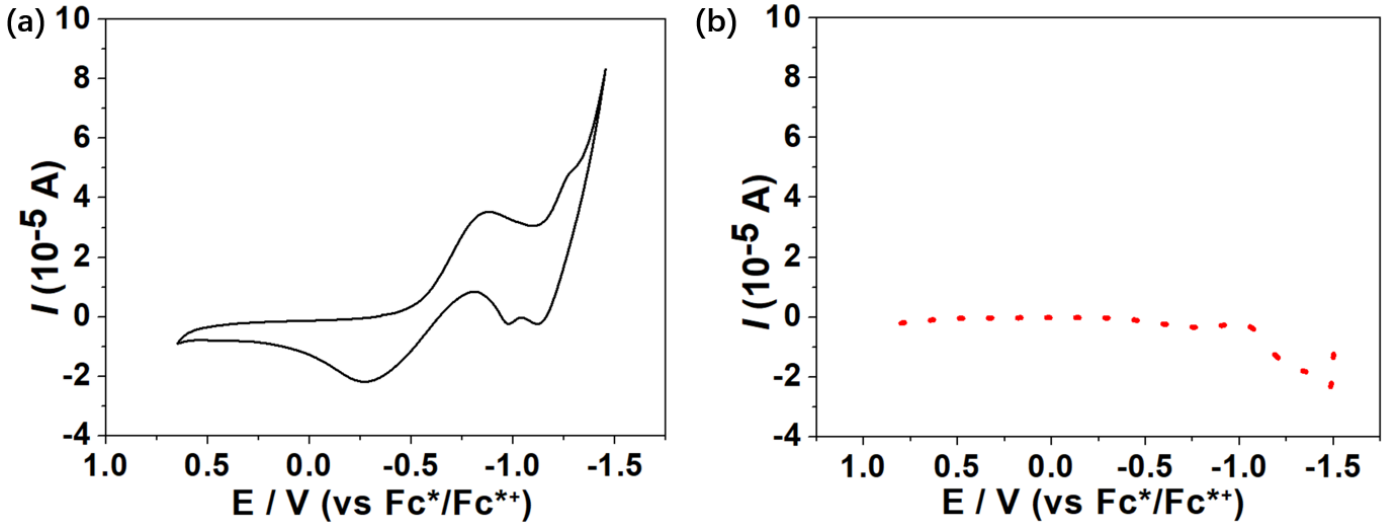

Figure S65. CV (black solid lines) (a) and DPV (red dashed lines) (b) curves of **TB(phen)**.

Section S5: *Single crystal X-ray diffraction analyses of [**1**•Zn^{2+}•$(NO_3^-)_2$]•CH_3OH and [**1**•Cd^{2+}•$(NO_3^-)_2$]•$2CH_3OH$.*

Table S3. Crystal data and structure refinement for [**1**•Zn^{2+}•$(NO_3^-)_2$]•CH_3OH and [**1**•Cd^{2+}•$(NO_3^-)_2$]•$2CH_3OH$.

	[**1**•Zn^{2+}•$(NO_3^-)_2$]•CH_3OH	[**1**•Cd^{2+}•$(NO_3^-)_2$]•$2CH_3OH$
Identification code	2305344	2305338
Empirical formula	$C_{29}H_{22}N_4O_9ZnCl_4$	$C_{28}H_{22}CdCl_2N_4O_{10}$
Formula weight	777.67	757.79
Temperature/K	170(2)	170(2)
Crystal system	orthorhombic	triclinic
Space group	Pnma	P-1
a/Å	10.9906(6)	7.1379(3)
b/Å	39.8868(16)	13.0556(3)
c/Å	13.6742(4)	15.0668(3)
α/°	90	88.113(2)
β/°	90	76.842(2)
γ/°	90	86.089(2)
Volume/$Å^3$	5994.5(4)	1363.80(7)
Z	8	2
$\rho_{calc}g/cm^3$	1.723	1.845
μ/mm^{-1}	4.978	8.835
F(000)	3152.0	760.0
Crystal size/mm^3	0.060 × 0.040 × 0.010	0.060 × 0.030 × 0.020
Radiation	CuK_α (λ = 1.54184)	CuK_α (λ = 1.54184)
2θ range for data collection/°	6.834 to 124.982	6.026 to 124.966
Index ranges	$-12 \le h \le 12$, $-36 \le k \le 45$, $-15 \le l \le 6$	$-8 \le h \le 8$, $-12 \le k \le 14$, $-17 \le l \le 17$
Reflections collected	20945	16700
Independent reflections	4848 [R_{int} = 0.0759, R_{sigma} = 0.0582]	4343 [R_{int} = 0.0542, R_{sigma} = 0.0502]
Data/restraints/parameters	4848/6/439	4343/2/412
Goodness-of-fit on F^2	1.020	1.034
Final R indexes [I>=2σ (I)]	R_1 = 0.0982, wR_2 = 0.2180	R_1 = 0.0361, wR_2 = 0.0861
Final R indexes [all data]	R_1 = 0.1194, wR_2 = 0.2319	R_1 = 0.0403, wR_2 = 0.0882
Largest diff. peak/hole / e $Å^{-3}$	1.84/-0.57	1.20/-0.43

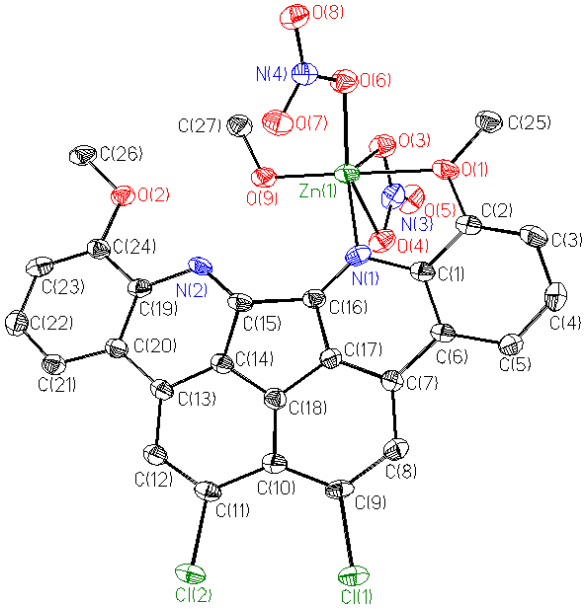

Figure S66. Ellipsoid form showing **1**•Zn^{2+}•$(NO_3^-)_2$ in the single crystal structure of [**1**•Zn^{2+}•$(NO_3^-)_2$•CH_3OH]. Displacement ellipsoids are scaled to the 50% probability level. All the other molecules and atoms have been omitted for clarity. Selected interatomic lengths (Å): Zn(1)…N(1) 2.11(6), Zn(1)…O(1) 2.20(7), Zn(1)…O(3) 2.10(6), Zn(1)…O(4) 2.36(6), Zn(1)…O(6) 2.03(6), Zn(1)…O(9) 2.01(6). Selected interatomic angles: ∠O(1)…Zn(1)…O(4) 86.3(2)°, ∠O(3)…Zn(1)…O(1) 85.1(2)°, ∠O(3)…Zn(1)…O(4) 57.0(2)°, ∠O(3)…Zn(1)…N(1) 134.4(3)°, ∠O(6)…Zn(1)…O(1) 84.4(3)°, ∠O(6)…Zn(1)…O(3) 88.6(3)°, ∠O(6)…Zn(1)…O(4) 144.9(2)°, ∠O(6)…Zn(1)…N(1) 128.3(3)°, ∠O(9)…Zn(1)…O(1) 175.5(2)°, ∠O(9)…Zn(1)…O(3) 90.7(3)°, ∠O(9)…Zn(1)…O(4) 90.2(2)°, ∠O(9)…Zn(1)…O(6) 97.0(3)°, ∠O(9)…Zn(1)…O(4) 90.2(2)°, ∠O(9)…Zn(1)…O(6) 97.0(3)°, ∠O(9)…Zn(1)…N(1) 107.5(2)°, ∠N(1)…Zn(1)…O(1) 74.7(2)°, ∠N(1)…Zn(1)…O(4) 80.9(2)°.

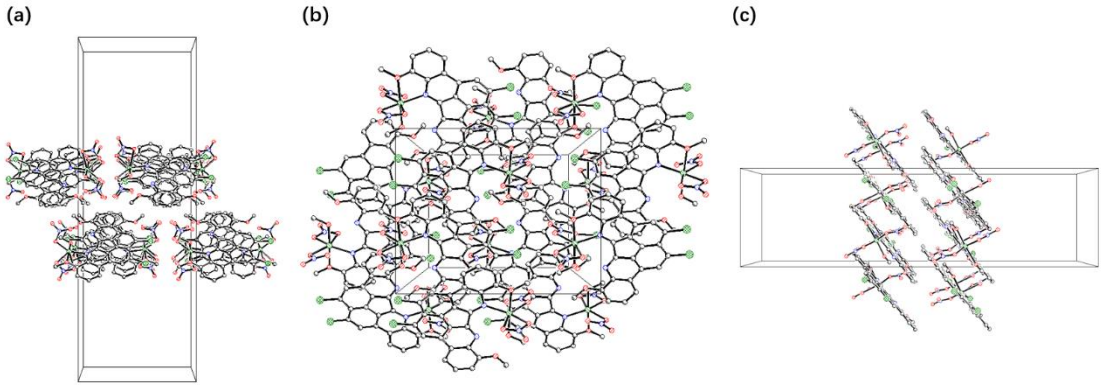

Figure S67. Packing diagram in the single crystal structure of [**1**•Zn^{2+}•$(NO_3^-)_2$]•CH_3OH along with *a* (a); *b* (b); *c* (c) cell axis.

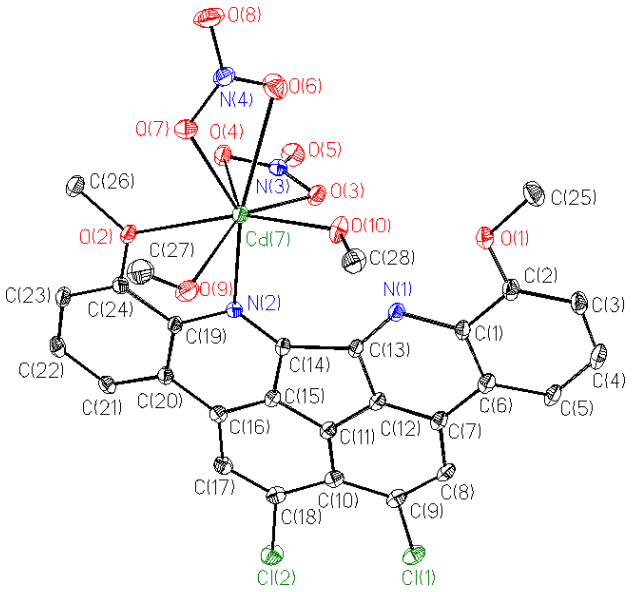

Figure S68. Ellipsoid form showing **1**•Cd^{2+}•$(NO_3^-)_2$ in the single crystal structure of [**1**•Cd^{2+}•$(NO_3^-)_2$•2CH_3OH]. Displacement ellipsoids are scaled to the 50% probability level. All the other molecules and atoms have been omitted for clarity. Selected interatomic lengths (Å): Cd(7)…N(2) 2.38(4), Cd(7)…O(2) 2.43(7), Cd(7)…O(3) 2.43(1), Cd(7)…O(4) 2.53(0), Cd(7)…O(6) 2.61(8), Cd(7)…O(7) 2.28(6), Cd(7)…O(9) 2.40(5). Selected interatomic angles: ∠O(2)…Cd(7)…N(2) 68.1(5)°, ∠N(2)…Cd(7)…O(10) 103.4(2)°, ∠O(10)…Cd(7)…O(3) 81.7(4)°, ∠O(3)…Cd(7)…O(4) 51.5(3)°, ∠O(4)…Cd(7)…O(2) 70.1(4)°, ∠O(2)…Cd(7)…O(9) 74.6(7)°, ∠N(2)…Cd(7)…O(9) 82.1(1)°, ∠O(10)…Cd(7)…O(9) 85.6(4)°, ∠O(3)…Cd(7)…O(9) 151.1(4)°, ∠O(4)…Cd(7)…O(9) 144.8(1)°, ∠O(2)…Cd(7)…O(7) 82.7(4)°, ∠N(2)…Cd(7)…O(7) 149.8(6)°, ∠O(10)…Cd(7)…O(7) 101.2(8)°, ∠O(3)…Cd(7)…O(7) 125.0(6)°, ∠O(4)…Cd(7)…O(7) 92.5(9)°, ∠O(2)…Cd(7)…O(6) 116.0(3)°, ∠N(2)…Cd(7)…O(6) 150.4(1)°, ∠O(10)…Cd(7)…O(6) 80.9(3)°, ∠O(3)…Cd(7)…O(6) 75.9(4)°, ∠O(4)…Cd(7)…O(6) 70.6(0)°, ∠O(6)…Cd(7)…O(7) 51.2(4)°.

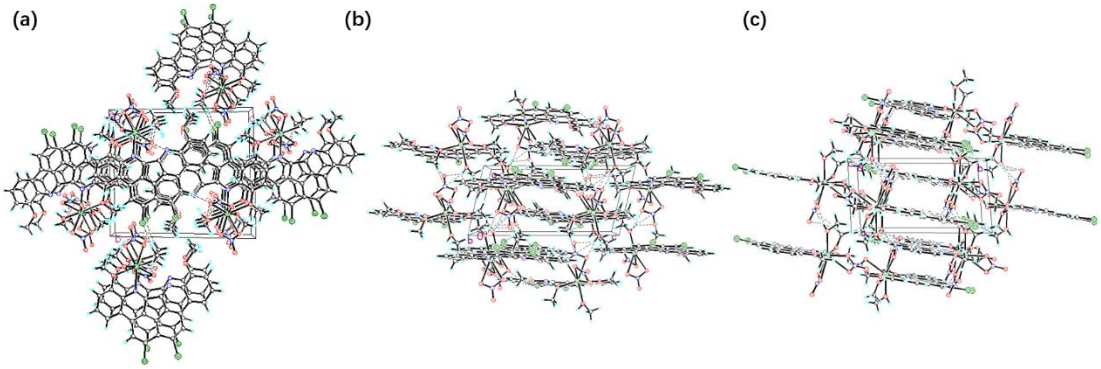

Figure S69. Packing diagram in the single crystal structure of [**1**•Cd^{2+}•$(NO_3^-)_2$]•CH_3OH along with *a* (a); *b* (b); *c* (c) cell axis.

Section S6: *Theoretical Calculations*

Theoretical calculations were carried out with the Gaussian 09 software package[8]. Geometry optimization was performed at the B3LYP level of density functional theory (DFT) with the 6-31G(d) basis set. The first ten vertical transition energies were calculated by time-dependent density functional theory (TD-DFT) at the B3LYP/6-31G(d) level (over optimized geometries at the same level). The first five states and corresponding main single electron transition for quinolino[2',3',4':3,4]indeno[2,1,7-*ghi*]phenanthridine (**2**), **1** and **TB(phen)** were listed in **Tables S4-S6**. Uv-vis absorption spectrum of **2**, **1** and **TB(phen)** were simulated according to TD-DFT results. The minimum structure of **2**, **1** and **TB(phen)** in the excited state S_1 were optimized at the B3LYP/6-31G(d) level of TD-DFT. Similarly, vibration frequency analysis confirmed local minima.

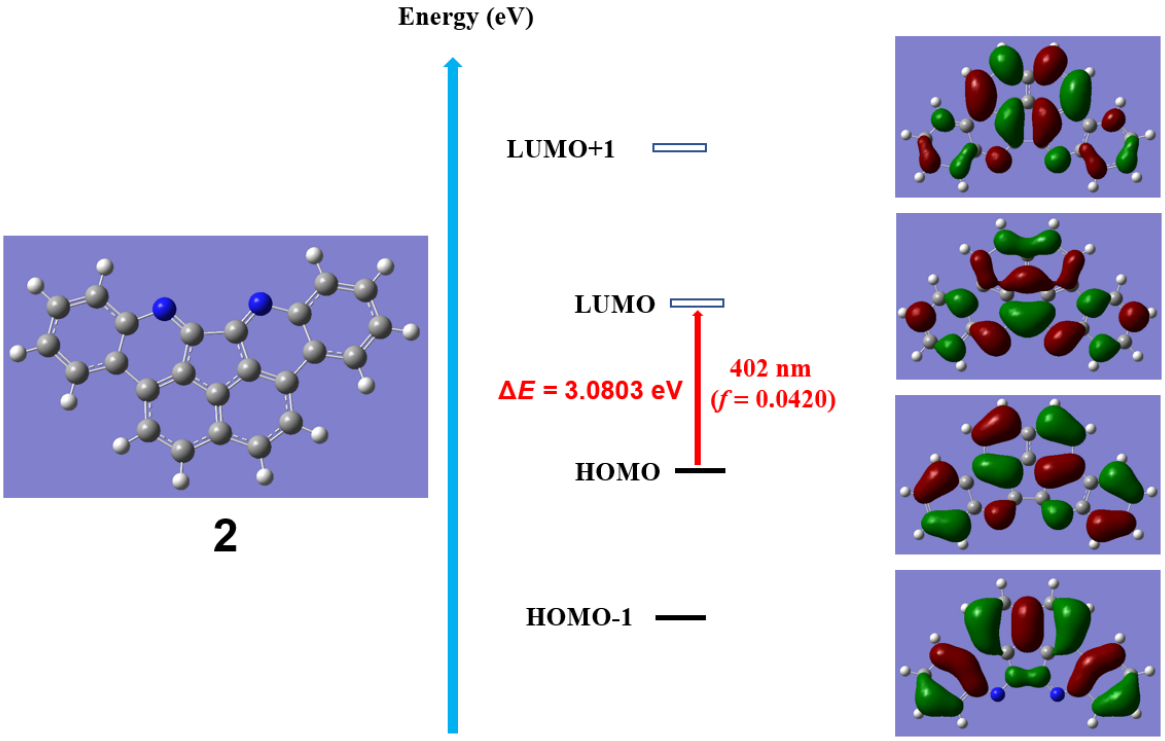

Figure S70. Molecular orbitals of **2**. TD-DFT result of the S_0-S_1 transition was indicated by a red arrow.

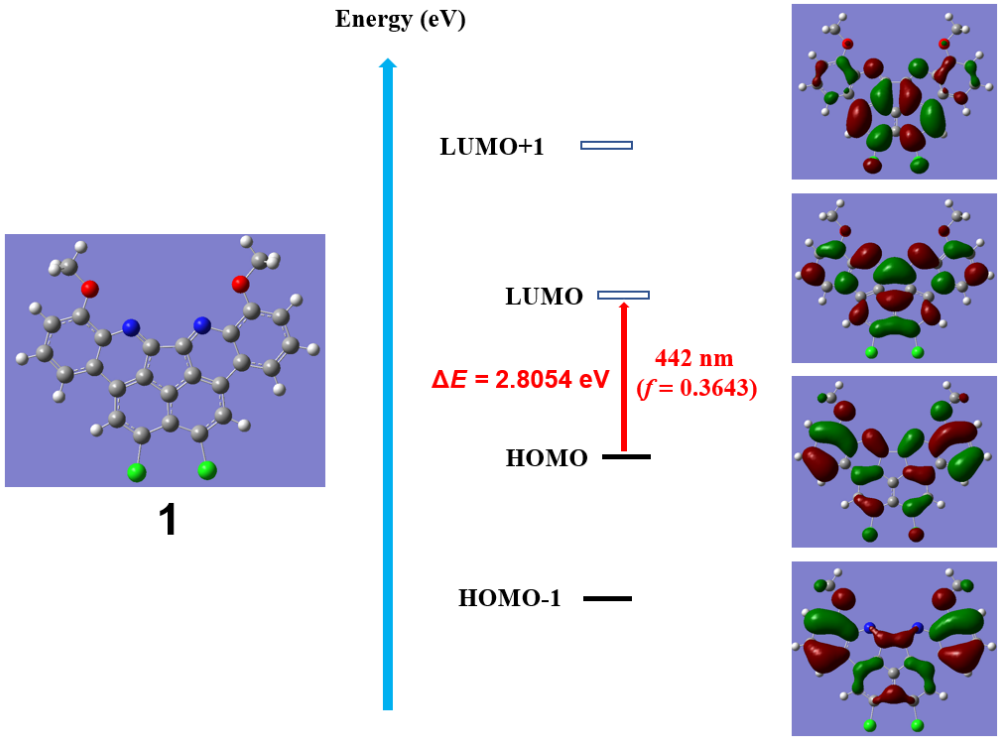

Figure S71. Molecular orbitals of **1**. TD-DFT result of the S_0-S_1 transition was indicated by a red arrow.

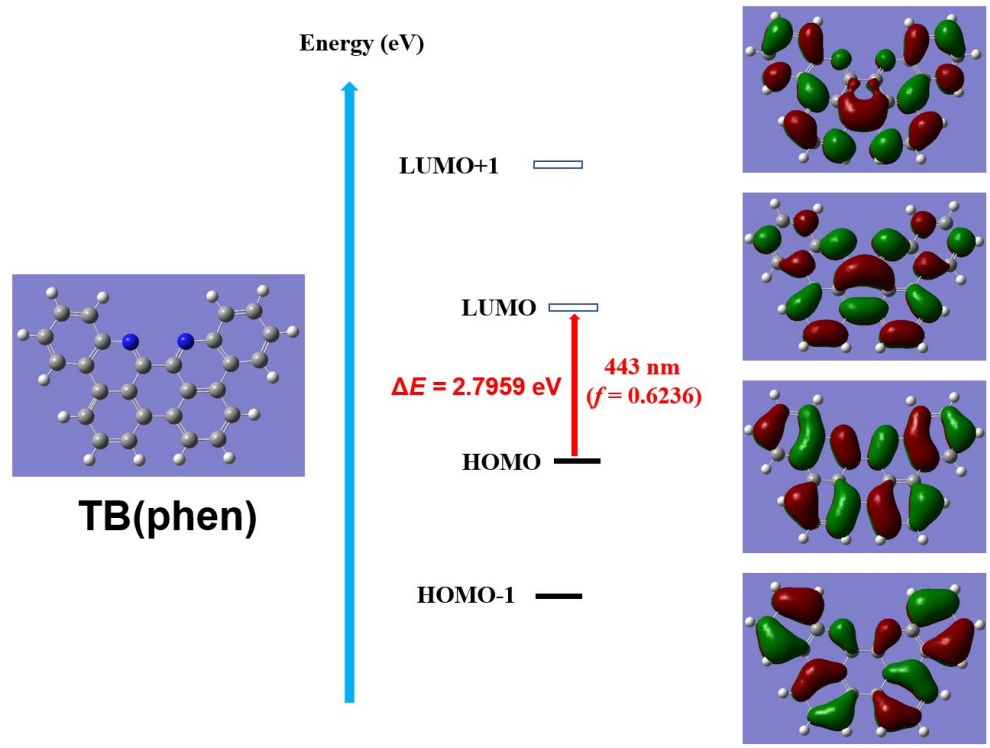

Figure S72. Molecular orbitals of **TB(phen)**. TD-DFT result of the S_0-S_1 transition was indicated by a red arrow.

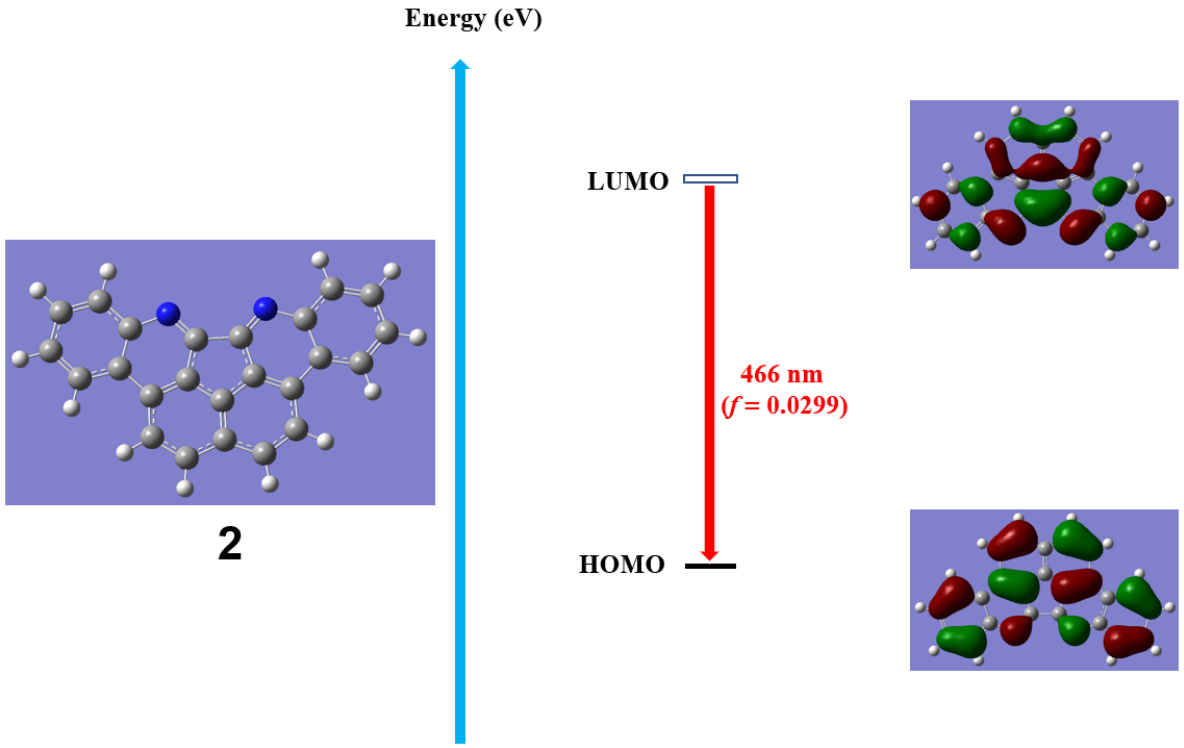

Figure S73. Molecular orbitals of **2** in excited state S_1. TD-DFT result of the S_1-S_0 transition was indicated by a red arrow.

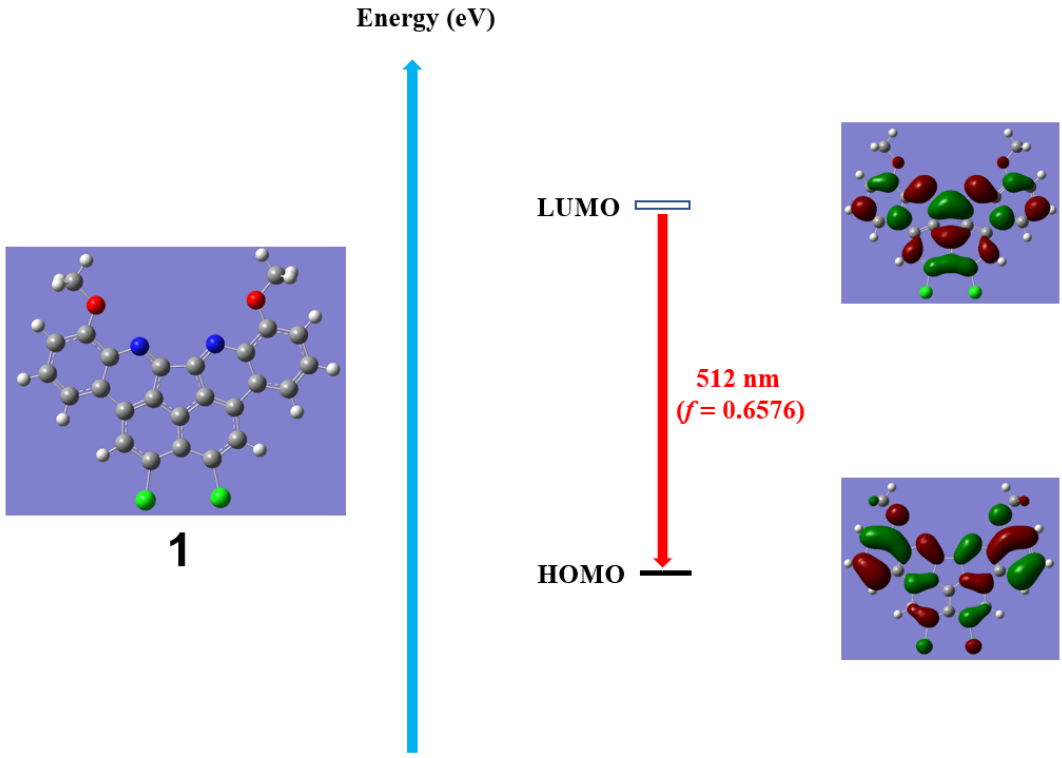

Figure S74. Molecular orbitals of **1** in excited state S_1. TD-DFT result of the S_1-S_0 transition was indicated by a red arrow.

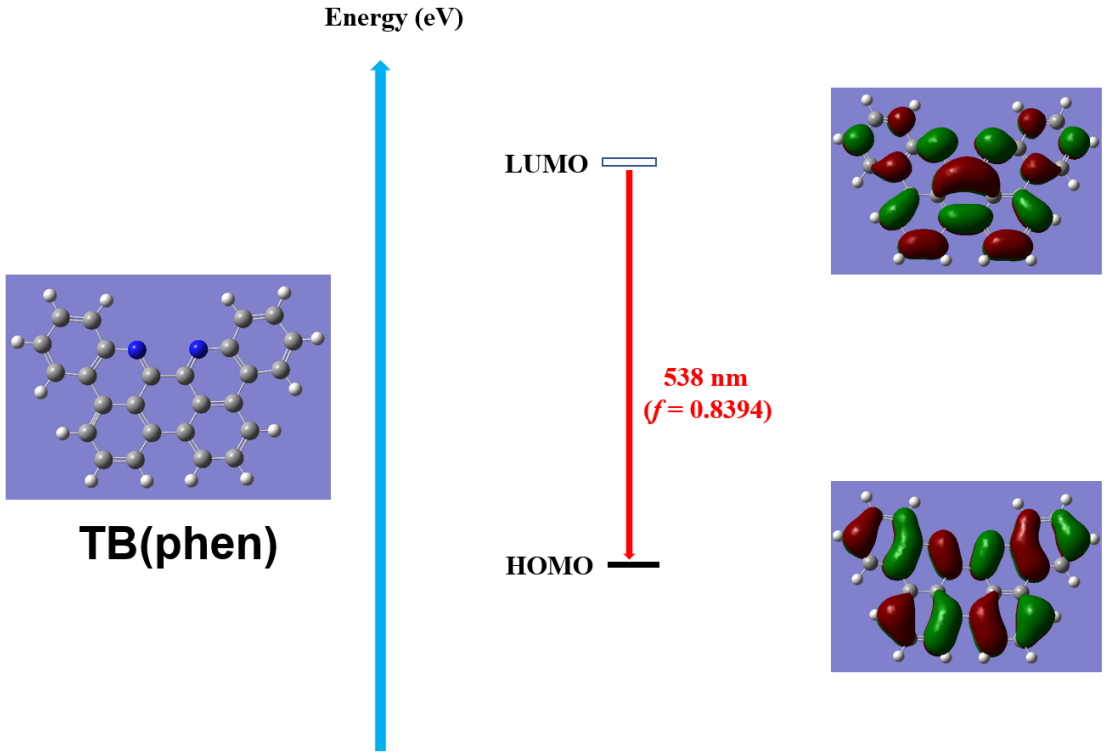

Figure S75. Molecular orbitals of **TB(phen)** in excited state S_1. TD-DFT result of the S_1-S_0 transition was indicated by a red arrow.

Table S4. TD-DFT calculation data for the ground state **2**.

Transition	Energy (eV)	Wavelength (nm)	Osc. Strength	Contributions
$S_0 \rightarrow S_1$	3.0803	402	0.0420	H-2→L (15%)
				H→L (83%)
$S_0 \rightarrow S_2$	3.3057	375	0.0094	H-1→L (95%)
				H→L+1 (4%)
$S_0 \rightarrow S_3$	3.5217	352	0.3239	H-2→L (78%)
				H-1→L+1 (6%)
				H→L (13%)
$S_0 \rightarrow S_4$				H-4→L (98%)
$S_0 \rightarrow S_5$	3.7939	326	0.0658	H-3→L (50%)
				H-2→L+1 (5%)
				H-1→L+2 (6%)
				H→L+1 (36%)

Table S5. TD-DFT calculation data for the ground state **1**.

Transition	Energy (eV)	Wavelength (nm)	Osc. Strength	Contributions
$S_0 \rightarrow S_1$	2.8054	442	0.3643	H→L (95%)
$S_0 \rightarrow S_2$	3.1153	398	0.1153	H-1→L (95%)
$S_0 \rightarrow S_3$	3.1963	388	0.0685	H-2→L (95%)
				H→L+2 (2%)
$S_0 \rightarrow S_4$	3.2576	381	0.0645	H-3→L (6%)
				H→L+1 (91%)

$S_0 \rightarrow S_5$	3.5688	347	0.0011	H-3→L (84%) H-2→L+1 (8%) H→L+1 (4%)

Table S6. TD-DFT calculation data for the ground state **TB(phen)**.

Transition	Energy (eV)	Wavelength (nm)	Osc. Strength	Contributions
$S_0 \rightarrow S_1$	2.7959	443	0.6236	H→L (98%)
$S_0 \rightarrow S_2$	3.2694	379	0.0239	H-1→L (83%) H→L+1 (14%)
$S_0 \rightarrow S_3$	3.3129	374	0.0015	H-3→L (95%) H-2→L (3%)
$S_0 \rightarrow S_4$	3.3924	365	0.0558	H-3→L (3%) H-2→L (87%) H→L+2 (9%)
$S_0 \rightarrow S_5$	3.6850	336	0.0016	H-6→L (97%)

Table S7. Cartesian coordinates of the DFT optimized ground state structure of **2**.

Center Number	Atom	Coordinates (Angstroms)		
		X	Y	Z
1	C	-1.132517	0.494647	0.000070
2	C	-0.763543	-0.889816	-0.000040
3	C	1.132604	0.494591	0.000207
4	C	0.763495	-0.889844	0.000024
5	N	1.662995	-1.834448	-0.000347
6	N	-1.663058	-1.834355	0.000236
7	C	-5.323752	-2.112875	0.000348
8	C	-5.746273	-0.770725	-0.000183
9	C	-4.814643	0.253985	-0.000549
10	C	-3.431290	-0.016732	-0.000229
11	C	-2.992966	-1.398443	0.000109
12	C	-3.973966	-2.414973	0.000438
13	H	-6.058396	-2.912048	0.000412
14	H	-6.806388	-0.536753	-0.000166
15	H	-5.150316	1.286603	-0.000776
16	H	-3.627324	-3.443173	0.000762
17	C	2.992906	-1.398499	-0.000305
18	C	3.431250	-0.016760	0.000133
19	C	4.814610	0.253973	0.000527
20	C	5.746250	-0.770727	0.000324
21	C	5.323747	-2.112926	-0.000254
22	C	3.973949	-2.415028	-0.000562
23	H	5.150261	1.286606	0.001043
24	H	6.806366	-0.536750	0.000661
25	H	6.058433	-2.912058	-0.000446
26	H	3.627275	-3.443213	-0.000877
27	C	0.000001	2.686851	-0.000085
28	C	1.327142	3.253298	-0.000324
29	C	2.467925	2.455341	-0.000004
30	H	1.453624	4.332336	-0.000456
31	H	3.433648	2.951019	-0.000210
32	C	0.000065	1.304218	-0.000006
33	C	-1.327123	3.253286	0.000171
34	H	-1.453638	4.332299	0.000229
35	C	-2.467854	2.455291	0.000034
36	H	-3.433623	2.950889	-0.000227
37	C	-2.407989	1.011396	0.000091
38	C	2.408057	1.011450	0.000203

Table S8. Cartesian coordinates of the DFT optimized ground state structure of **1**.

Center Number	Atom	Coordinates (Angstroms)		
		X	Y	Z
1	C	1.127520	-0.412705	0.000033
2	C	0.759096	0.969509	-0.000057
3	C	-1.127525	-0.412712	-0.000079
4	C	-0.759100	0.969511	-0.000088
5	N	-1.661138	1.912665	-0.000065
6	N	1.661141	1.912649	-0.000170
7	C	5.334974	2.192012	0.000098
8	C	5.738612	0.847102	0.000261
9	C	4.811477	-0.178192	0.000363
10	C	3.434050	0.113647	0.000208
11	C	2.985983	1.490413	0.000025
12	C	3.983050	2.520924	0.000018
13	H	6.088644	2.968938	0.000126
14	H	6.799612	0.617358	0.000341
15	H	5.141876	-1.211486	0.000418
16	C	-2.985976	1.490410	0.000011
17	C	-3.434007	0.113629	0.000140
18	C	-4.811434	-0.178226	0.000369
19	C	-5.738603	0.847043	0.000437
20	C	-5.334998	2.191963	0.000218
21	C	-3.983081	2.520895	-0.000010
22	H	-5.141791	-1.211536	0.000530
23	H	-6.799597	0.617268	0.000631
24	H	-6.088671	2.968886	0.000227
25	C	-0.000001	-2.625172	-0.000032
26	C	-1.350044	-3.154134	-0.000103
27	C	-2.483172	-2.345183	-0.000068
28	H	-3.446947	-2.840546	-0.000116
29	C	0.000006	-1.234497	-0.000092
30	C	1.350079	-3.154109	0.000064
31	C	2.483189	-2.345150	0.000157
32	H	3.446954	-2.840536	0.000207
33	C	2.407493	-0.910197	0.000186
34	C	-2.407492	-0.910226	0.000017
35	O	3.514482	3.790921	-0.000045
36	O	-3.514538	3.790904	-0.000239
37	C	4.455091	4.863254	-0.000377
38	H	3.860560	5.776728	-0.000562
39	H	5.087953	4.840863	0.894002
40	H	5.087827	4.840426	-0.894833
41	C	-4.455188	4.863199	-0.000145
42	H	-5.087828	4.840627	0.894386
43	H	-3.860693	5.776697	-0.000324

44	H	-5.088147	4.840503	-0.894446
45	Cl	1.646634	-4.888639	-0.000030
46	Cl	-1.646595	-4.888657	-0.000322

Table S9. Cartesian coordinates of the DFT optimized ground state structure of **TB(phen)**.

Center Number	Atom	Coordinates (Angstroms)		
		X	Y	Z
1	C	3.569936	2.072760	-0.048077
2	C	2.871002	0.847027	-0.020124
3	C	1.447095	0.867212	-0.008663
4	C	0.738630	2.105137	-0.014026
5	C	2.877585	3.268543	-0.063808
6	C	0.744003	-0.394708	0.006254
7	C	-0.738613	2.105157	0.014127
8	C	-1.447091	0.867220	0.008522
9	C	-0.744002	-0.394708	-0.006596
10	C	-2.870990	0.847019	0.019980
11	H	4.653126	2.085634	-0.059007
12	H	3.421285	4.207744	-0.089075
13	C	3.538774	-0.439400	-0.001740
14	C	2.720630	-1.604754	0.026675
15	C	-3.538783	-0.439403	0.001766
16	C	-2.720644	-1.604735	-0.026932
17	C	-1.477026	3.287342	0.046499
18	H	-0.978978	4.248822	0.061632
19	C	1.477037	3.287337	-0.046359
20	H	0.978974	4.248808	-0.061493
21	N	1.350539	-1.558003	0.027506
22	N	-1.350550	-1.557969	-0.027950
23	C	-4.698135	-3.016817	-0.045371
24	H	-5.154337	-4.001771	-0.063391
25	C	-3.324584	-2.886324	-0.051331
26	H	-2.669268	-3.750869	-0.073313
27	C	-5.511249	-1.865185	-0.014619
28	H	-6.592100	-1.967253	-0.008939
29	C	-4.942810	-0.604150	0.008309
30	H	-5.592840	0.263293	0.031020
31	C	-3.569951	2.072778	0.047974
32	H	-4.653141	2.085616	0.058789
33	C	-2.877582	3.268552	0.063772
34	H	-3.421256	4.207772	0.088886
35	C	5.511255	-1.865173	0.015262
36	C	4.698132	-3.016817	0.045549
37	C	3.324586	-2.886334	0.051052
38	C	4.942805	-0.604143	-0.007786
39	H	6.592107	-1.967242	0.010078

40	H	5.154338	-4.001769	0.063616
41	H	2.669261	-3.750883	0.072667
42	H	5.592833	0.263310	-0.030224

Table S10. Cartesian coordinates of the DFT optimized structure in excited state S_1 of **2**.

Center Number	Atom	Coordinates (Angstroms)		
		X	Y	Z
1	C	1.11437300	0.48252000	-0.00001800
2	C	0.72858600	-0.92208100	-0.00001600
3	C	-1.11437300	0.48252100	-0.00001900
4	C	-0.72858100	-0.92208300	-0.00002800
5	N	-1.67627000	-1.86318000	-0.00003100
6	N	1.67627800	-1.86317800	-0.00000300
7	C	5.33859700	-2.08280100	0.00002400
8	C	5.76152900	-0.73905200	0.00003300
9	C	4.81248400	0.26884700	0.00002700
10	C	3.42824800	-0.01662600	0.00001400
11	C	2.98144100	-1.40854900	0.00001200
12	C	3.98898800	-2.40259100	0.00001300
13	H	6.07625400	-2.87995600	0.00002600
14	H	6.81892500	-0.49675000	0.00004300
15	H	5.13268900	1.30693700	0.00003300
16	H	3.66308400	-3.43753500	0.00000700
17	C	-2.98143400	-1.40855400	-0.00002400
18	C	-3.42824500	-0.01663000	-0.00001400
19	C	-4.81248400	0.26884000	-0.00001700
20	C	-5.76152500	-0.73906100	-0.00002600
21	C	-5.33858900	-2.08280900	-0.00003200
22	C	-3.98897800	-2.40259600	-0.00003200
23	H	-5.13269200	1.30693000	-0.00001900
24	H	-6.81892200	-0.49676300	-0.00003100
25	H	-6.07624300	-2.87996600	-0.00003800
26	H	-3.66307300	-3.43754000	-0.00003800
27	C	-0.00000600	2.69720700	0.00001200
28	C	-1.31512900	3.25487900	0.00004900
29	C	-2.46641300	2.43610600	0.00003500
30	H	-1.45569400	4.33177800	0.00007100
31	H	-3.43029800	2.93462100	0.00005700
32	C	-0.00000400	1.30421300	-0.00002000
33	C	1.31511000	3.25488100	0.00001600
34	H	1.45567700	4.33177900	0.00004100
35	C	2.46640100	2.43610600	0.00001700
36	H	3.43028300	2.93462700	0.00003400
37	C	2.41189700	1.00918600	0.00000500
38	C	-2.41190200	1.00918300	-0.00000100

Table S11. Cartesian coordinates of the DFT optimized structure in excited state S_1 of **1.**

Center Number	Atom	Coordinates (Angstroms)		
		X	Y	Z
1	C	1.11727300	0.41312300	0.00002200
2	C	0.73383900	-0.96782100	0.00005900
3	C	-1.11726500	0.41312800	0.00001300
4	C	-0.73383900	-0.96781700	0.00004200
5	N	-1.67210200	-1.93266300	0.00004800
6	N	1.67209600	-1.93267100	0.00008600
7	C	5.35164800	-2.19156400	0.00010300
8	C	5.75017400	-0.85145100	0.00006100
9	C	4.80017100	0.16737500	0.00002400
10	C	3.42197300	-0.11833300	0.00002600
11	C	2.96281700	-1.49813700	0.00007300
12	C	3.99266300	-2.52237100	0.00011100
13	H	6.10246400	-2.97144100	0.00012700
14	H	6.80733100	-0.60804900	0.00005800
15	H	5.12776300	1.20218800	-0.00000100
16	C	-2.96282000	-1.49812100	0.00002200
17	C	-3.42196800	-0.11831500	-0.00001800
18	C	-4.80016500	0.16740100	-0.00004900
19	C	-5.75017500	-0.85141800	-0.00003700
20	C	-5.35165800	-2.19153300	0.00000900
21	C	-3.99267600	-2.52234700	0.00003800
22	H	-5.12774900	1.20221700	-0.00008400
23	H	-6.80733100	-0.60800900	-0.00006000
24	H	-6.10247800	-2.97140700	0.00002200
25	C	0.00001000	2.64432600	-0.00006800
26	C	-1.34286800	3.16436400	-0.00009200
27	C	-2.47990900	2.34414500	-0.00007300
28	H	-3.44383100	2.83970800	-0.00009800
29	C	0.00000600	1.24353600	-0.00000300
30	C	1.34289100	3.16435700	-0.00010600
31	C	2.47992700	2.34413200	-0.00007700
32	H	3.44385200	2.83969000	-0.00011200
33	C	2.40219600	0.91384700	-0.00000900
34	C	-2.40218500	0.91386000	-0.00002600
35	O	3.53616300	-3.78359600	0.00015100
36	O	-3.53619700	-3.78357700	0.00008400
37	C	4.46578700	-4.87160800	0.00023900
38	H	3.85695700	-5.77463000	0.00031400
39	H	5.09501600	-4.85025700	-0.89526300
40	H	5.09502200	-4.85010900	0.89573200
41	C	-4.46585000	-4.87156400	0.00008200
42	H	-5.09506200	-4.85013500	-0.89543000
43	H	-3.85704400	-5.77460200	0.00011200

44	H	-5.09510100	-4.85010400	0.89556500
45	Cl	1.65443400	4.89742200	-0.00019100
46	Cl	-1.65440200	4.89743100	-0.00015600

Table S12. Cartesian coordinates of the DFT optimized structure in excited state S_1 of **TB(phen).**

Center Number	Atom	Coordinates (Angstroms)		
		X	Y	Z
1	C	-3.54685200	2.07029500	0.02503500
2	C	-2.85539300	0.84774700	0.00984300
3	C	-1.42776400	0.86012700	0.00414500
4	C	-0.72101200	2.10812200	0.00744300
5	C	-2.85712300	3.28974500	0.03521500
6	C	-0.72363200	-0.38643600	-0.00346900
7	C	0.72101200	2.10812200	-0.00744300
8	C	1.42776400	0.86012700	-0.00414600
9	C	0.72363200	-0.38643600	0.00346700
10	C	2.85539300	0.84774700	-0.00984300
11	H	-4.63032500	2.08430700	0.03101600
12	H	-3.41388900	4.22088500	0.05052000
13	C	-3.52703500	-0.43890400	0.00045400
14	C	-2.69501700	-1.61738600	-0.01438500
15	C	3.52703500	-0.43890400	-0.00045300
16	C	2.69501700	-1.61738600	0.01438400
17	C	1.47547800	3.31355200	-0.02638200
18	H	0.97248300	4.27186600	-0.03809000
19	C	-1.47547800	3.31355200	0.02638200
20	H	-0.97248300	4.27186600	0.03808900
21	N	-1.34939500	-1.58625300	-0.01539500
22	N	1.34939500	-1.58625300	0.01539100
23	C	4.69439800	-3.01964500	0.02382300
24	H	5.15861100	-4.00132100	0.03305900
25	C	3.32467900	-2.90188600	0.02721700
26	H	2.67604200	-3.77169500	0.03876200
27	C	5.50512100	-1.86026200	0.00777100
28	H	6.58640700	-1.95602100	0.00459700
29	C	4.92602100	-0.60062700	-0.00380200
30	H	5.57395800	0.26910000	-0.01553500
31	C	3.54685200	2.07029500	-0.02503500
32	H	4.63032500	2.08430700	-0.03101700
33	C	2.85712300	3.28974500	-0.03521500
34	H	3.41388900	4.22088500	-0.05052100
35	C	-5.50512100	-1.86026200	-0.00776600
36	C	-4.69439800	-3.01964500	-0.02382200
37	C	-3.32467900	-2.90188600	-0.02721900
38	C	-4.92602100	-0.60062700	0.00380600
39	H	-6.58640700	-1.95602100	-0.00459000

40	H	-5.15861100	-4.00132100	-0.03305900
41	H	-2.67604200	-3.77169500	-0.03876600
42	H	-5.57395800	0.26910000	0.01554200

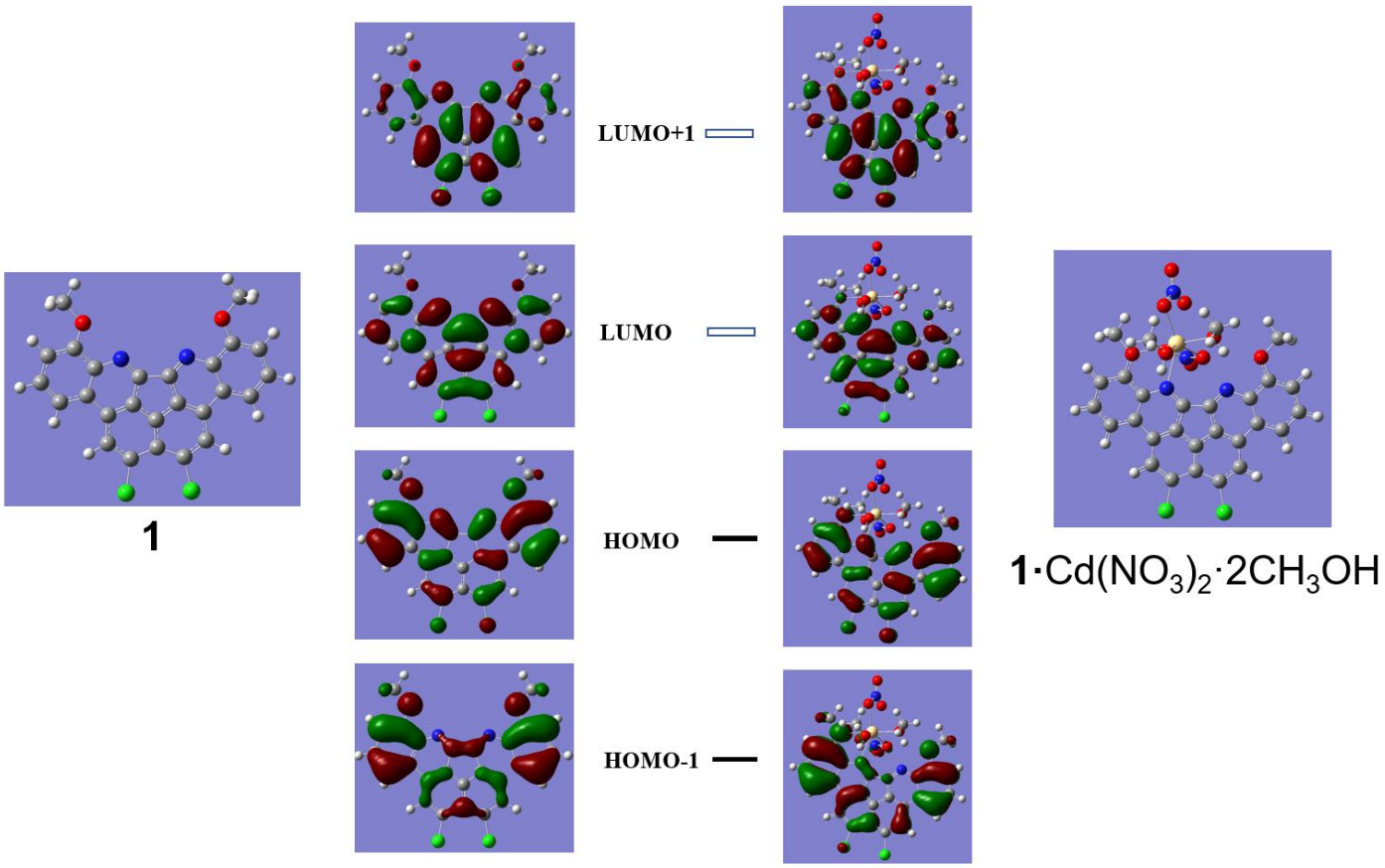

Figure S76. Molecular orbitals of **1** and **1**·$Cd(NO_3)_2$·$2CH_3OH$.

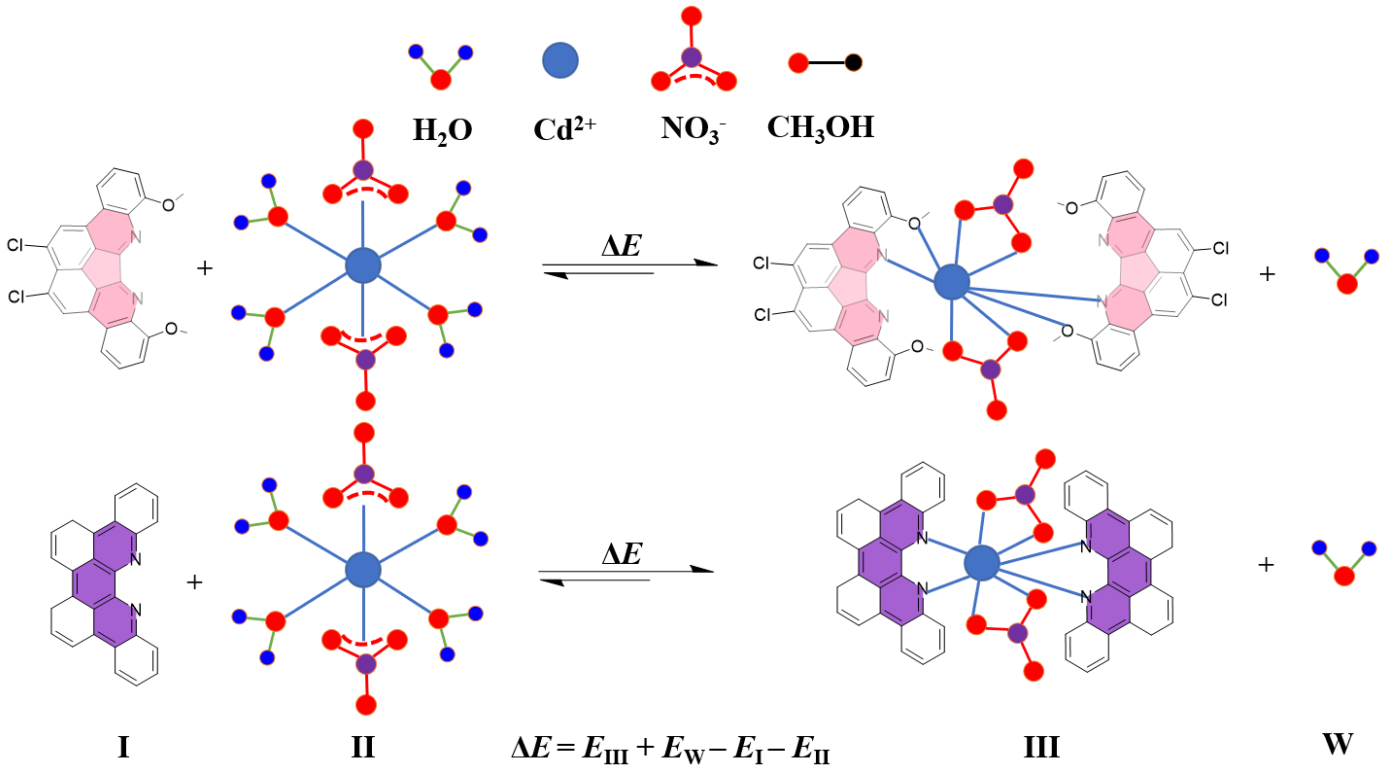

Figure S77. Complexation equilibriums between $Cd(NO_3)_2·4H_2O$ and **1** or **TB(phen)** with 2:1 ratio.

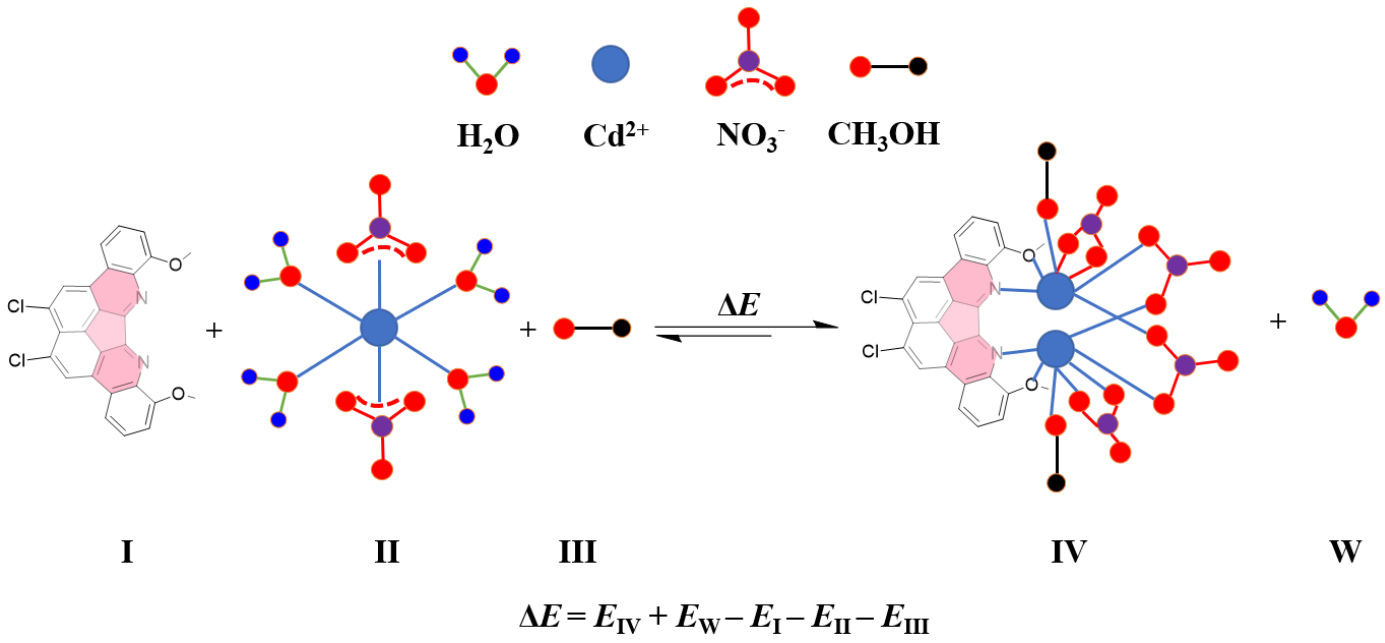

$$\Delta E = E_{IV} + E_{W} - E_{I} - E_{II} - E_{III}$$

Figure S78. Complexation equilibriums between $Cd(NO_3)_2 \cdot 4H_2O$ and **1** with 1:2 ratio.

Section S7: *Protonation study of* ***1*** *in* CH_2Cl_2/CH_3OH *(4:1, v/v)*

General procedure for the Uv-vis and fluorescence spectral studies

In this case, 2000 μL of **1** (2.00×10^{-5} M in CH_2Cl_2/CH_3OH (4:1, *v/v*)) was added to quartz cell. The tested trifluoroacetic acid (CF_3SO_3H, 4.00×10^{-2} M in CH_2Cl_2/CH_3OH (4:1, *v/v*)) was stepwise added and fully mixed for further detection. All data were collected after each aliquot was added and mixed.

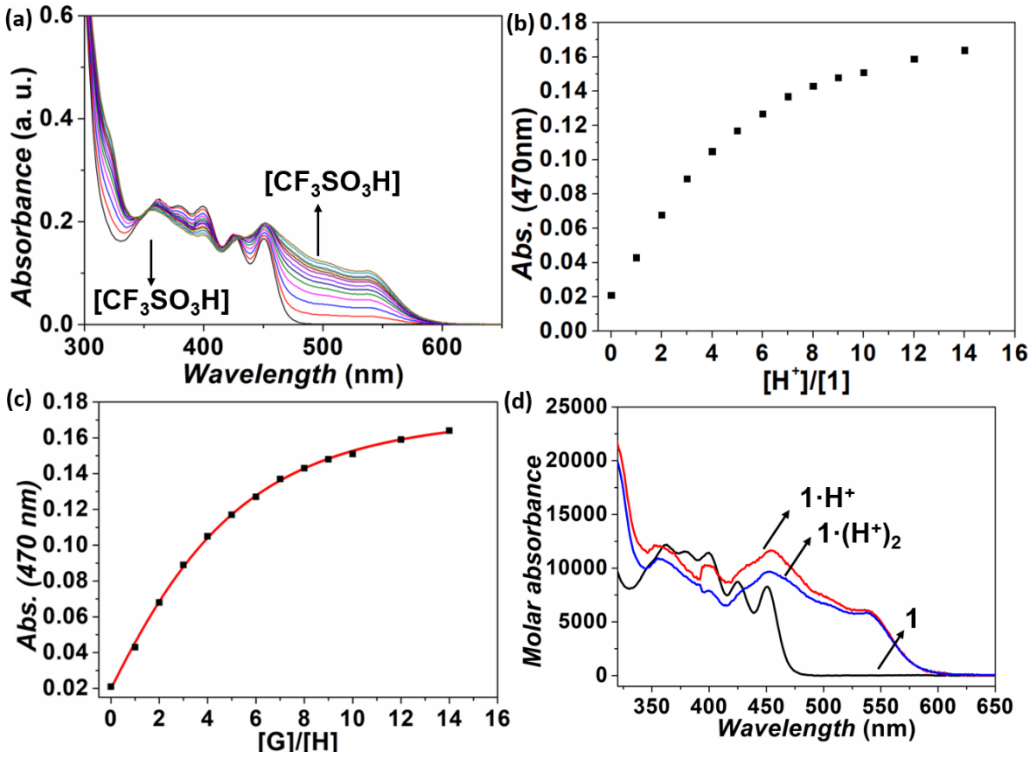

Figure S79. (a) Uv-vis spectra recorded for corresponding to **1** (2.00×10^{-5} M in CH_2Cl_2/CH_3OH (4:1, *v/v*)) with increasing [CF_3SO_3H] (G: from 0 to 20 molar equiv.) at 298 K. (b) The absorbance changes at 470 nm ("■"). And (c) the results of the corresponding nonlinear curve fitting according calculated model (red line) Hyperquad 2003. (d) The calculated molar absorbance of **1** and its protonated products. The equilibriums and related K_a calculation results as shown: $2M + L \overset{K_2}{\rightleftarrows} M_2L$; $\log K_2 = 8.0(5)$; $M + L \overset{K_1}{\rightleftarrows} ML$; $\log K_1 = 3.9(5)$.

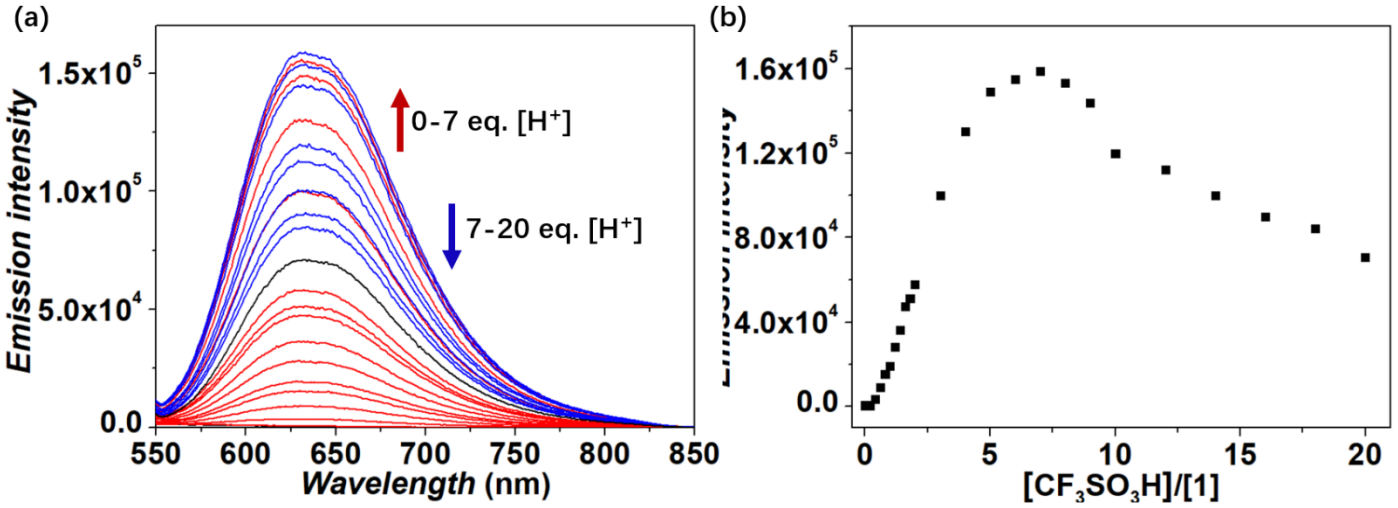

Figure S80. (a) Fluorescent emission spectra corresponding to **1** (2.00×10^{-5} M in CH_2Cl_2/CH_3OH (4:1, *v/v*)) with increasing [CF_3SO_3H] (from 0 to 20.0 molar equiv.) at 298 K. (b) The fluorescence intensity changes at 630 nm ("▪") (λ_{ex} = 540 nm, voltage = 400 V, entrance slit width = 9 nm, exit slit width = 9 nm).

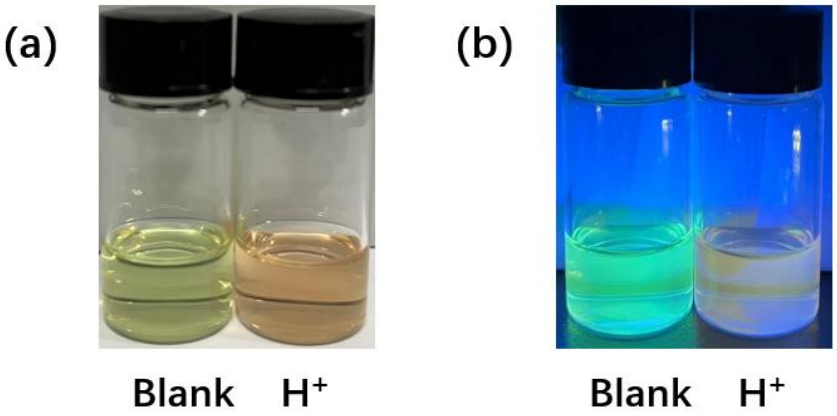

Figure S81. Photographs of **1** (2.00×10^{-5} M) coordination with CF_3SO_3H (20 molar equiv.) in CH_2Cl_2/CH_3OH (4:1, *v/v*) under (a) visible light and (b) 365 nm UV light, respectively.

Reference

(1) H. E. Gottlieb, V. Kotlyar, A. Nudelman, *J. Org. Chem.*, 1997, **62**, 7512-7515.

(2) G. M. Sheldrick, *SHELXL97*. Program for the Refinement of Crystal Structures, University of Göttingen, Göttingen, 1994.

(3) O. V. Dolomanov, L. J. Bourhis, R. J. Gildea, J. A. K. Howard, *J. Appl. Cryst.*, 2009, **42**, 339-341.

(4) G. M. Sheldrick, *Acta Cryst. A.*, 2015, **71**, 3-8.

(5) $R_W(F^2) = \{w(|F_O|^2 - |F_C|^2)^2/w(|F_O|)^4\}^{1/2}$ where w is the weight given each reflection. $R(F) = (|F_O| - |F_C|)/|F_O|\}$ for reflections with $F_O > 4((F_O))$. $S = [w(|F_O|^2 - |Fc|^2)^2/(n - p)]^{1/2}$, where n is the number of reflections and p is the number of refined parameters.

(6) Y. Fei, Y. Fu, X. Bai, L. Du, Z. Li, H. Komber, K.-H. Low, S. Zhou, D. L. Phillips, X. Feng and J. Liu, *J. Am. Chem. Soc*., 2021, **143**, 2353.

(7) T. Ishiyama, M. Murata and N. Miyaura, *J. Org. Chem*., 1995, **60**, 7508.

(8) Gaussian 09, Revision D.01, M. J. Frisch, G. W. Trucks, H. B. Schlegel, G. E. Scuseria, M. A. Robb, J. R. Cheeseman, G. Scalmani, V. Barone, B. Mennucci, G. A. Petersson, H. Nakatsuji, M. Caricato, X. Li, H. P. Hratchian, A. F. Izmaylov, J. Bloino, G. Zheng, Sonnenberg, J. L.; Hada, M.; Ehara, M.; Toyota, K.; Fukuda, R.; Hasegawa, J.; Ishida, M.; T. Nakajima, Y. Honda, O. Kitao, H. Nakai, T. Vreven, J. A. Montgomery, J. E. Peralta, F. Ogliaro, M. Bearpark, J. J. Heyd, E. Brothers, K. N. Kudin, V. N. Staroverov, R. Kobayashi, J. Normand, K. Raghavachari, A. Rendell, J. C. Burant, S. S. Iyengar, J. Tomasi, M. Cossi, N. Rega, M. J. Millam, M. Klene, J. E. Knox, J. B. Cross, V. Bakken, C. Adamo, J. Jaramillo, R. Gomperts, R. E. Stratmann, O. Yazyev, A. J. Austin, R. Cammi, C. Pomelli, J. W. Ochterski, R. L. Martin, K. Morokuma, V. G. Zakrzewski, G. A. Voth, P. Salvador, J. J. Dannenberg, S. Dapprich, A. D. Daniels, Ö. Farkas, J. B. Foresman, J. V. Ortiz, J. Cioslowski, D. J. Fox, Gaussian, Inc., Wallingford CT, 2013.